LA-UR-04-1227

|  |  |
|---|---|
| *Title:* | GSI-191: Experimental Studies of Loss-of-Coolant-Accident-Generated Debris Accumulation and Head Loss with Emphasis on the Effects of Calcium Silicate Insulation |
| *Author(s):* | C. J. Shaffer, ARES Corporation<br>M. T. Leonard, dycoda, LLC<br>B. C. Letellier, D V Rao, W. A. Roesch, and<br>J. D. Madrid, Los Alamos National Laboratory<br>A. K. Maji, K. Howe, A. Ghosh, and J. Garcia, The University of New Mexico |
| *Submitted to:* | US Nuclear Regulatory Commission |

# GSI-191: Experimental Studies of Loss-of-Coolant-Accident-Generated Debris Accumulation and Head Loss with Emphasis on the Effects of Calcium Silicate Insulation

Principal Investigator: B. C. Letellier

Prepared by
C. J. Shaffer,[†] M. T. Leonard,[*] B. C. Letellier, D V Rao,
A. K. Maji,[‡] K. Howe, [‡] A. Ghosh, J. Garcia, [‡] W. A. Roesch, and J. D. Madrid

Los Alamos National Laboratory
Los Alamos, NM 87545

Subcontractors:
[*]dycoda, LLC
 Belen, NM 87002

[†]ARES Corporation
 Albuquerque, NM 87106

[‡]The University of New Mexico
 Department of Civil Engineering
 Albuquerque, NM 87110

Tsun-Yung Chang, NRC Project Manager

## CONTENTS

**CONTENTS (cont)**

# FOREWORD

by
The United States Nuclear Regulatory Commission

In the event of a loss-of-coolant accident (LOCA) within the containment of a nuclear power plant, thermal insulation and other materials in the vicinity of the pipe break may be dislodged by the high-energy steam/water jet impingement. Fragmented and dislodged insulation and other materials such as paint chips and concrete dust may be transported to the containment floor by the steam/water flows from the break and by the containment sprays, if actuated. Some of this debris will eventually be transported to and accumulated on the sump screens in pressurized water reactor (PWR) containments or on pump suction strainers in boiling water reactor (BWR) containments. Debris accumulation on sump screens/suction strainers and the ensuing head loss (pressure drop) across sump screens/suction strainers could challenge the plant's ability to provide adequate, long-term cooling water to the emergency core cooling system (ECCS) and the containment spray system (CSS) pumps. Therefore, adequate test data for debris accumulation and head loss for various debris types are essential for the realistic assessment of the post-LOCA sump performance.

The NRC-sponsored parametric study of BWR ECCS strainer blockage due to LOCA-generated debris resulted in the publication of NUREG/CR-6224 in 1995. Among the important findings of this study was the head loss correlation. This correlation was developed by performing extensive experiments to measure the head loss effects of mixed particulate and fibrous debris beds. The particulate debris investigated was U.S. BWR suppression pool sludge, which includes primarily corrosion products, along with dirt, dust, and other residues commonly found in the U.S. BWR suppression pools. The fibrous insulation used for the tests was NUKON™ fiberglass.

Although there is an extensive body of head loss test data, including the NRC-sponsored study documented in NUREG/CR-6224 and tests done by others in the U.S. and in Europe, tests performed to date have not addressed the full range of potential debris characteristics postulated for PWR containments. Of the 69 PWR plants operating in the U.S. today, close to 40% use calcium silicate (CalSil) thermal insulation (see NUREG/CR-6762, Vol. 2, August 2002), often with other insulation materials such as fiberglass or reflective metallic insulation (RMI). The primary objectives of this experimental program were to generate data on debris accumulation on PWR sump screens and head loss associated with CalSil insulation and to determine the suitability of the NUREG/CR-6224 head loss correlation for CalSil head loss calculations. The tests encompass a range of test parameters that are representative of those in typical U.S. PWR plants during recirculation phase, such as screen approach velocities, water temperatures, and mixed debris beds of CalSil and fiber/RMI.

This report documents the experiments conducted to determine the head loss associated with CalSil insulation accumulated on a sump screen (with or without fiber/RMI). The experiments confirmed that CalSil could degenerate into very fine particulates in the post-LOCA containment environment, and debris bed formed by a combination of fine CalSil particulates and fibrous insulation on a sump screen can cause substantial head loss across the sump screen. The recommended head loss parameters to be used in the NUREG/CR-6224 correlation were established with consideration of uncertainties in test parameters and the variance in the manufacture of the particular brand of CalSil insulation tested. The experiments demonstrated that the NUREG/CR-6224 head loss correlation performed reasonably well for CalSil insulation if the head loss parameters used in the correlation (e.g., specific surface area, particle density) are adequately determined by experiments. The results from this research enhance the understanding of the important Generic Safety Issue (GSI) 191, "Assessment of Debris Accumulation on PWR Sump Performance."

# GSI-191: Experimental Studies of Loss-of-Coolant-Accident-Generated Debris Accumulation and Head Loss with Emphasis on the Effects of Calcium Silicate Insulation

## EXECUTIVE SUMMARY

This report describes a series of experiments that generated data needed to support the resolution of Generic Safety Issue 191. The experiments were performed under the direction of Los Alamos National Laboratory (LANL) in facilities operated by the Civil Engineering Department of the University of New Mexico.

The tests provide data and qualitative insights not available from earlier experimental work in two respects. First, head loss across a debris bed consisting of fragments of Calcium Silicate (CalSil) insulation had not been measured in prior experiments sponsored by the United States (US) Nuclear Regulatory Commission. Second, prior experimental work did not explicitly examine the geometric configuration(s) with which transportable forms of loss-of-coolant-accident (LOCA)-generated debris would collect on a typical pressurized-water reactor (PWR) recirculation sump screen. A prior industry examination of CalSil head-loss characteristics [performed to support the redesign of recirculation strainers in a boiling-water reactor (BWR)] suggested that the head loss caused by this material could be disproportionately higher than that of other forms of insulation debris with comparable mass/volume. When it was recognized that the specific design features of recirculation sump screens differ considerably among the fleet of US PWRs, experimental data were needed to understand the basic configuration with which debris would collect on a typical PWR sump screen. Therefore, tests were conducted to observe the geometric pattern with which debris would accumulate on a prototypic screen in representative configurations.

Significant findings from the current experiments are the following.

1. Debris accumulation on a simulated (vertical) PWR sump screen was examined for several different types of LOCA-generated debris, including shredded fiberglass, crushed CalSil, mixtures of NUKON™ and CalSil, and crumpled stainless-steel foils from the interior of reflective metal insulation (RMI). With the exception of RMI foils, debris was observed to accumulate on the screen in a relatively uniform manner for conditions in which the local fluid velocity was significantly greater than the bulk transport velocity of debris fragments. The RMI foils accumulated primarily near the bottom of the screen; however, continuous hydraulic forces gradually caused late-arriving foils to "climb" over the pile of debris that accumulated earlier. Over time, this created a "bottom-skewed" profile in which most of the screen surface (1 ft in height) was covered with debris; however, roughly one-half of the total RMI debris remained stationary at the bottom of the screen.

2. Head-loss measurements were made in a closed-loop test facility located at the University of New Mexico. Before conducting experiments with debris containing CalSil, qualification tests were run to measure the head loss caused by debris that has been examined in prior studies (in other test facilities). In particular, tests were performed to measure head loss caused by shredded NUKON™ fiber and mixtures of NUKON™ fiber and a sand-and-concrete-dust particulate. Measurements were compared to predictions of the head loss using the NUREG/CR-6224 correlation with excellent agreement.

3. The application of the NUREG/CR-6224 head-loss correlation to a bed of debris requires certain parameters (e.g., specific surface area) as input to the correlation. These parameters have been determined for NUKON™ insulation debris and for some other materials, such as BWR suppression pool corrosion products, but not for many types of insulation and particulate debris typically found in PWR containments; in particular, these parameters have not previously been determined for CalSil. The determination of these parameters is

experimental, and one method is to vary the parameter numerically in the correlation while simulating an appropriate test until the correlation results reasonably predict the data. The analysis of the results described herein show that the specific surface area for CalSil is quite large, which should be expected because of the fine nature of its components, as shown in scanning electron microscopy photos taken of the debris tested. The analyses herein strongly indicate that the high specific surface area of CalSil is responsible for the high head losses it is known to generate. For perspective, the generally accepted value for the specific surface area of NUKON™ is 171,000/ft; while the experimentally determined values for CalSil are roughly 3-5 times this value. The leading term of the NUREG/CR-6224 correlation depends on the square of this number, and the second term is linear with the specific surface area. Testing difficulties have included the establishment of reasonably uniform and homogeneous debris beds under conditions where nearly the entire test quantity of CalSil is filtered from the flow stream and the accurate measurement of debris bed head losses, flow rates, temperatures, and water clarity; however, these challenges were handled successfully in a second group of tests. Recommendations for the input parameters to the NUREG/ CR-6224 correlation were developed to ensure conservative simulation of head loss associated with fibrous debris beds that contain the brand of CalSil insulation debris obtained from Performance Contracting Inc. The recommendations focus on the prediction of thin-bed behavior, where the debris has been compacted until further compaction is limited by the CalSil particulate. The recommendations are 115 lbm/ft$^3$ for the particle density, 22 lbm/ft$^3$ for the sludge density, and 880,000 ft$^2$/ft$^3$ for the specific surface area. This specific surface area includes a 10 to 20% safety factor to cover uncertainties.

4.  Tests conducted using only CalSil fragments to form the debris bed clearly demonstrated that CalSil debris can accumulate on a 1/8-in. mesh screen and cause substantial head loss without the aid of another form of fiber to hold it in place. Further, it was clearly demonstrated that CalSil creates substantially higher head losses than does a comparable quantity of low-density fiberglass. Experimentally, it was found even more difficult to form a truly uniform bed of CalSil debris than it was to form a NUKON™/CalSil bed. The thickest beds of CalSil formed in these tests were ~1/4-in. thick (on average) so that the fragments of CalSil formed lumps and unevenness in the bed and small portions of the screen were not covered by the CalSil, thereby forming a bypass. However, the analysis strongly indicates that once the CalSil head-loss parameters have been adequately determined, the form of the NUREG/CR-6224 correlation where the correlation is modified to simulate a granular bed (without significant fiber) will perform well for a uniform CalSil debris bed.

5.  Measured head losses for mixtures of CalSil and RMI were higher than those measured for the base RMI debris. Head loss doubled in magnitude when 75 g CalSil/ft$^2$ of screen area was added to a 1-in. bed of crumpled RMI foils; significantly less CalSil (~30 g/ft$^2$ of screen area) doubled the head loss across an 8-in. bed of RMI foils. The LANL correlation for characterizing head loss in RMI debris beds was shown to provide an excellent prediction of data measured for baseline test conditions involving 1-in. and 8-in. debris beds of pure stainless-steel RMI.

# 1. INTRODUCTION

In the event of a loss-of-coolant accident (LOCA) within the containment of a pressurized-water reactor (PWR), piping thermal insulation and other materials in the vicinity of the break will be dislodged by break jet impingement. A fraction of this dislodged insulation and other materials, such as paint chips and concrete dust, will be transported to the containment floor by the steam/water flows induced by the break and the containment sprays. Some of this debris may eventually be transported to and accumulated on the suction sump screens of the emergency core cooling system (ECCS) pumps. Debris accumulation increases the differential pressure across the sump screen and in some cases may degrade ECCS performance to the point of failure.

The Generic Safety Issue (GSI)-191 study addresses the issue of debris accumulation on the PWR sump screen and consequential loss of ECCS pump net positive suction head (NPSH). Los Alamos National Laboratory (LANL) has been supporting the United States (US) Nuclear Regulatory Commission (NRC) in the resolution of GSI-191. Among the tasks being performed by LANL is experimental determination of head loss across a PWR sump screen for flow conditions representative of those expected during ECCS recirculation and for debris types and quantities that might accumulate on the screen during a LOCA. This document describes the experimental facilities and tests conducted to address this topic with emphasis on the effects of calcium silicate insulation.

## 1.1. Rationale for Test Program

The program plan described here acknowledges the extensive body of published literature on debris-induced head loss. However, experiments performed to date had not addressed the full range of potential debris characteristics postulated for PWR containments. In particular, the efficiency with which calcium silicate (CalSil) debris is captured by a PWR sump screen (with or without fibrous debris present) has not been characterized, nor has the resulting head loss been measured at prototypic flow conditions. It was known that CalSil fragments can accumulate on a clean screen whereas the fine CalSil particulate will pass through the screen. The presence of fibrous debris increases the efficiency of filtration for the CalSil. Further, the vertical geometry and horizontal entrance flow through most PWR sump screens raises significant questions regarding the extent to which debris would accumulate in a uniform manner across the sump screen area, as many head-loss models assume. These issues and others are addressed in the test program described herein.

## 1.2. Objectives and Scope of the Experiments

The test program described here is designed to achieve the following objectives:

1. Establish a technical basis for extending the applicability of the NUREG/CR-6224 correlation from porous debris beds on boiling-water reactor (BWR) suppression pool strainers to debris beds on PWR sump screens or other flow blockages.

2. Generate data to support confirmatory evaluation of sump screen performance for plants with CalSil insulation and suitability of NUREG/CR-6224 correlation to CalSil head-loss predictions.

To accomplish these objectives, experiments were performed that focus on two properties of a LOCA-generated debris bed: (1) debris accumulation on a vertical sump screen and (2) sump screen head loss.

### 1.2.1. Debris Accumulation
Information regarding the manner in which debris accumulates on a vertical screen is needed to answer at least two questions: (1) Under what conditions is the debris bed that forms on a submerged recirculation sump screen uniform in thickness and composition? Direct application of the NUREG/CR-6224 head-loss correlation to PWR sump screens requires an understanding of the range of conditions in which the debris bed is spatially uniform. (2) Can debris accumulate against a vertical screen in a manner that would block flow near the base of the screen and create a weir?

### 1.2.2. Sump Screen Head Loss

Head-loss data collected in several past experimental programs are limited in two areas critical to a robust assessment of PWR sump screen performance. First, head loss has not been measured across debris beds formed on PWR sump screens. Data generated to date have concentrated on BWR strainer configurations, which typically involve a perforated plate rather than a wire-mesh screen. Second, data are not available regarding head losses associated with debris beds containing CalSil. The test program described here is designed to address these topics.

To accomplish these objectives, vertical screen experiments were conducted in an open flume apparatus primarily to determine the debris-accumulation characteristics of NUKON™, CalSil, and reflective metal insulation (RMI) debris on a vertically oriented screen. Limited head-loss data were taken for selected debris accumulations. Experiments were also conducted in a closed-loop test apparatus where the screen was horizontal but the focus was the measurement of the debris bed head loss associated with a variety of debris beds including NUKON™ debris, NUKON™, and a sand and concrete dust particulate, CalSil debris, mixed NUKON™ and CalSil debris, RMI debris, and mixed RMI and CalSil debris. These head-loss measurements were subsequently used to deduce head-loss parameters for the NUREG/CR-6224 head-loss correlation.

The closed-loop head-loss tests were conducted in two groups. After the first group of tests was completed, analysis of those results indicated that test apparatus procedure and instrumentation enhancements were required to refine the test results. Once these enhancements were completed, a second group of tests was performed. Both the testing experience and the test results are discussed. The recommendations regarding the application of the NUREG/CR-6224 head-loss correlation were developed primarily from the data gathered during the second group of tests.

### 1.3. Report Outline

The technical approach to the experiments is described in Section 2. This discussion includes a brief summary of the test apparatus for observing debris accumulation and the apparatus for measuring debris head loss (Section 2.1). A description of the major test variables is also provided in Section 2, which concludes with a tabulated delineation of the values used to define individual experiments.

Results of the experiments from the first group of closed-loop head-loss tests are described in Section 3. The results include a summary of measurements and qualitative observations made during the experiments.

Section 4 provides analysis of the test data from the first group of closed-loop head-loss tests. In particular, the ability of the NUREG/CR-6224 correlation to provide reasonable estimates of head loss is evaluated for the test conditions examined.

Section 5 provides the experimental results and analysis of the test data from the second group of closed-loop head-loss tests. The procedure and instrumentation enhancements for the second group of tests are also discussed herein. Recommendations for the application of the NUREG/CR-6224 correlation to fibrous debris beds containing CalSil insulation debris were developed from this test data.

Major conclusions drawn from the experiments are described in Section 6. All references provided in the text of this report are listed in Section 7.

Several appendices are attached to the report and provide additional detail on several topics, such as the design and construction details of the experimental apparatuses, test procedures, and a listing of raw data collected in each test.

## 2.    TECHNICAL APPROACH

The technical approach is to simulate appropriate PWR containment debris accumulation and head-loss conditions, with flexibility for controlling local flow conditions, debris quantity and other important parameters and with the capability of taking applicable measurements and visual observations of the phenomena under examination.

### 2.1.    Test Facilities

Two facilities were used to conduct the experiments described in this document: a large linear flume and a closed-loop hydraulic test apparatus. The large flume was used primarily to record visual observations of debris accumulation on a vertical, fully submerged screen, but coarse measurements of the associated head loss across the screen were also taken for a limited range of conditions. The closed-loop hydraulic test apparatus was used exclusively for measuring the head loss across a debris-laden screen. Major features of these two facilities are described below.

#### 2.1.1.    Large Flume Debris-Accumulation Tests

The debris-accumulation tests were conducted in an open-channel linear flume, referred to as the "large flume," located in the open-channel hydraulics laboratory at the University of New Mexico (UNM). This facility was used to measure debris transport characteristics in the separate-effects test series conducted in support of GSI-191 [Rao, 2002a]. The large-flume apparatus is illustrated schematically in Figure 2.1. The flume consists of an open-top box 20 ft long, 3 ft wide, and 4 ft high. The water inlet and flow conditioning occurs in the first 4 ft of the flume. In the central portion of the flume (i.e., the 10-ft length between the flow straightener and the test screen), the active width of the flume was reduced from 3 ft to 1 ft by installing 1-in.-thick plywood walls. This converging section of the flume was necessary to allow tests to be conducted with volume-average approach velocities at the screen above 1 ft/s.

The walls of the 2-ft linear section of the flume, immediately upstream of the screen, are constructed of 1/2-in.-thick, transparent Plexiglas™, allowing experimenters to observe the behavior of transported debris as it accumulates on the screen. Downstream of the debris screen, an exit tunnel (1-ft x 1-ft square in cross section) was mated to the end of the linear portion of the flume to simulate a submerged recirculation sump enclosure and attached suction piping. The tunnel is sealed from other upstream portions of the flume, except for a 1-ft x 1-ft entrance doorway through which all water flowing through the flume must pass to reach the exit drain at the opposite end of the tunnel. A 1/8-in. mesh screen covers the entire cross section of the doorway, simulating flow conditions at the surface of a fully submerged recirculation sump.

Additional details of the flume construction, operation during experiments, and instrumentation are provided in Appendix A.

#### 2.1.2.    Closed-Loop Head-Loss Measurement Facility

Experiments to measure head loss across a debris-laden screen were conducted in a closed-loop hydraulic test apparatus also operated by the Civil Engineering Department of UNM. As illustrated in Figure 2.2, the primary section of the experimental apparatus is a vertically oriented nominal 12-in. polyvinyl chloride (PVC) pipe (inside diameter of 11.4 in.). A support ring, ~7/16-in. thick, was mounted approximately mid-height in the transparent section inside the PVC pipe to support the test screen (ring inside diameter of ~11.05 in.). A course supporting steel grating and then the actual 1/8-in. rectangular mesh screen similar to those used as PWR recirculation sump screens (both 11.25 in. in diameter) were placed on the support ring.

Additional details of the flume construction, operation during experiments, and instrumentation are also provided in Appendix A.
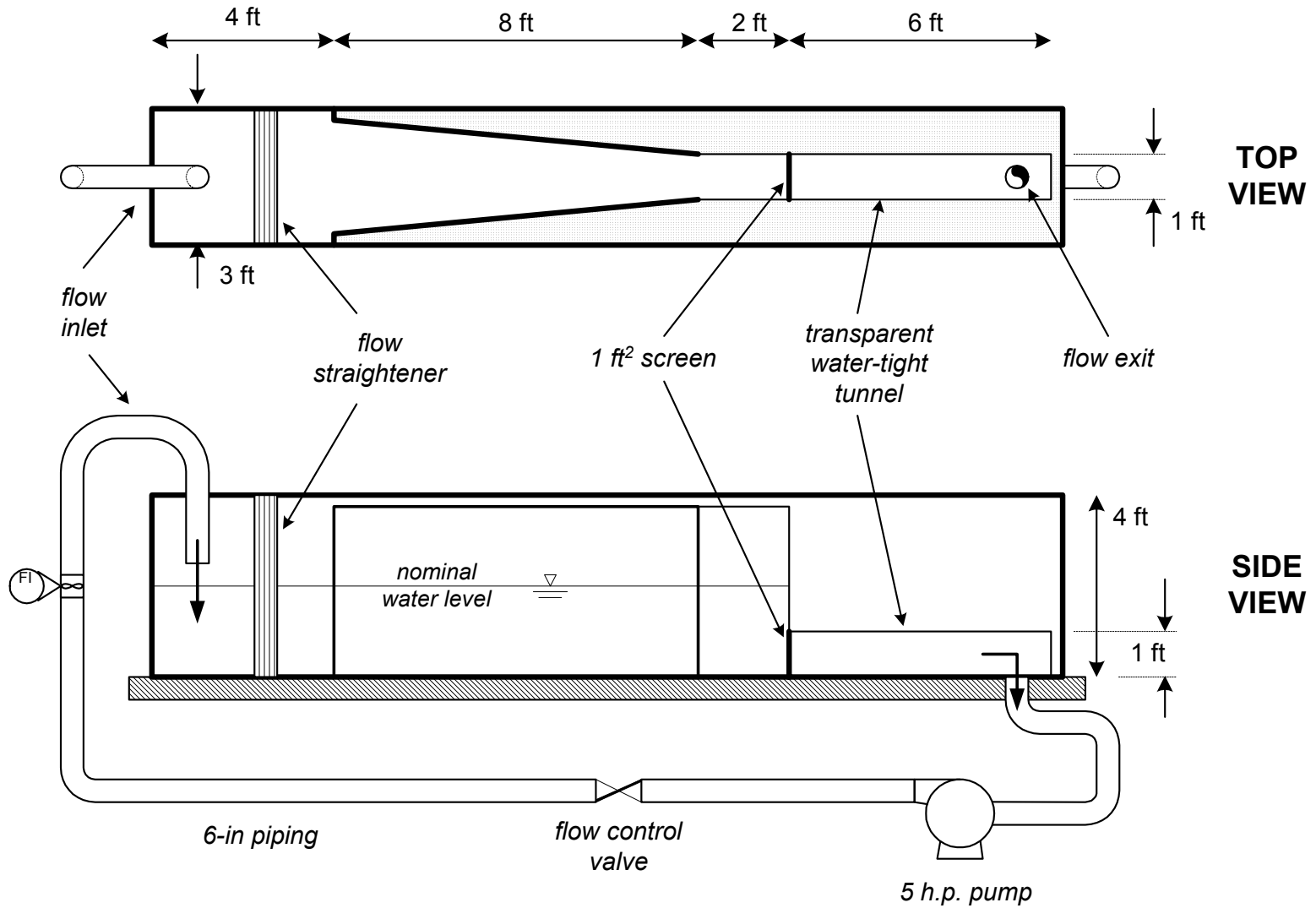
**Figure 2.1. Plan and elevation views of the large flume used in debris-accumulation tests.**
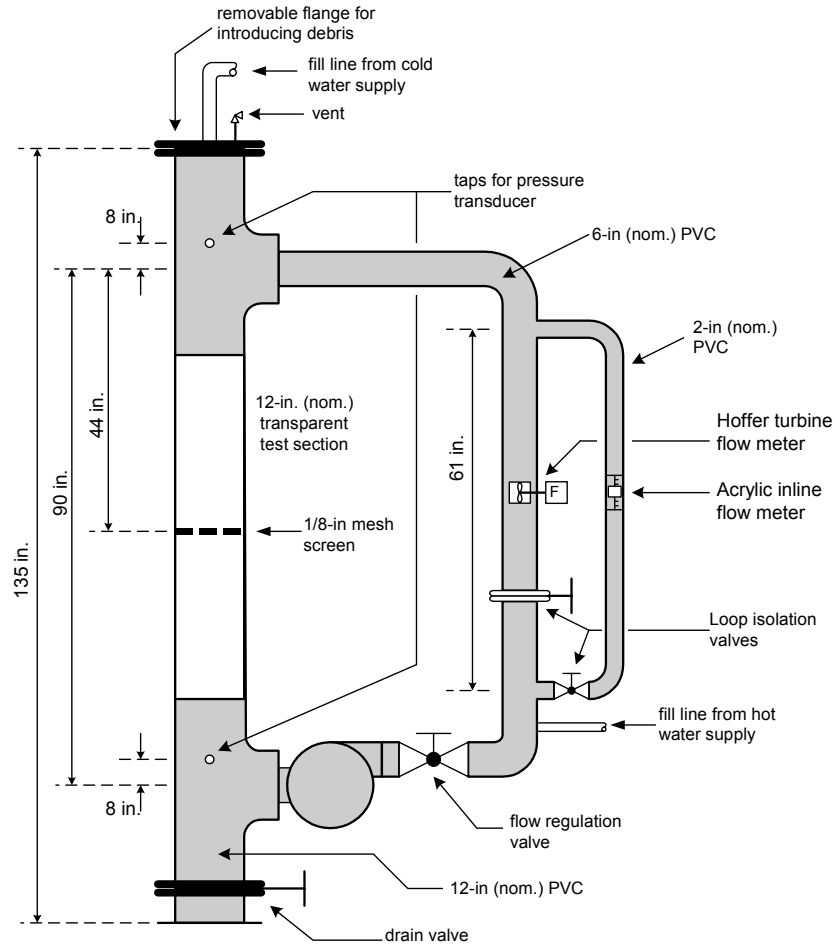
**Figure 2.2. Configuration of the closed-loop head-loss test facility.**

## 2.2. Test Variables

### 2.2.1. Large-Flume Debris-Accumulation Tests
The parameters varied during the debris-accumulation tests were the following:

- screen approach velocity,
- total quantity of debris available for capture by the screen,
- debris type(s), and
- the presence or absence of large-scale turbulence in the flume.

#### 2.2.1.1. Approach Velocity
Analysis of information gathered in a survey of ECCS recirculation sump configurations at US PWRs indicates that ~85% of US PWRs have minimum approach velocities less than 0.5 ft/s and 40% have minimum approach velocities less than 0.1 ft/s [Rao, 2002b]. The latter value was found in separate-effects debris transport tests to be near the minimum velocity required to move small fragments of fiber along the containment floor in uniform nonturbulent flow [Rao, 2002a]. Slightly higher values were required to move CalSil fragments (~0.25 ft/s). The maximum approach velocities in a few plants can exceed 1 ft/s, with the largest maximum velocity in the neighborhood of 2 ft/s. Based on these observations and the physical limitations of the large-flume test facility, tests were performed to span a range of approach velocity from 0.2 to 1 ft/s.

5

### 2.2.1.2. Debris Type and Size Distribution
Debris-accumulation tests were performed using the following types of debris:

- shredded fiberglass from the core insulating material in NUKON™ blankets,
- fragments of CalSil insulation,
- mixed beds of NUKON™ fiber and CalSil fragments,[1] and
- RMI foils constructed of stainless steel.

Photographs of typical fiberglass, CalSil, and RMI debris used in these experiments are shown in Figure 2.3. Fiberglass debris was generated by running cut sections of NUKON™ base fiber blanket material through a common leaf shredder. This process produced a mixture of debris with sizes ranging from small collections of individual fibers to roughly 1-in. loose clumps of fibers. CalSil fragments were generated by hand-crushing intact segments of initially intact insulation. For comparison, LOCA generated debris ranges from individual fibers to large pieces of relatively intact insulation.

Tests were not performed for RMI foils constructed of aluminum because results of the PWR industry survey indicated that this type of insulation is only used as reactor vessel insulation. Accident analyses generally do not postulate that a credible amount of reactor vessel insulation could be destroyed and subsequently transported to the containment sump.

### 2.2.1.3. Quantity of Fibrous Debris
The quantities of debris that could potentially collect on sump screens were roughly estimated as part of the parametric evaluation of PWR sump performance [Rao, 2002b]. These estimates considered both the degree of insulation destruction within the zone of influence and the subsequent transport to the sump screens. To facilitate scaling of the full-scale PWR analysis to the experimental facility, results of this evaluation were expressed in terms of the quantity of debris that could accumulate on the sump screen divided by the total area of the sump screen, i.e., cubic feet of fiber per unit area of screen. In the parametric evaluation, values of this ratio were generated for each of the 69 cases studied in the parametric analysis, and based on this evaluation, the following observations were made.

- For small and medium LOCAs, the quantity of fibrous debris that could accumulate on the sump screen is bounded by 1 $ft^3/ft^2$. Representative (i.e., industry-average) values for these sequences are closer to 0.05 to 0.1 $ft^3/ft^2$.

- Larger quantities of debris would be expected following large-LOCAs than small or medium LOCAs. In 64 of the 69 cases studied, the maximum estimated quantity of fibrous debris was less than 10 $ft^3/ft^2$. A representative (i.e., industry-average) value would be close to 2 to 5 $ft^3/ft^2$.

Existing debris test data have indicated that it takes a minimum quantity of debris to form a uniform layer of debris on a screen. For fine NUKON™ debris, this minimum quantity of debris would form a uniform layer ~1/8 in. thick (~0.01 $ft^3/ft^2$), but it is possible for significant head loss to occur with a layer somewhat less than 1/8in., say 1/10 in., i.e., the process is not a discontinuous step change in head loss. Without a uniform bed, portions of the screen remain exposed, allowing flow to bypass the debris.

The range of debris quantities examined in the accumulation tests was selected to span as much of this range as possible without exceeding the physical capabilities of the UNM large-flume test facility. In particular, the maximum quantity of debris that could be tested was limited by the corresponding head loss it would produce across the screen. Screen head loss is a physical limitation in the large-flume facility because the "exit tunnel" was constructed of transparent Plexiglas™ (to facilitate visualization), which could collapse if a sufficiently large vacuum were to develop within the tunnel. With these considerations in mind, experiments were performed with debris quantities over the range of 0.01 to 1 $ft^3/ft^2$.

---

[1] The NUKON™ and CalSil insulation samples used in these tests were obtained from Performance Contracting Inc. (PCI), Lenexa, Kansas.

Shredded fiberglass debris


CalSil fragments


Crumpled RMI foil

**Figure 2.3. Typical fiberglass, CalSil, and RMI debris used in the current experiments.**

### 2.2.1.4.    *Relative Quantities of CalSil Debris*

The parametric evaluation estimates of the quantities of debris that could collect on a sump screen included information regarding CalSil debris [Rao, 2002b]. The same estimates can be used to characterize the amount of CalSil that might accompany fibrous debris, i.e., the ratio of the volume of CalSil to volume of fibrous debris transported to the containment sump. This ratio was found to span an extremely wide range from nearly zero to values greater than 10. Unfortunately, the quality of information used to generate these estimates is relatively poor (e.g., specific quantities of fiber and/or CalSil were often not reported by the various PWR plants in their responses to the industry survey; rather, survey respondents often simply reported the presence or absence of each debris type). As a result, the specific numerical values of this ratio should not be given much credit. Based on experience and engineering judgment, it was decided that a reasonable representation of actual CalSil/fiber mass ratios that should be examined in these tests ranged from ~0.5 to 2.0.

### 2.2.2.  Closed-Loop Head-Loss Testing

The parameters varied during the closed-loop head-loss tests were the following:

- the screen approach velocity,
- the water temperature, and
- the type(s) and quantities of debris in the debris bed.

The screen approach velocity was varied from near zero to as high as ~2 ft/s depending on the conditions of the tests (consistent with the range from the industry survey). The maximum velocity was generally limited by the head loss across the bed of debris, i.e., when the head loss approached the limitation of the apparatus, the pump flow rate could not be further increased.

The water temperature was either at the nominal room temperature or initially heated to ~125°F.

The types of debris tested in the closed-loop facility included NUKON$^{TM}$ fiberglass insulation debris, calcium silicate insulation debris, sand-and-concrete-dust particulate, and crumpled foils from RMI insulation constructed of stainless steel. The quantities of debris are discussed in Section 2.4.2.

### 2.3.    Test Procedures

Initial or exploratory testing was used to develop suitable test procedures for the conduct of the structured tests.

### 2.3.1.  Large-Flume Debris-Accumulation Tests

The limitations in experiment conditions (i.e., debris loading and flow velocity) in terms of the structural integrity of the Plexiglas$^{TM}$ exit tunnel were determined during the exploratory testing phase. These tests were also used to establish the optimum method of establishing the flow, develop appropriate methods of introducing the debris into the flume once flow conditions were established, and refine instrumentation. The exploratory tests involved a total of 13 different experiments (labeled cases A through M) spanning a wide range of test variables. For each case, notes and photographs were taken to record the observed geometric pattern that debris assumed as it collected on the screen. Detailed results of the exploratory tests are described in Appendix B.

### 2.3.1.1.    *Major Observations and Conclusions of Exploratory Tests*

Three major observations were noted from the exploratory tests.

1.  The debris-accumulation profile that developed during each test could be described by one of three distinct categories:

- Category I [uniform]—Debris was distributed uniformly across the surface of the screen,

- Category II [bottom-skewed]—Some debris covered the entire surface of the screen, but the distribution was not uniform; most debris tended to collect on the bottom of the screen rather than at the top, or

- Category III [curb]—Debris accumulated almost entirely on flume floor where it intersected the lower edge of the screen, effectively forming a short "curb."

Although minor variations could be seen within each profile, these broad categories provided a convenient, initial description of the extent to which debris covered the screen. Example photographs and a graphical illustration of each of these patterns are shown in Figure 2.4.



| (I) Uniform | (II) Bottom-skewed | (III) Curb |
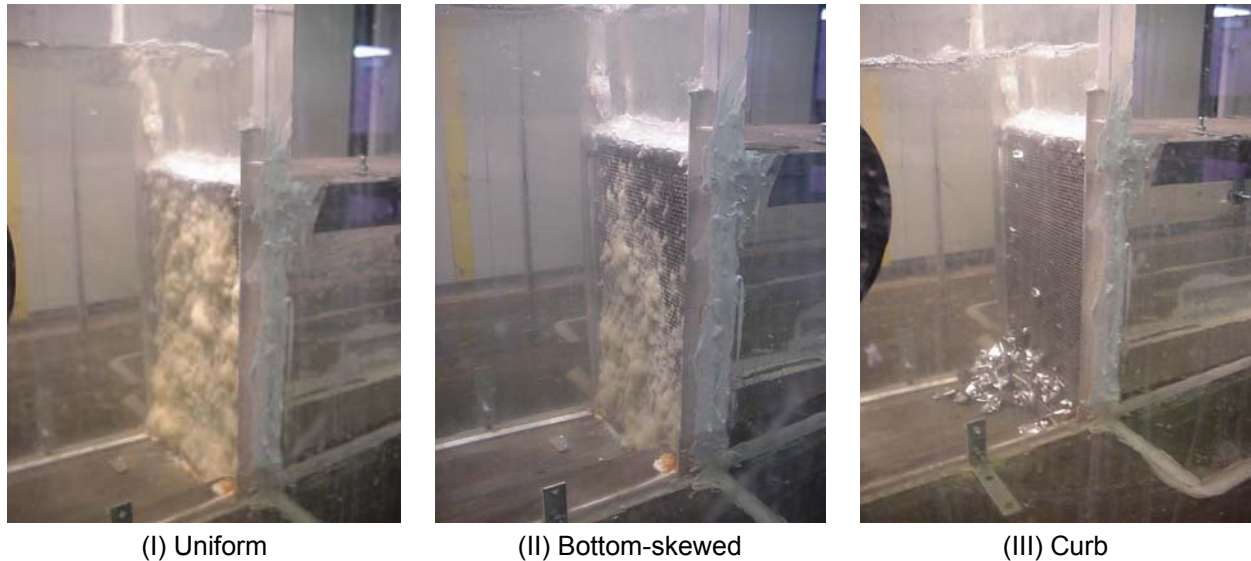
**Figure 2.4. General variations in debris-accumulation patterns observed in exploratory tests.**

2. The analog pressure gauges did not provide a convenient or accurate measurement of head loss across the screen. In subsequent testing (described in the main body of the report), these gauges were replaced with electronic pressure transducers equipped with digital readouts.

3. Large quantities of air became entrained into the flume exit tunnel during exploratory tests in which significant head losses were measured across the screen. In this case, "significant" meant greater than ~1 in. Hg (~1.1 ft of water). The source of this air was not initially discernible. However, exploratory tests conducted near the end of the exploratory phase (i.e., Tests I and K, as described in Appendix B) resulted in the formation of a large, highly turbulent, but stable air pocket along the roof of the exit tunnel. When this occurred, water and entrained air were observed to pour over the top of the edge of the debris screen through a gap between the screen and the upper edge of the exit tunnel doorway. The gap grew in size as the screen "bowed" inward due to hydraulic forces caused by debris accumulation. The flow of water through the screen itself appeared to decrease to nearly zero as the gap grew, and the flow of water over the top of the screen increased. The high velocity of water rolling over the top of the screen generated a sufficient level of turbulence in the pool above the screen that air was entrained into the flow from the free surface of the flume. In some of the exploratory tests, air was also observed to be drawn into the exit tunnel through cracks in the corners of the Plexiglas[TM] sheeting used to form the tunnel.

This observed behavior is contrary to the hydraulic conditions that would occur at a nuclear power plant, thus a pathway for water to bypass the screen is not representative of the situation being modeled. As a result, these observations led to two significant changes in the construction of the debris screen and exit tunnel:

1. The top edge of the screen was firmly mated to the upper edge of the exit tunnel doorway and sealed with silicone caulking.

2. The exit tunnel itself was disassembled and reconstructed with angle iron mounted along its corners to reinforce the walls under conditions of high head loss (i.e., vacuum within the tunnel).

After these design changes were completed, two of the exploratory tests were re-run to verify that all water drawn into the exit tunnel by the recirculation pump properly passed through the debris screen. Both tests involved a moderate quantity of NUKON™ fibers. Results of these two tests (labeled Tests L and M) are recorded in Appendix B.

A significant observation was made during these two repeated exploratory tests. The debris-accumulation profile changed from one that was primarily skewed toward the bottom of the screen to one that was very uniform. The gap at the top edge of the screen obviously caused a sufficient change in the local velocity profile in advance of the screen to alter the debris deposition pattern. All subsequent testing in the large flume was performed using the sealed debris screen.

### 2.3.2. Closed-Loop Head-Loss Testing

The initial qualifying tests for the closed-loop facility were used to refine testing procedures, as well as to show that this facility was capable of simulating head-loss results that were used to develop and validate the NUREG/CR-6224 correlation, thus the term "qualifying tests." These tests and their results are included in the main test matrix and discussed in Section 3.

Leading up to the qualifying tests, the loop was operated to check out equipment, which included the pump, flow meters, and pressure transducers. The method of introducing debris into the test section evolved from gravitational settling with the pump off to introducing the debris while the pump was at slow flow to allow the flow to more thoroughly distribute the debris. Using techniques developed in previous testing, such as the separate-effects debris transport tests, the debris was pretreated to ensure complete saturation, i.e., to eliminate all air from the debris.

In the fashion used by other researchers, once the debris bed was established, the flow velocity was incrementally increased (by adjusting the throttle valve) so that the head loss could be measured for various flow velocities for the same debris bed. The general idea was to increase the flow, then wait until the head loss became relatively stable, record the head loss and flow, and then move on to the next velocity. Once a practical maximum flow was reached, as determined by the head loss and debris bed stability, the flow was sequentially decreased with the data recorded on the descent, as well. This process is shown schematically in Figure 2.5. By measuring the head losses while decreasing the flow, as well as increasing the flow, the hysteresis effect associated with fibrous debris bed compression was examined (i.e., the failure of a debris bed to fully recover in thickness when fluid velocity is decreased after an initial period of high-velocity flow.)

### 2.4. Test Matrices

The considerations described above, along with insights from exploratory testing, led to a series of tests in the large flume and closed-loop test facility to study debris accumulation and head loss.
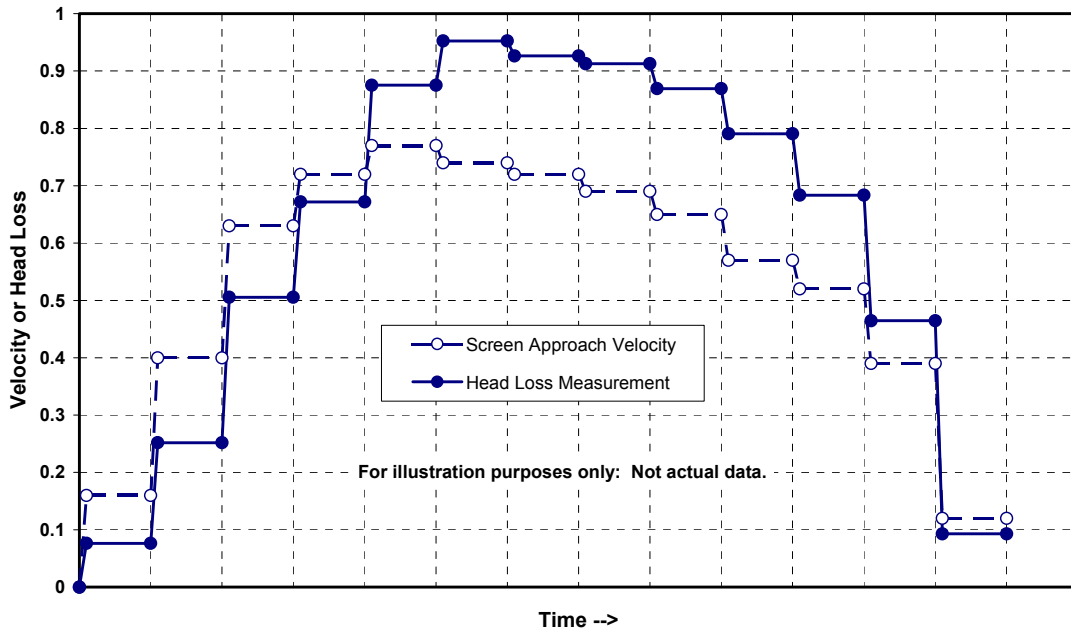
**Figure 2.5. Schematic illustration of the flow increment increase/decrease procedure.**

### 2.4.1. Large Flume Debris-Accumulation Tests

The range of specific test conditions studied in the large flume debris-accumulation tests is outlined in Table 2.1.

**Table 2.1. Test Matrix for Debris-Accumulation Tests**

| Test ID | Approach Velocity (ft/s) | | Debris Type | | | Fiber Quantity (ft³/ft²) | | CalSil/Fiber Mass Ratio | |
|---|---|---|---|---|---|---|---|---|---|
| | 0.5 | 0.9 | NUKON™ | CalSil | SS RMI | 0.023 | 0.046 | 0.5 | 1.0 |
| 1a | X | | X | | | X | | | |
| 1b | X | | X | | | | X | | |
| 1c | | X | X | | | X | | | |
| 1d | | X | X | | | | X | | |
| 2a | X | | X | X | | X | | X | |
| 2b | X | | X | X | | X | | | X |
| 2c | | X | X | X | | X | | X | |
| 3a | X | | | X | | | X | | |
| 3b | | X | | X | | | X | | |
| 4 | | X | | | X | | | | |

### 2.4.2. Closed-Loop Head-Loss Tests

The range of specific test conditions studied in the closed-loop head-loss tests is outlined in Table 2.2. These tests were grouped into four series and each series had the following primary test objectives:

- The first test series (1a through 1d) was conducted to qualify the test apparatus and procedures by performing tests where substantial data already existed, i.e., to show that the debris bed behavior of those tests could be reasonably well reproduced.

11

- The second test series (2a through 2f) was conducted to illustrate the ability of CalSil debris to accumulate and cause substantial head loss without the aid of additional fibrous debris to hold the CalSil in place on the screen and to measure those head losses.

- The third test series was conducted to measure the head loss associated with mixed beds of fibrous and CalSil debris at various bed thicknesses and particulate-to-fiber mass ratios.

- The fourth test series (5a through 5g)[2] was conducted to measure the head loss associated with mixed beds of RMI and CalSil debris at various bed thicknesses and quantities of CalSil.

**Table 2.2. Test Matrix for Debris Head-Loss Tests**

| Test ID | Water Temp | Debris Type | | | Fiber Bed Thickness* (in.) | | | CalSil/Fiber Mass Ratio | | |
|---|---|---|---|---|---|---|---|---|---|---|
| | | NUKON™ | CalSil | SS RMI | Low | Med | High | Low | Med | High |
| 1a | Room | X | | | | | 1.72 | | | |
| 1a' | Room | X | | | | 0.86 | | | N/A | |
| b | 125°F | X | | | | | 1.72 | | | |
| c | Room | X** | | | | 0.86 | | | | |
| d | Room | X** | | | | | 1.72 | | | |
| 2a | Room | | X | | 0.02 | | | | | |
| b | Room | | X | | | 0.14 | | | | |
| c | Room | | X | | | | 0.28 | | N/A | |
| d | 125°F | | X | | 0.02 | | | | | |
| e | 125°F | | X | | | 0.14 | | | | |
| f | 125°F | | X | | | | 0.28 | | | |
| 3a | Room | X | X | | 0.11 | | | 0.5 | | |
| b | Room | X | X | | 0.11 | | | | 1.0 | |
| c | Room | X | X | | 0.11 | | | | | 2.0 |
| d | Room | X | X | | | 0.86 | | 0.5 | | |
| e | Room | X | X | | | 0.86 | | | 1.0 | |
| f | Room | X | X | | | 0.86 | | | | 2.0 |
| g | Room | X | X | | | | 1.72 | 0.5 | | |
| h | Room | X | X | | | | 1.72 | | 1.0 | |
| i | Room | X | X | | | | 1.72 | | | 2.0 |
| j | 125°F | X | X | | | 0.86 | | 0.5 | | |
| k | 125°F | X | X | | | 0.86 | | | 1.0 | |
| l | 125°F | X | X | | | 0.86 | | | | 2.0 |

| Test ID | Water Temp | Debris Type | | | RMI Quantity (in.) | | CalSil Mass (g) | | |
|---|---|---|---|---|---|---|---|---|---|
| | | NUKON™ | CalSil | SS RMI | 1.0 | 10. | 10. | 20. | 50. |
| 5a | Room | | | X | X | | | | |
| b | Room | | | X | | X | | | |
| c | Room | | X | X | X | | X | | |
| d | Room | | X | X | X | | | X | |
| e | Room | | X | X | X | | | | X |
| f | Room | | X | X | | X | X | | |
| g | Room | | X | X | | X | | X | |

\* Fiber bed thickness was based on the as-manufactured insulation density.
\*\* Sand-and-concrete-dust particulate was added to the fibrous debris bed with a particulate-to-fiber mass ratio of 1.

---

[2] Test Series Four was deleted from the original matrix.

## 3. TEST RESULTS

Debris accumulation and the head-loss test results are reported in Sections 3.1 and 3.2, respectively.

### 3.1. Debris Accumulation

Debris-accumulation data were taken for low-density fiberglass (LDFG), mixtures of fiberglass and CalSil, CalSil, and RMI debris.

#### 3.1.1. Low-Density Fiberglass Insulation

Debris-accumulation Tests 1a through 1d (refer to Table 2.1) examined the debris-accumulation pattern for low-density fiberglass. Fragments of NUKON™ fiber were used to represent this broad class of insulation. Tests were conducted at the two approach velocities of 0.5 to 0.9 ft/s and at the two debris quantities of 0.023 to 0.046 ft³/ft² (i.e., theoretical bed thickness[3] of 0.29 in. and 0.58 in.), as shown in Table 3.1.

**Table 3.1. Fiber Fragment Accumulation Test Results**

| Test | Screen Approach Velocity (ft/s) | Debris Quantity (ft³/ft²) | Accumulation Pattern |
|------|------|------|------|
| 1a | 0.5 | 0.023 | Uniform |
| 1b | 0.5 | 0.046 | Uniform |
| 1c | 0.9 | 0.023 | Uniform |
| 1d | 0.9 | 0.046 | Uniform |

Photographs of the observed debris-accumulation patterns for these tests are shown in Figure 3.1. In all four cases, the accumulation pattern was relatively uniform.[4]

#### 3.1.2. Mixtures of Fiberglass and CalSil

Tests 2a through 2c examined the accumulation pattern for mixtures of low-density fiberglass and CalSil. As in Tests 1a-1d, shredded NUKON™ insulation was used to represent the broad class of fiberglass fragments. Crushed fragments of CalSil were added to flow stream (separately from the shredded fiberglass), as described in Appendix C.

All three cases involved the same quantity of fiberglass fragments (0.023 ft³/ft²). However, the approach velocity at the screen and the relative quantity of NUKON™ fiber and CalSil fragments varied, as shown in Table 3.2.

**Table 3.2. Mixed Fiber/CalSil Debris-Accumulation Test Results**

| Test | Screen Approach Velocity (ft/s) | CalSil/Fiber Mass Ratio | Accumulation Pattern |
|------|------|------|------|
| 2a | 0.5 | 0.5 | Uniform |
| 2b | 0.5 | 1.0 | Uniform |
| 2c | 0.9 | 0.5 | Uniform |

---

[3] The theoretical bed thickness is the thickness that would result if the density of the debris was that of the as-manufactured insulation. As such, it is proportional to mass per unit area.

[4] An example of very uniform debris accumulation on a vertical screen is found in the test report on the integrated debris transport tests, Figure 6-7 in NUREG/CR-6773, [Rao, 2002c]. The uniformity in this bed can be attributed to the fineness of the approaching debris, which consisted primarily of suspended fibers.

Test 1a



Test 1b



Test 1c



Test 1d

**Figure 3.1. Debris accumulation in Tests 1a through 1d.**[5]

No change in the overall accumulation pattern was observed from tests with fiberglass fragments alone; i.e., the debris mixture was uniformly distributed across the screen. The relative distribution of fiber and CalSil fragments within the mixed debris bed could not be determined precisely. However, visual observations made through the transparent walls of the flume clearly indicated the transport and

---

[5] Note: The photograph shown for Test 1c was taken before the debris had completely accumulated on the screen. This photograph provides a visual indication of the manner in which this type of debris transported to the screen from its upstream release location.

accumulation of fiber fragments was essentially uniform. A photograph of the suspended debris approaching the screen is shown in Figure 3.2(i). Visual inspection of the debris bed after the flume water was cleared of suspended material showed CalSil particles across the entire surface of the debris bed. A photograph of the final (uniform) debris bed is shown in Figure 3.2(ii).

Post-test examination of the debris bed composition was not possible in these tests because the debris bed did not remain attached to the screen when the test was terminated. When flow through the flume ceased at the end of the accumulation test (by turning off the pump), the pressure on either side of the debris bed equilibrated and the debris bed "bounced" back into the flume and collapsed as a pile of mixed debris at the base of the screen. The pile of rejected debris is shown in Figure 3.2(iii).



(i) Debris transport and accumulation on screen.



(ii) Final debris-accumulation pattern.



(iii) Pile of debris formed in front of the screen when flow through the flume was terminated.

**Figure 3.2. Debris-accumulation behavior observed in Tests 2a through 2c.**

### 3.1.3. Calcium Silicate (CalSil)

Tests 3a and 3b examined the debris-accumulation pattern for CalSil fragments alone (i.e., no base fiber or other debris for the CalSil to adhere to). The tests examined debris accumulation at two values of approach velocity; i.e., 0.5 and 0.9 ft/s. The total debris quantity in both cases was 0.023 $ft^3/ft^2$. Results are summarized in Table 3.3.

**Table 3.3. CalSil Fragment Accumulation Test Results**

| Test | Screen Approach Velocity (ft/s) | Debris Quantity $(ft^3/ft^2)$ | Accumulation Pattern |
|------|------|------|------|
| 3a | 0.5 | 0.023 | Nonuniform, bottom-skewed |
| 3b | 0.9 | 0.023 | Nonuniform, bottom-skewed |

In both cases, the accumulation pattern was thin, nonuniform, and highly skewed toward the bottom of the screen. Photographs of the observed debris-accumulation patterns for these tests are shown in Figure 3.3. Although sufficient CalSil material was added to the flume to form a bed with a theoretical thickness slightly greater than 1/4 in., relatively little material actually accumulated on the screen. As shown in the photographs in Figure 3.3, larger pieces of CalSil fragments collected in patches near the bottom of the screen, but most of the suspended material passed through the 1/8-in. webbing of the screen. Because the large flume was operated in a recirculation configuration, suspended CalSil fragments were provided several opportunities to pass through the screen. After several min of operation, however, debris did not appear to accumulate further and the tests were terminated.

### 3.1.4. Reflective Metal Insulation (RMI)

Test 4 examined the debris-accumulation pattern for crumpled foils of stainless-steel RMI. Accumulation of this type of debris was tested at one approach velocity (0.9 ft/s). Lower values would not be sufficient to transport the debris to the screen;[6] higher values were not achievable in the current UNM flume configuration. The total debris quantity added to the flume (695 g) was sufficient to generate a debris bed with a theoretical thickness of ~2.5 in.

When the entire quantity of debris was released into the flume as a coherent mass, the entire mass slid along the bottom of the flume and stopped near the base of the screen (see left-hand side of Figure 3.4). Individual pieces of debris slowly piled up near the base of the screen in a pattern similar to the "curb" geometry described earlier. Over time (several min), a few pieces of debris climbed over the curb and covered a debris-free portion of the screen. However, large sections of the screen remained free of debris until the end of the test.

This test was then repeated, but the debris was released gradually into the flume. In this case, the foils transported as individual debris fragments or in small clumps. Again, the debris initially stopped near the base of the screen. However, as more debris arrived, new pieces rolled over pieces that had arrived earlier. Gradually, the screen surface area was covered with foils—with the accumulation developing from the bottom upward. As shown in the photograph on the right-hand side of Figure 3.4, the entire screen eventually was covered with at least some amount of debris. However, the final debris-accumulation pattern was nonuniform (i.e., bottom-skewed). Variations in the depth of the debris bed with height could not be measured precisely. However, visual estimates indicated the depth at the top of the screen was ~1 in., which corresponded to the depth of 1 or 2 crumpled RMI foils. Near the bottom of the screen, the depth was ~6 in. (i.e., roughly half of the total debris mass rested at the bottom of the screen.)

---

[6]  Based on data collected in earlier tests conducted in the UNM large flume [Rao, 2002a].

Test 3a

Test 3b

**Figure 3.3. Debris accumulation in Tests 3a and 3b.**



Test 4 (top view during transport)

Test 4 (final accumulation profile)

**Figure 3.4. Debris accumulation in Test 4.**

## 3.2.    Head Loss

The head-loss tests were conducted in the closed-loop facility.

### 3.2.1.  Low-Density Fiberglass Debris

Tests 1a-1d measured head loss across a debris bed consisting of fiberglass insulation fragments. Head loss for this type of debris has been studied extensively.[7] In the current study, Tests 1a through 1d established a technical basis for comparing measurements made in the UNM facility with measurements made in other facilities in previous studies. The current tests also provide a basis for comparing measurements with contemporary correlations of head loss; e.g., the correlation published in NUREG/CR-6224 and validated for fiber beds in NUREG/CR-6367. Comparisons of current measurements with other published data and with the NUREG/CR-6224 correlation are described in Chapter 4 of this report.

The first two tests measured head loss across a NUKON™ fiber bed, and the difference between Tests 1a and 1b was the temperature of water passing through the debris bed (72°F vs. 125°F). Test 1b was run three times to examine variance in measured results for the same test conditions. Results for these two tests are shown in Figure 3.5. Individual data points are tabulated in Appendix B.

Data collected from the three trials of Test 1b (125°F) show reasonably good repeatability.[8] Further, measured head loss for a given approach velocity with 125°F water is consistently lower than head loss at 72°F. This observation is consistent with earlier analysis of the hydraulic performance of fibrous debris beds and is explained primarily by the decrease in dynamic viscosity with increasing temperature (a factor of ~1.8 lower at 125°F than 72°F).
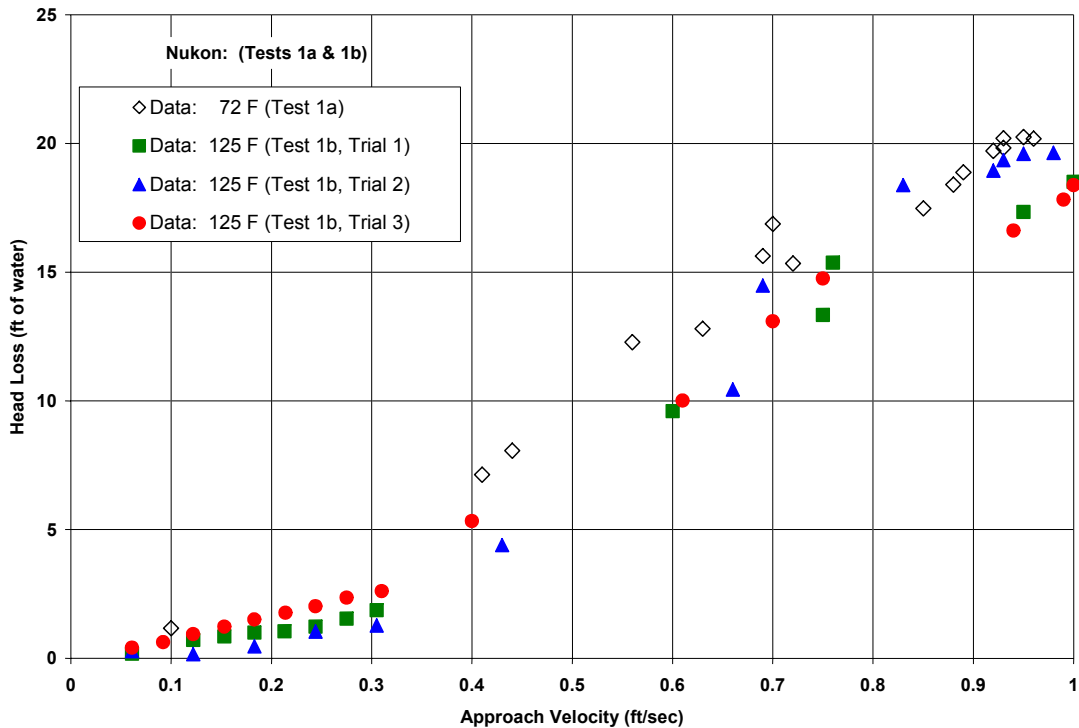


**Figure 3.5. Measured head loss for NUKON™ fiber bed at two temperatures.**

---

[7]   A detailed review of prior head-loss testing for fiber-based debris beds can be found in the Knowledge Base Report [Rao, 2003, Section 7].

[8]   Applying a simple second-order polynomial fit to these data ($y = ax + bx^2$) produces a value of $R^2$ of 0.97.

To further qualify the UNM facility, Test 1a was repeated as Test 1a' with roughly half the amount of fiber, reducing the theoretical bed thickness from ~1.72 to 0.86 in. The test data for Tests 1a and 1a' are compared in Figure 3.6, and the dashed lines in the figure indicate the order in which the data were taken, i.e., the data taken as the velocity were incrementally increased vs. when the velocity was incrementally decreased. The decreasing curves for both tests were somewhat higher than the increasing curves. This behavior is the typical compression hysteresis behavior, i.e., the bed does not expand as readily as it was compressed by the flow.
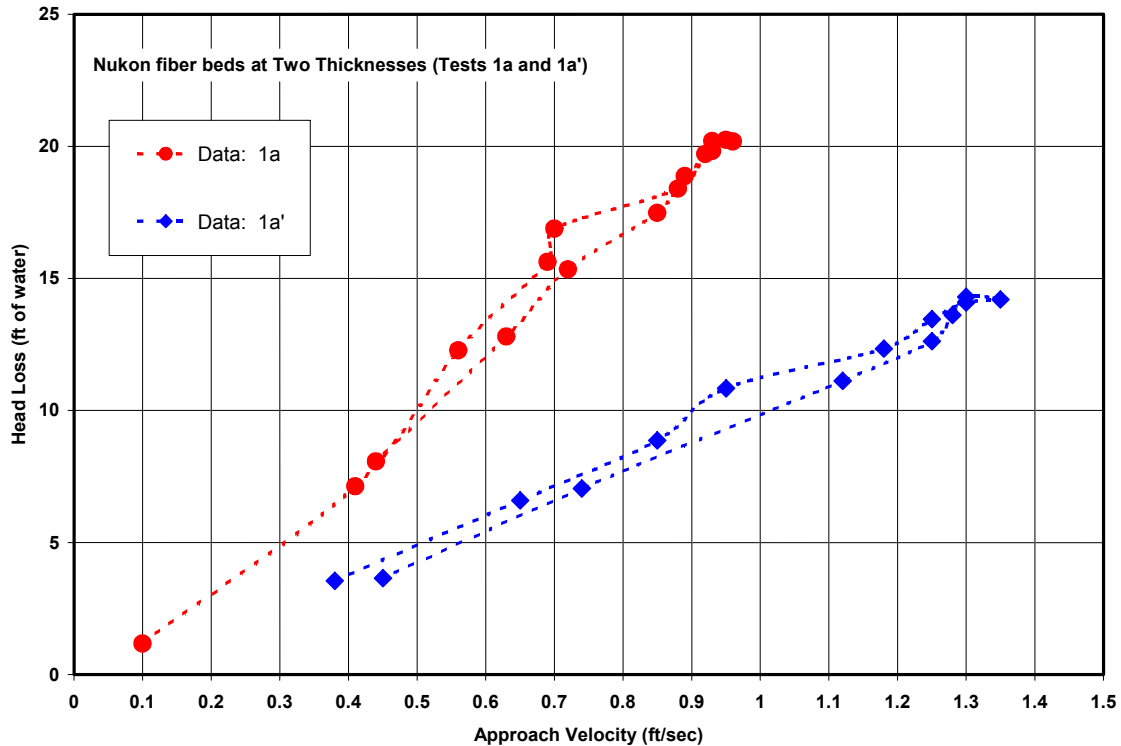


**Figure 3.6. Measured fiber bed head loss at two thicknesses (72°F).**

Tests 1c and 1d were conducted using a sand-and-concrete-dust particulate mixed in with the NUKON™ fibrous debris. Previous testing used to validate the NUREG/CR-6224 correlation [Rao, 1996] was performed using principally iron oxide (rust) particulate that accumulates in the suppression pool of a BWR reactor. For PWRs, the principal particulate is likely the common dirt and dust washed down from the containment, but it can also be particulate from such materials as paint and concrete erosion. Because the characteristics of the PWR containment materials have not been determined, a surrogate particulate was used in Tests 1c and 1d. This surrogate particulate was obtained by collecting dirt and dust from the floor of the Concrete Laboratory at UNM; sifting the particulate through a series of sieves with differing sizes (2 mm, 250 micron, 160 micron and 75 micron); and combining its constitutes by taking equal amounts (by mass) of material from each of these size classes. Both tests involved a mass ratio of particulate to fiber of one but with different quantities of fiber.

The head-loss data for Tests 1c and 1d are shown in Figure 3.7. The arrows shown in Figure 3.7 indicate the sequence of head-loss measurements as flow through the test facility was increased, then decreased. On the surface, this behavior appears to be a hysteresis effect, but it is not hysteresis behavior. When the flow velocity is first decreased from its maximum value in each test, the head loss increased significantly. Since there is no phenomenological reason for the head loss to increase with a velocity decrease for a given debris bed configuration, it appears that the debris bed was altered with the flow reduction. The debris bed must have become more uniform, and therefore the higher head losses associated with the

decreasing velocity are more valid than the head losses associated with the increasing velocity. This type of behavior is also seen in several of the NUKON™/CalSil tests.
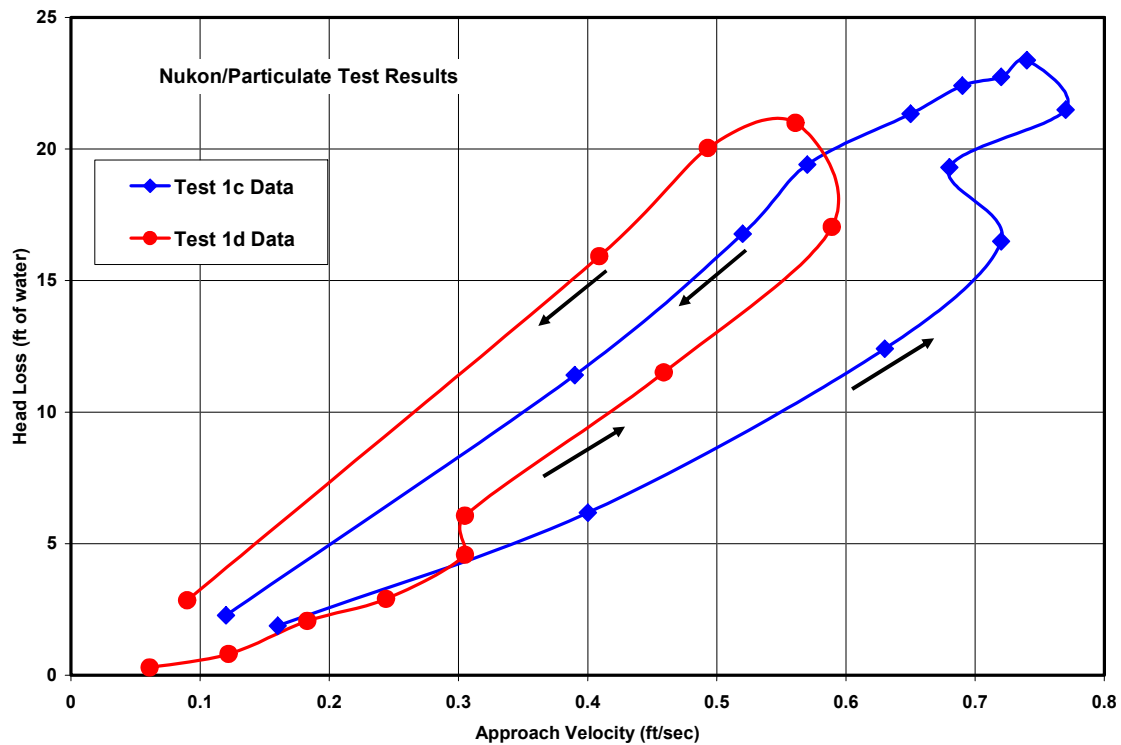


**Figure 3.7.  Measured head loss for NUKON™ fiber bed with particulate for two fiber bed thicknesses.**

### 3.2.2.  Calcium Silicate (CalSil)

Head-loss Tests 2a through 2f were conducted with debris beds of CalSil only. Tests were conducted at three debris loadings[9] and at two temperatures. The three debris loadings were 7.2, 58, and 116 g of CalSil, which resulted in a theoretical bed thickness of 0.02, 0.14, and 0.28 in., respectively.[10] The temperatures included room temperature water and water heated to 125°F. The test results are shown in Figure 3.8. Photographs of the debris beds from Tests 2b and 2c are shown in Figure 3.9. Head-loss measurements with room temperature water were made using the sequential increase and subsequent decrease in approach velocity, but at the higher temperature, the velocities were only incrementally increased.

Significant head loss was measured for all the CalSil debris beds formed on the 1/8-in.-mesh screen, even the thinnest bed with a theoretical bed thickness of only ~0.02 in. However, a significant fraction of the screen area was effectively uncovered, as seen in Figure 3.9. Therefore, it must be concluded that higher head losses would have occurred if the bed had been truly uniform. If the CalSil had been totally pulverized before insertion into the test, its accumulation would likely have been less than shown in these tests where the debris was not completely turned into fine particulate.

---

[9]  The term loading, as used here, refers the quantity of a particular debris on the test screen. At times, the loading may be given as quantity per unit area.

[10]  Thicknesses were calculated using a representative value for the as-manufactured density of CalSil of 14.5 lbm/ft$^3$ obtained from the spec-sheet for a high-temperature molded CalSil pipe insulation found on the Johns-Manville internet site.
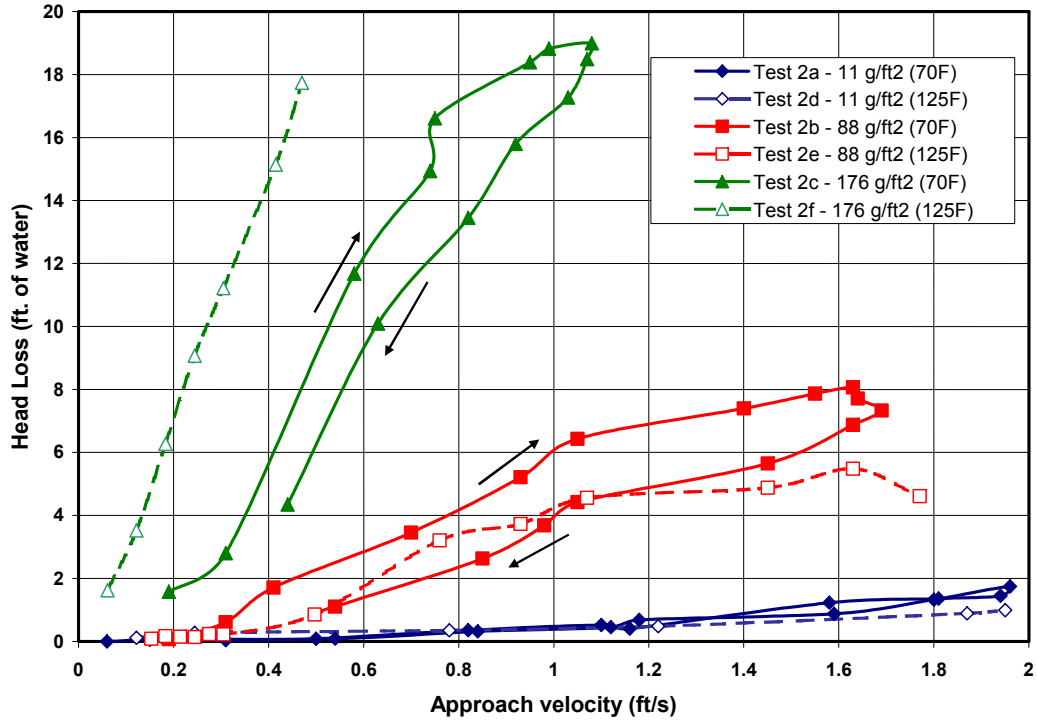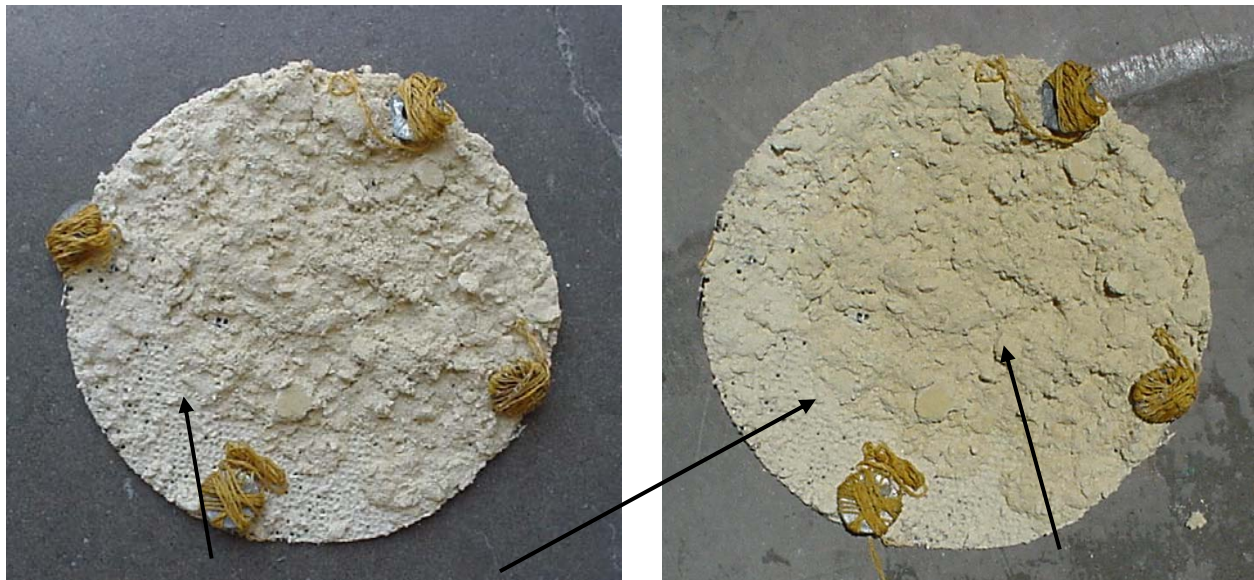
**Figure 3.8. Head-loss measurements for three different quantities of CalSil at two different water temperatures.**



Test 2b. Screen visible through debris

Test 2c. Agglomerated clumps of CalSil resin

**Figure 3.9. CalSil debris bed formed in Tests 2b and 2c.**

The return cycle on the room temperature water tests has the appearance of a reverse hysteresis effect, i.e., the head losses were somewhat less when the flow velocity was being decreased than when the velocity was increasing. The reasons for this behavior are not clear, but the effect is not compression hysteresis. It may be possible that the debris bed was disturbed and subsequently shifted into a less uniform configuration so that its resistance to flow was lessened.

The temperature affected the head loss in two ways. First, the water viscosity decreased with temperature, thereby also decreasing the head loss. Second, the dissolution or disintegration of CalSil is enhanced by temperature, which was clearly demonstrated during the separate-effect debris characterization tests [Rao, 2002a]. Therefore, it should be expected that the lumps of CalSil will more readily disintegrate in the higher temperature test and subsequently form a more uniform bed. At the highest debris loading (116 g), the head loss for the heated water test was substantially higher than for the cold water test, yet the viscosity associated with the heated water was approximately half that of the room temperature water. It is likely that the CalSil in Test 2f (125°F and 116 g) disintegrated substantially more than the CalSil in Test 2c (room temperature and 116 g) and that this disintegration reconfigured the debris bed into a more uniform bed with a resultant higher head loss. The quality of this data was affected by debris bed uniformity concerns. In addition, the filtration of the CalSil from the flow stream was somewhat problematic, in that an incomplete debris bed would not completely filter the CalSil from the flow; thus, the true quantity of CalSil in the debris bed was less than the quantity introduced into the test.

### 3.2.3. Mixtures of Fiberglass and CalSil

The hydraulic behavior of mixtures of fiberglass and CalSil debris were examined in a series of tests labeled Tests 3a through 3l (see Table 2.2). This series examined a range of debris bed thickness, varied the relative amount of fiberglass and CalSil fragments, and considered two different water temperatures. In each case, head loss was measured over a range of approach velocities.

#### 3.2.3.1. Room Temperature Tests

The results of Tests 3a through 3c conducted with debris beds of mixed NUKON™ and CalSil and room temperature water are shown in Figure 3.10; Test 3d through 3f in Figure 3.11; and Tests 3g through 3i in Figure 3.12. Photographs of the debris beds for tests 3a, 3b, and 3c are shown in Figure 3.13. Three loadings of NUKON™ debris (7.2, 58, and 116 g), resulting in three bed thicknesses, were each tested with three different CalSil loadings such that the particulate-to-fiber mass ratios were 0.5, 1.0, and 2.0, thus nine tests. Some of the tests were repeated.

The addition of CalSil to a fiberglass debris bed clearly resulted in substantial increases in the head loss over the head loss associated with the fibers alone. These test results, as a whole, illustrated some rather complex and somewhat erratic behavior on the head-loss measurements.

- In some tests, head loss increased as the flow velocity was decreased (e.g., Test 3i).

- The head losses associated with the incremental velocity decreases were generally much larger than the head losses associated with the incremental velocity increases; much more than can be explained as a hysteresis effect (e.g., Test 3h).

- Repeated tests generally poorly replicated the original test (e.g., Test 3e).

The erratic behavior associated with these tests is likely due to transient debris bed behavior as the lumps of CalSil disassociate or disintegrate due to soaking in the water along with flow turbulence. Disintegrated CalSil subsequently deposited in the bed again, whereby the bed tended to become more uniform, thus incurring increased head loss. The poor repeatability also indicates initially uneven debris where the unevenness of the original and repeat were substantially different. In addition, the filtration of the CalSil from the flow stream was somewhat problematic, in that under certain conditions, the CalSil was not completely filtered from the flow; thus, the true quantity of CalSil in the debris bed was less than the quantity introduced into the test. The filtration efficiency appeared to increase with bed compression, i.e., bed compression reduced the interfiber spacing, resulting in greater entrapment of the CalSil particulate.
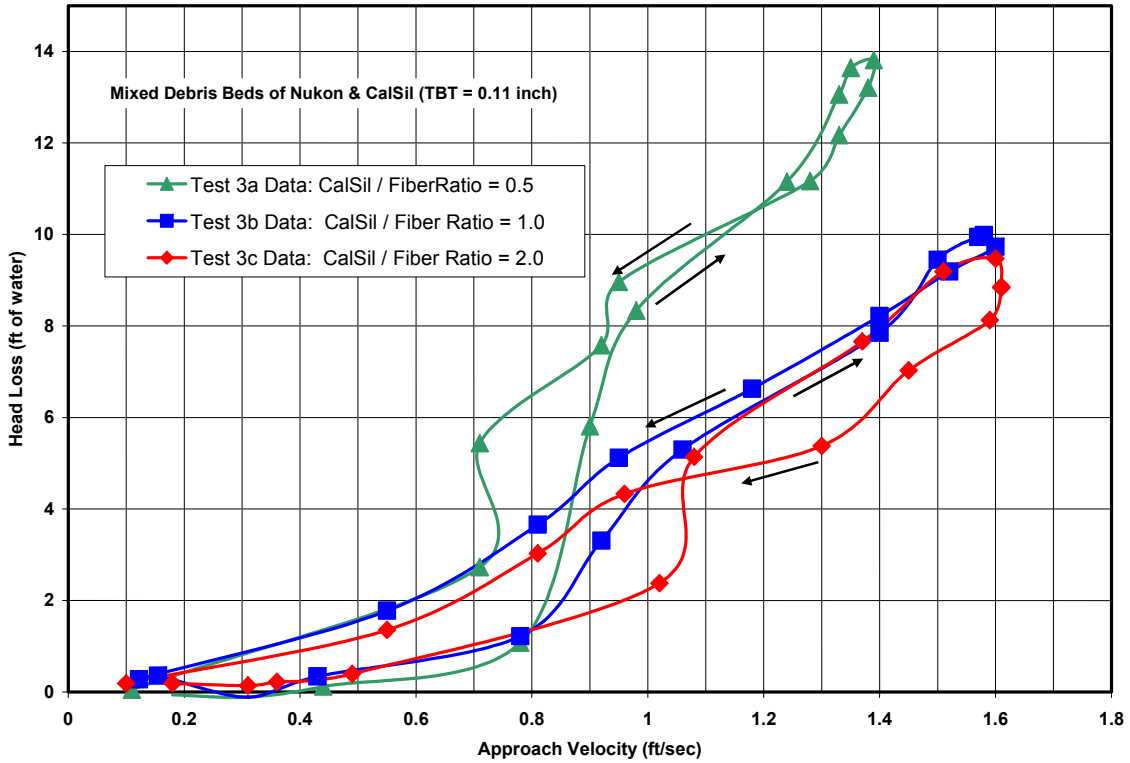
**Figure 3.10. Head-loss measurements for CalSil/fiber debris mixtures: Tests 3a, 3b, and 3c.**
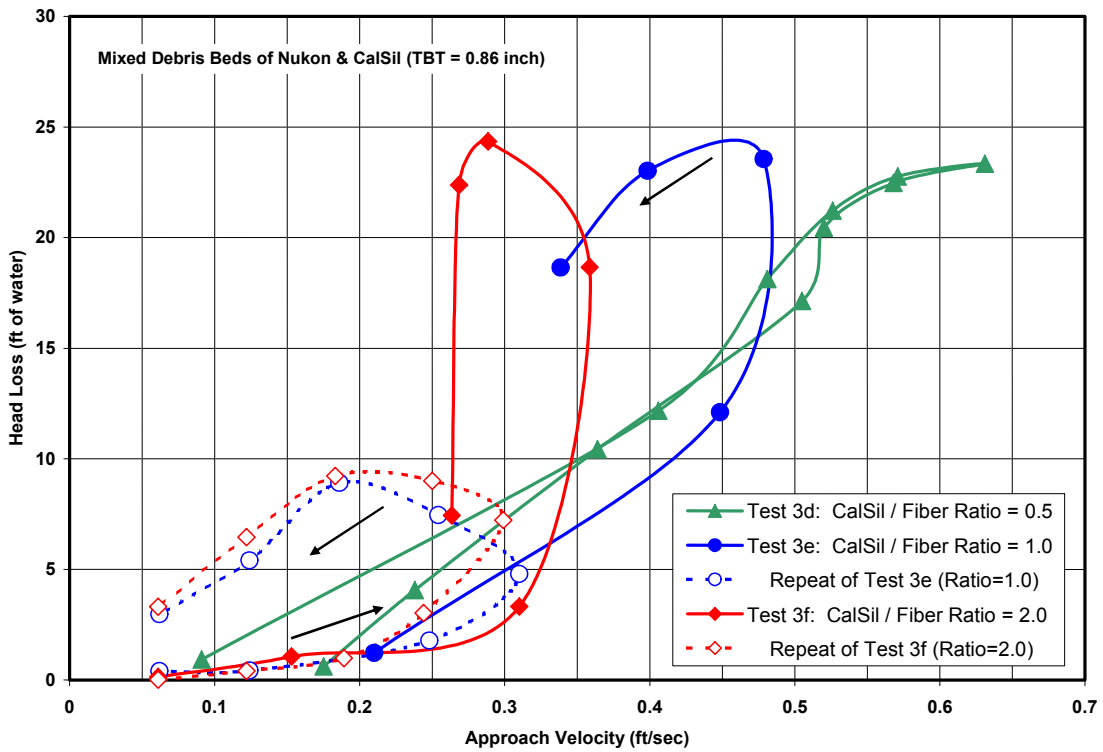


**Figure 3.11. Head-loss measurements for CalSil/fiber debris mixtures: Tests 3d, 3e, and 3f.**

23
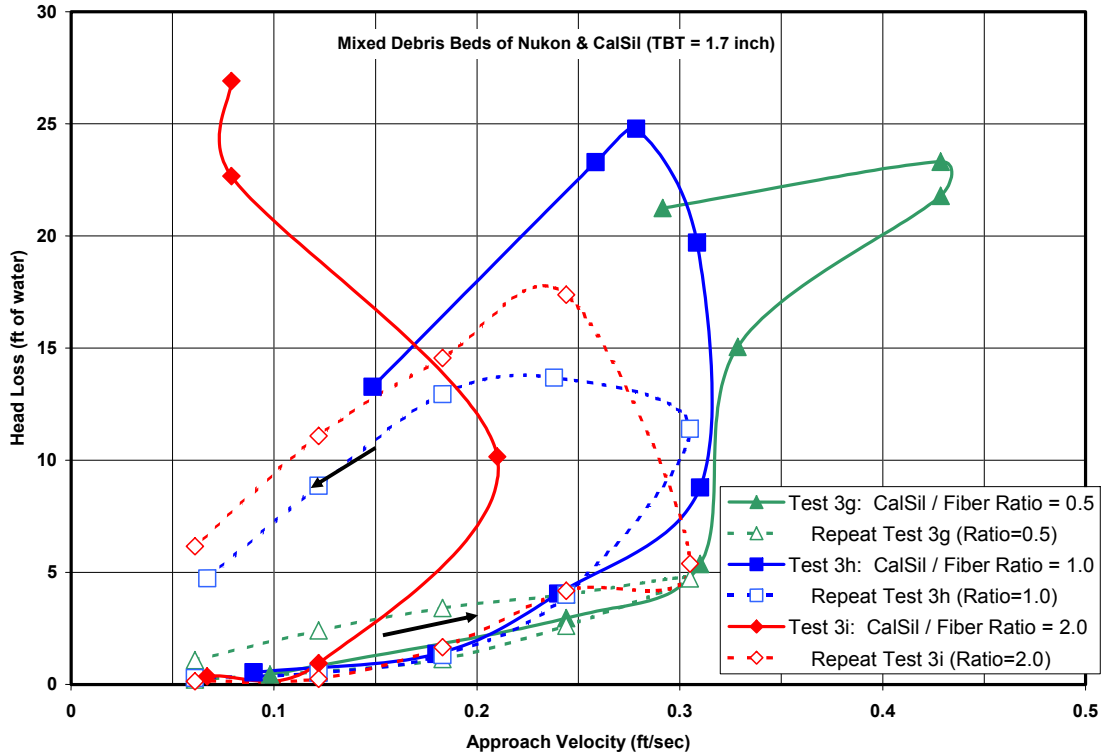
**Figure 3.12. Head-loss measurements for CalSil/fiber debris mixtures: Tests 3g, 3h, and 3i.**



| Test 3a | Test 3b | Test 3c |

**Figure 3.13. Post-test debris distribution on horizontal screens in thin-bed mixed debris Tests 3a-c.**

### 3.2.3.2.  Heated Water Tests

Tests 3j through 3l were conducted using water heated to a nominal temperature of 125°F to examine the effect of water temperature on head loss. The temperature affected the head loss in two ways. First, the water viscosity decreases with temperature, thereby also decreasing the head loss. Second, the dissolution or disintegration of CalSil is enhanced by temperature, which was clearly demonstrated during the separate-effect debris characterization tests [Rao, 2002a]. Therefore, it should be expected that the lumps of CalSil will more readily disintegrate in the higher temperature test and subsequently form a more uniform bed. A comparison of the data from these tests is shown in Figure 3.14.

**Figure 3.14. Head-loss measurements for CalSil/fiber debris mixtures: Tests 3j, 3k, and 3l.**

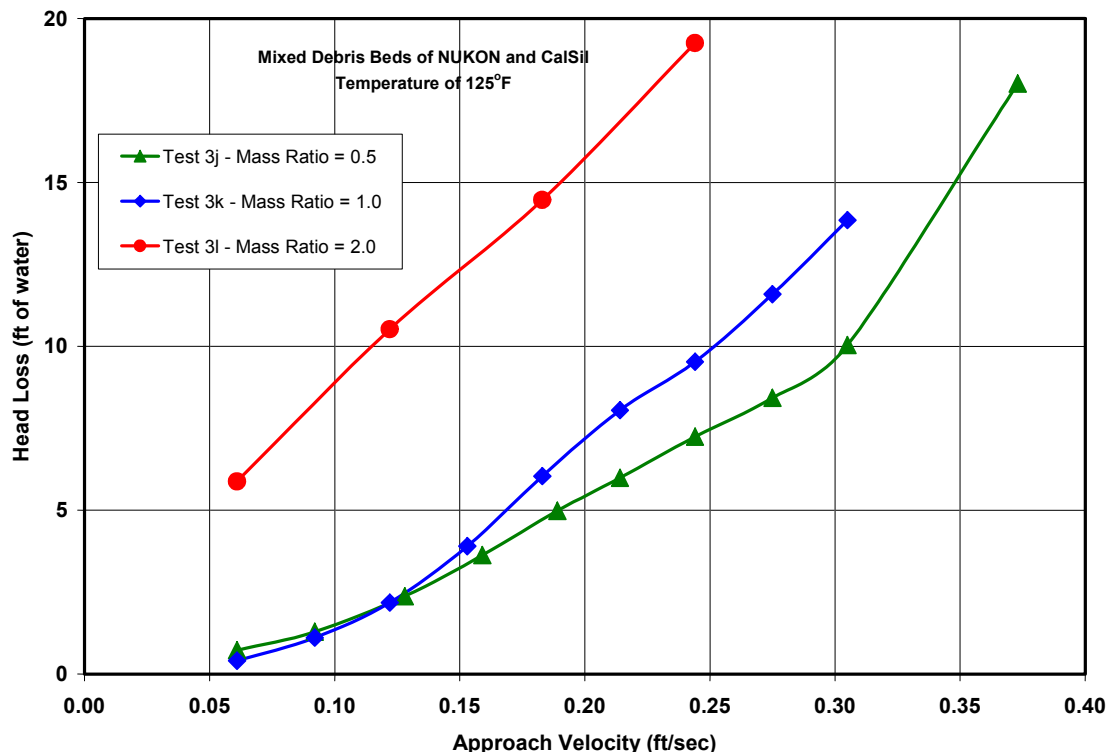At first glance, temperature did not appear to have substantial effect on the head loss, as illustrated in the comparison of the data from Tests 3d and 3j shown in Figure 3.15. Both tests used 58 g of NUKON™ and 29 g of CalSil, and the only test parameter difference was the temperature. Test 3d should have had the higher head loss because the viscosity of its room temperature water was nearly twice that of Test 3j, which used water heated to ~125°F. However, the head losses for Test 3j were somewhat higher than the head losses for Test 3d. This implies that something more than viscosity caused a difference in the test data between the two tests; a likely explanation is that the higher temperature of Test 3j enhanced the disintegration of the CalSil, thereby creating a more uniform debris bed with its correspondingly higher head loss. Thus, the effect of disintegration was more significant than the effect of viscosity, and the head losses for Test 3j were higher than for Test 3d. The quality of the test data seemed to have improved with temperature.

### 3.2.3.3. *Head-Loss Measurements across a Vertical Screen*

Although the primary objective of tests performed in the large flume was to characterize debris-accumulation patterns on a vertically oriented screen (with horizontal transport of debris), head loss was also measured in some tests. The pressure transducers used above and below the debris screen in the closed-loop (head-loss measurement) tests were installed immediately upstream and downstream of the vertical screen in the flume. Flow rate (approach velocity) was fixed at a constant value, and pressure measurements were recorded as the debris bed developed.

Results of these measurements are shown in Figure 3.16 for accumulation Tests 2a through 2c from the flume test matrix (refer to Table 2.1). These tests involved a base fiber bed with a theoretical bed thickness of 0.276 in. and CalSil with a mass ratio to fiber of 0.5. This bed thickness lies between those examined in the closed-loop facility, making a direct comparison of results between the two facilities difficult. Two of the tests were performed with a constant approach velocity of 0.5 ft/s; the third test was performed at 0.9 ft/s. Tests 2b and 2c were terminated 2-1/2 and 3 min after initial debris accumulation, respectively, to prevent the Plexiglas™ exit tunnel from collapsing due to the reduced internal pressure created by high head losses.
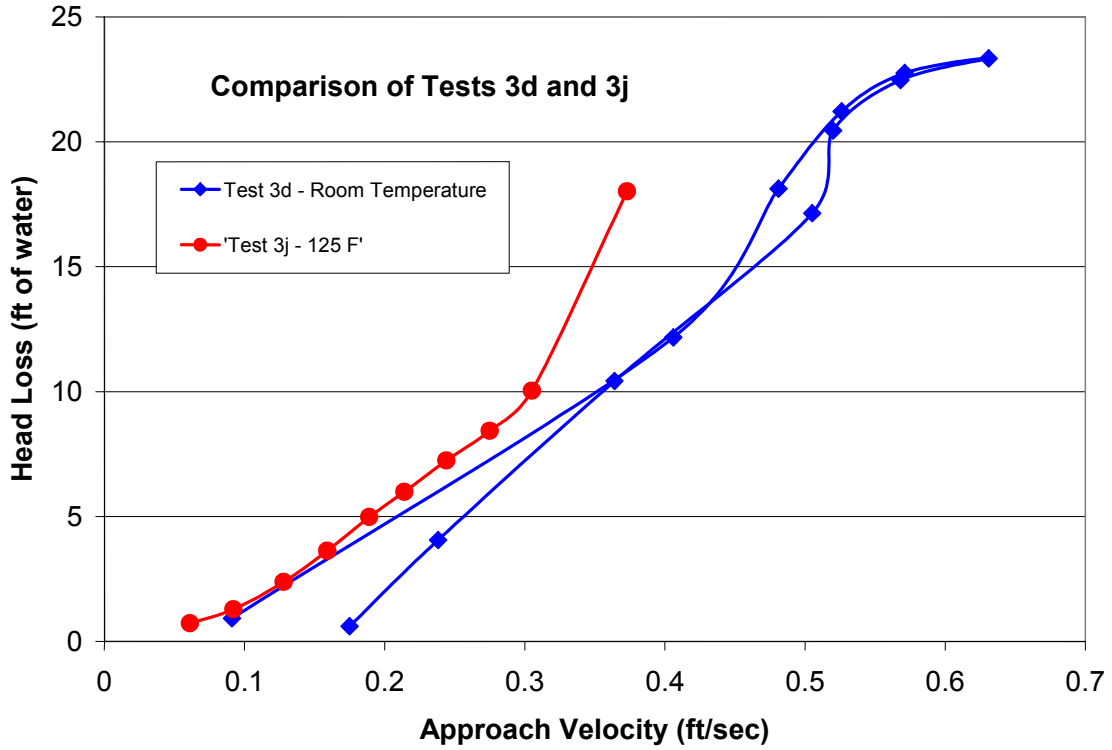
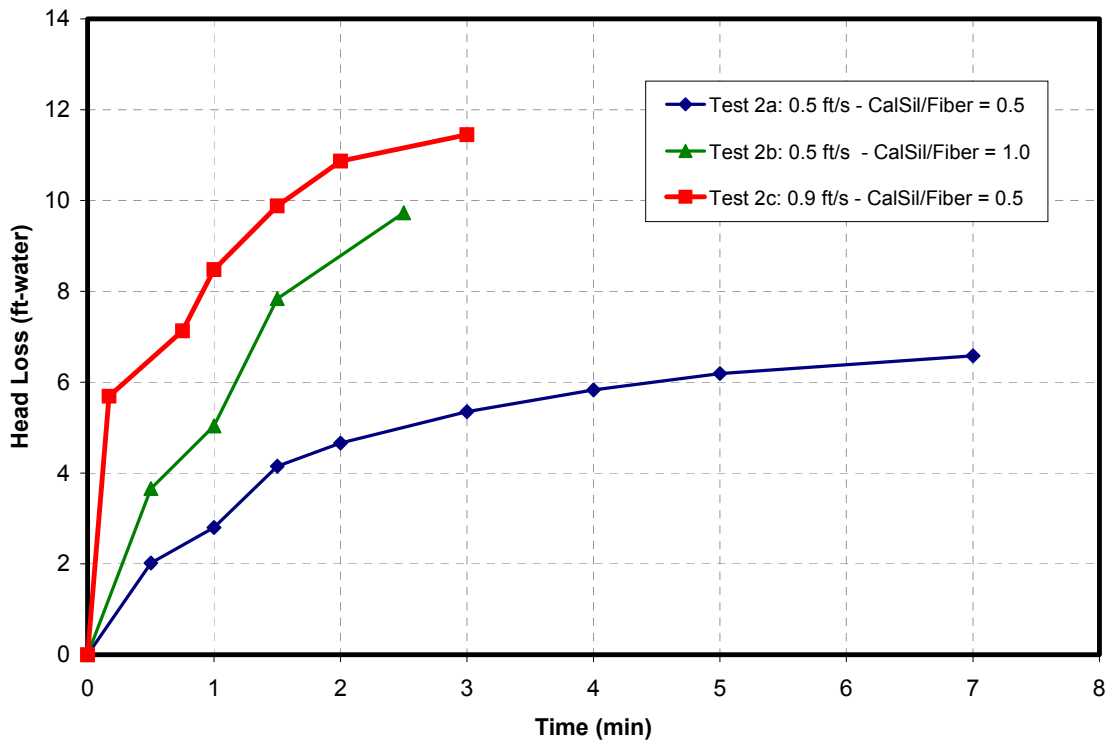**Figure 3.15. Comparison of Tests 3d and 3j head-loss measurements.**



**Figure 3.16. Time-dependent head-loss measurements during debris-accumulation Tests 2a–2c.**

### *3.2.3.4.  Physical Behavior of the Mixed Bed*

Various aspects of the physical behavior of a mixed bed of fiber and CalSil were also of interest in the current experiments. Before the experiments, several questions had been raised regarding how the bed responds to persistent hydraulic stress, such as

- does a debris bed with significant quantities of CalSil physically compress during high-flow conditions?

- does the particulate matter in CalSil remain adhered to the fiber bed or does it erode and escape the bed? and

- how do the CalSil resin and other particulate distribute themselves within a base fibrous-debris bed?

The following observations were made during the mixed bed tests, which shed some light on these and perhaps other questions.

1.  The minimum quantity of fiberglass debris (7.3 g of NUKON™) used in the mixed bed experiments corresponded to a theoretical bed thickness for the fiber of ~0.11 in. Previous studies concluded that a theoretical bed thickness of ~0.125 in. was the minimum needed to generate a fibrous debris bed of sufficient thickness, uniformly distributed, for the models inherent in the NUREG/CR-6224 correlation to be valid. For example, considerations of particle filtration in a fiber bed are rooted in assumptions related to filtration efficiency, which in turn assume a uniform porous bed medium. However, the actual distribution of debris in Tests 3a through 3c was not uniform. Post-test photographs of the debris screen (removed from the closed loop) in Figure 3.13 clearly indicate a scattered distribution of material; a significant portion of the screen is visible through the debris in all three cases.

2.  Nonuniform coverage of the screen likely explains why data trends from these tests are not consistent throughout the testing. However, it is important to note that these "open" portions of the screen were not visible during the test itself. Rather, the debris appeared to cover nearly the entire surface of the screen. The discrepancy between the visual appearance of the debris during and after the test could be caused by a significant loss of CalSil from the debris bed at the conclusion of the test. When flow through the loop was terminated after the final head-loss measurement, a white suspension was released into the water from the debris bed; it is assumed that this suspension was CalSil particulate and possible small fine binding fibers. The "open" areas of the screen shown in Figure 3.13 could therefore be the result of debris ejection after the test. Although some debris ejection was also observed at the conclusion of tests with larger quantities of debris, it had a negligible effect on debris coverage of the screen (based solely on visual observations.)

3.  Post-test examination of debris beds developed in tests with a fiber bed thickness of 0.86 or 1.72 in. (Tests 3d-3l), revealed CalSil fragments dispersed through the base fiber bed. This is partially because the method by which debris was introduced to the head-loss apparatus allowed the debris constituents to commingle in the column of water above the screen and gradually settle together. CalSil fragments (both small and larger pieces) were visible as "inclusions" in a web of tightly woven fiber. A typical cross section of a deep, mixed bed is shown in Figure 3.17.
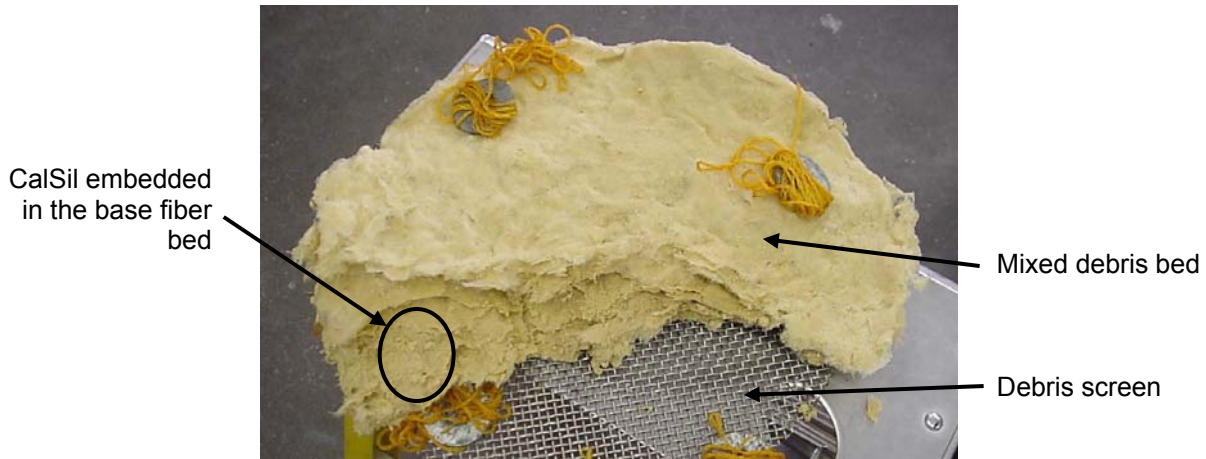
**Figure 3.17. Cross section of a 2-in.-thick mixed bed of CalSil and fiberglass debris.**

4.  Physical changes occurred in mixed debris bed(s) during several experiments when head loss exceeded ~10 ft-$H_2O$. The texture of the top surface of the debris bed, which initially was smooth and 'wavy' in appearance, took on a sharper, rugged look, with clearly defined lumps and depressions. As flow and head loss increased, a few of the depressions suddenly collapsed and small holes appeared to puncture through the debris bed. The number and location of these holes changed with time; as some appeared, others vanished. Disintegration of a piece of CalSil could be a factor. An example of these perforations in the debris bed is shown in Figure 3.18, which shows the (post-test) appearance of the debris bed in Test 3k. The effect of these holes in the debris bed was not obvious during the experiment. Head loss (or more precisely, the pressure readings above and below the screen) fluctuated by as much as $\pm$ 50% before and after the holes formed in the bed.

5.  Bubbles spontaneously formed beneath (downstream) the debris screen during experiments conducted with heated water (nominally 125°F) when the head loss exceeded ~10 ft-$H_2O$. The number of bubbles increased during each subsequent step in velocity and corresponding rise in head loss. A photograph of the bubble swarm that formed in Test 3j when the flow rate reached 0.25 ft/s is shown in Figure 3.19.

    The cause or source of these bubbles is believed to be de-aeration of water flowing through the closed test loop due to the reduced pressure immediately below the debris screen. The temperature of the heated water was sufficiently below saturation to preclude vapor (steam) formation by simple thermodynamic considerations. The water used in the "high-temperature" tests was drawn from a pair of standard, domestic hot-water heaters that maintain water at ~130°F and are pressurized to a maximum of 10 in.-$H_2O$ (gauge). The heaters are filled with tap water from the UNM general (potable) water supply. If this water is assumed to be fully saturated with dissolved air, a simple application of Henry's Law suggests that ~1 liter of air would be released from the water due to a 10 ft-$H_2O$ (~ 5psi) reduction in pressure.

    Bubble formation below the screen did not appear to adversely affect the measured head loss across the debris bed, provided that water velocity was maintained below values that would sweep bubbles into the closed-loop flow stream. Due to the relatively low flow velocities through the closed loop (i.e., less than 1 ft/s) and the long vertical distance between the debris screen and the return leg of the loop piping, the bubbles were not swept downward into the return flow leg of the test loop and generally remained suspended below the screen.
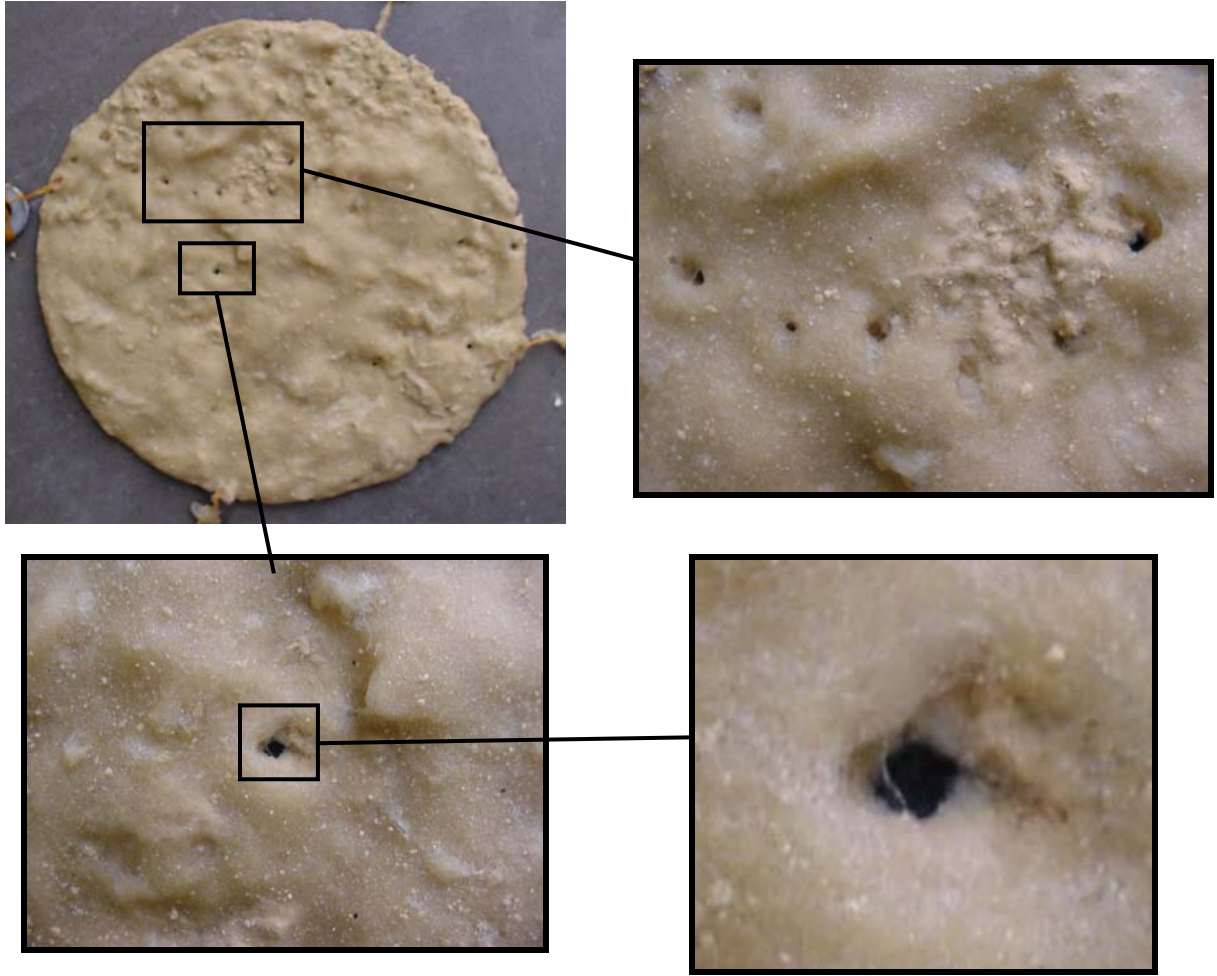
**Figure 3.18. Surface morphology of mixed CalSil/fiber debris beds after experiencing high head loss (Test 3k).**



← Debris screen

Bubbles dispersed in downstream water

Flow direction
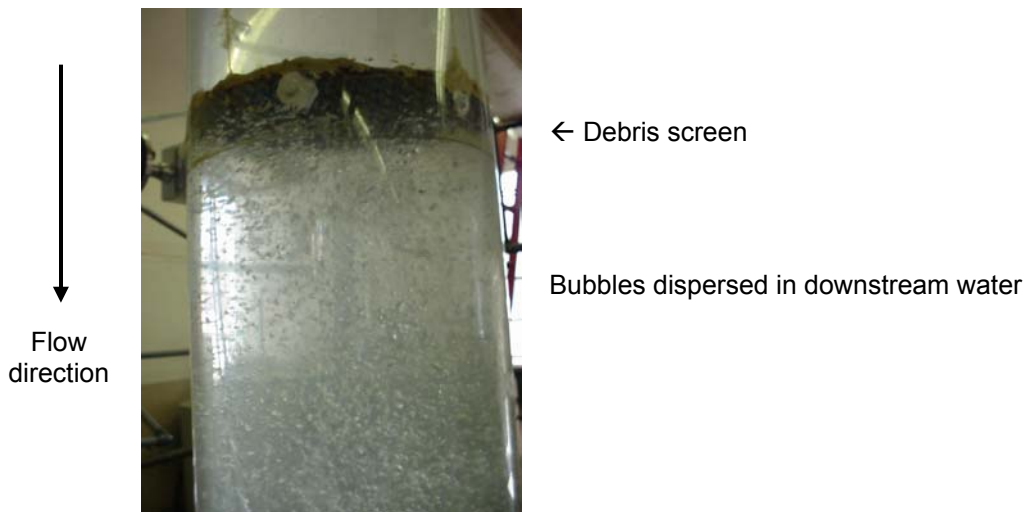
**Figure 3.19. Bubbles form beneath the debris screen at 0.25 ft/s in Test 3j (head loss ~10 ft-H₂O).**

### 3.2.4.  Reflective Metal Insulation (RMI)

Tests 5a and 5b establish a baseline of head-loss data for crumpled stainless-steel RMI foil. The baseline data allow the incremental effects of CalSil to be examined in Tests 5c through 5g; the latter are described in Section 3.2.5. The baseline data were collected for debris beds with an uncompressed thickness of 1 in. (Test 5a) and 8 in. (Test 5b.) Photographs of the two baseline debris beds are shown in Figure 3.20 (before testing). Head-loss measurements are shown in Figure 3.21.
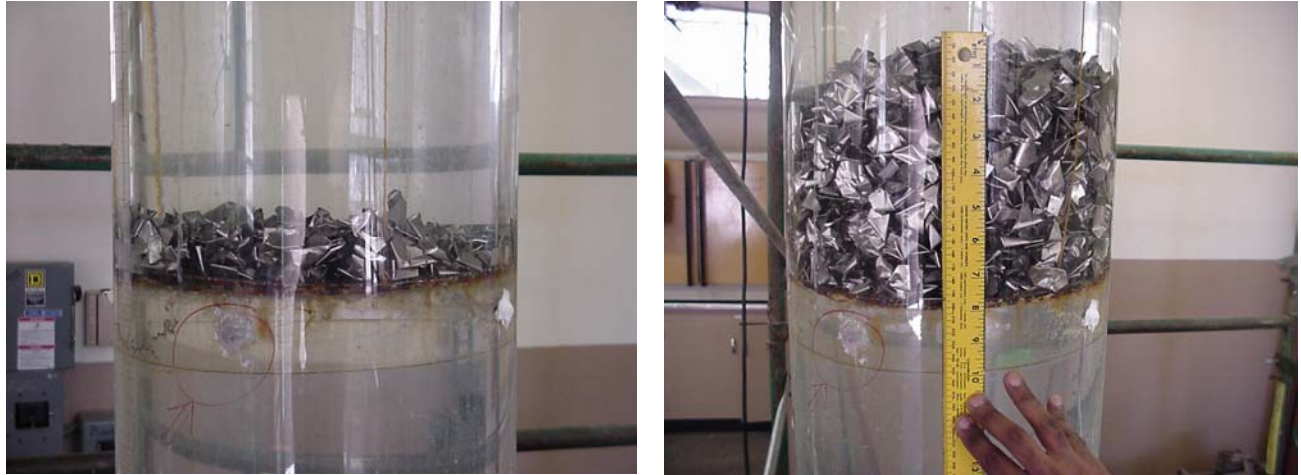


**Figure 3.20. Stainless-steel RMI foil debris beds—1 in. (left) and 8 in. (right) in thickness.**
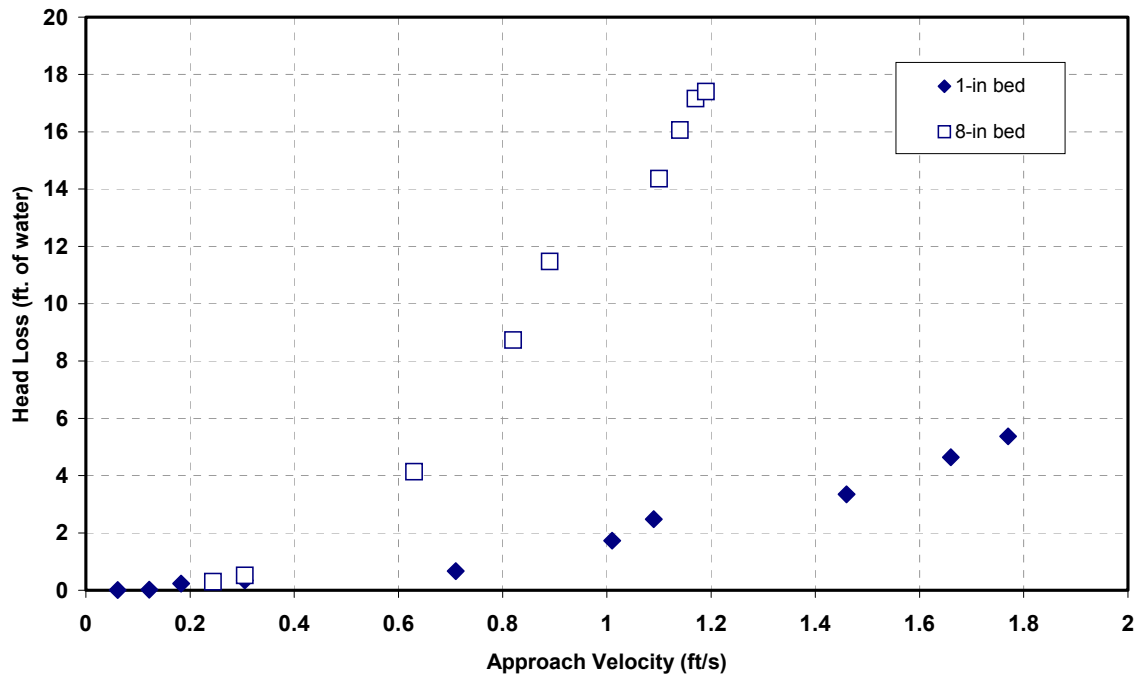


**Figure 3.21. Stainless-steel RMI foil head-loss data.**

### 3.2.5.  Mixtures of RMI and CalSil

Tests 5c through 5g examined the incremental effects of CalSil on the head loss generated by 1-in. and 8-in. beds of stainless-steel RMI debris. Results for the 1-in. RMI debris bed are shown in Figure 3.22; results for the 8-in. RMI debris bed are shown in Figure 3.23.
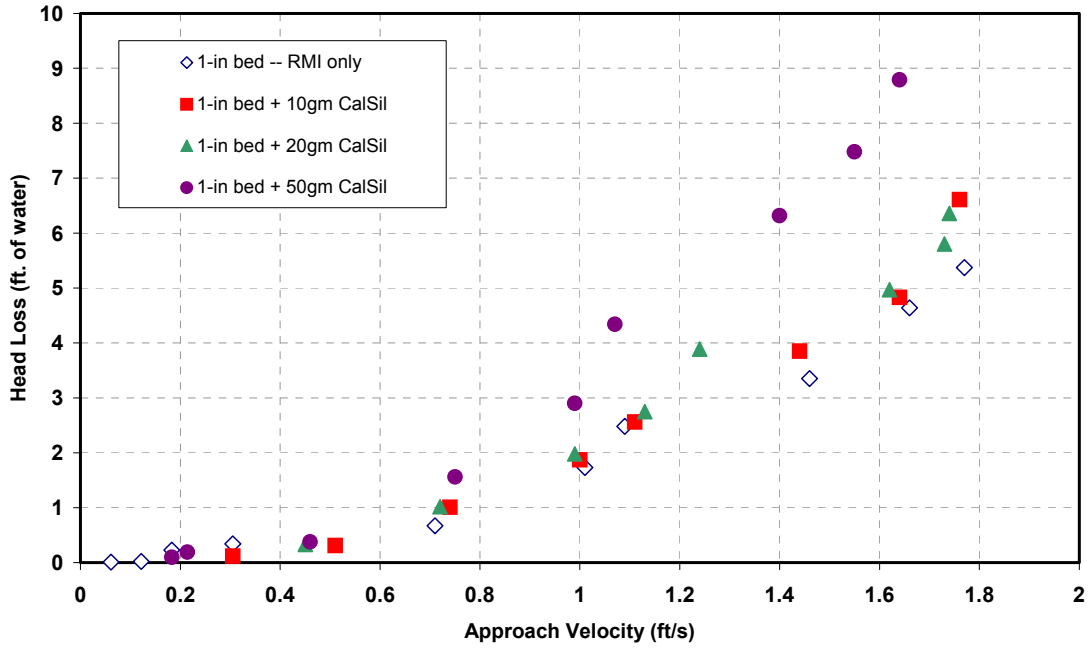


Figure 3.22. Incremental head loss due to the addition of CalSil to a 1-in. stainless-steel RMI debris bed.
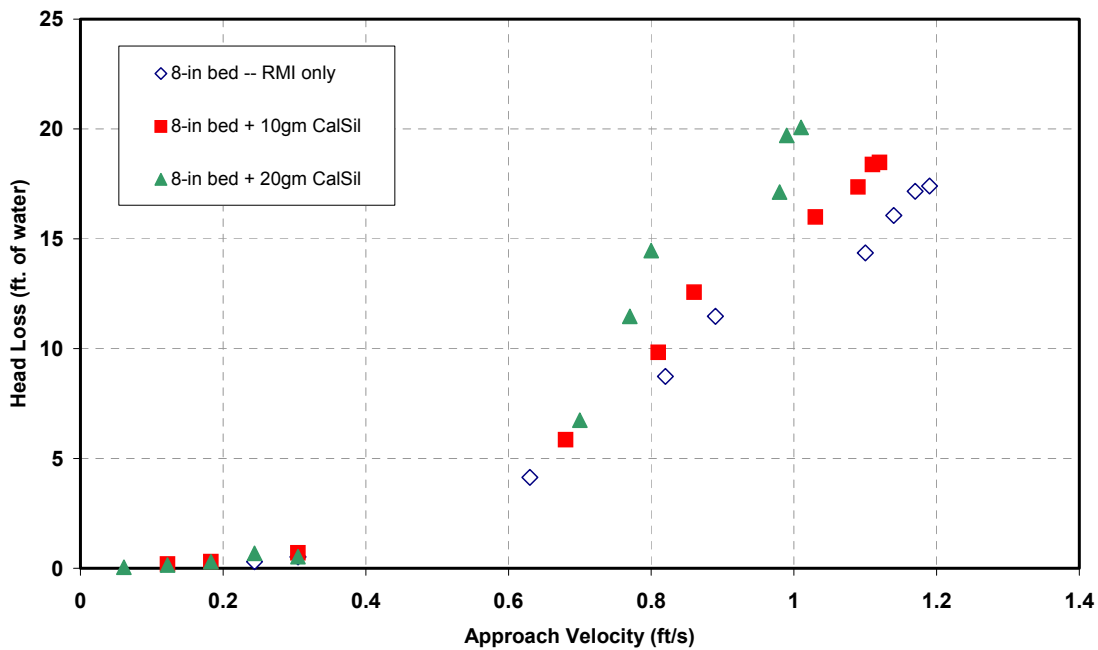


Figure 3.23. Incremental head loss due to the addition of CalSil to an 8-in. stainless-steel RMI debris bed.

Head loss is clearly shown to increase with increasing amounts of CalSil. For the 1-in. debris bed, relatively little change is observed until the quantity of CalSil exceeded 20 g. Noticeable increases in head loss were measured with lower quantities of CalSil in the 8-in. RMI debris bed. Head loss doubled in magnitude when 50 g of CalSil was added to a 1-in. bed of crumpled RMI foils. It is interesting to note that the head loss across an 8-in. bed of RMI foils nearly doubled with considerably less CalSil.

The distribution of CalSil within the RMI debris bed appeared to be nearly uniform in tests at each bed thickness. Photographs of typical post-test debris mixtures are shown in Figures 3.24 and 3.25 for the 1-in. and 8-in. beds, respectively.



**Figure 3.24. CalSil/RMI debris mixture in a typical 1-in. debris bed.**



**Figure 3.25. CalSil/RMI debris mixture in a typical 8-in. debris bed.**

## 4. ANALYSIS OF RESULTS

The analyses of the head-loss testing are organized with the fibrous/particulate beds presented in Section 4.1 and the CalSil/RMI beds in Section 4.2.

### 4.1. Debris Beds Formed of Fibrous and Particulate Debris

An important objective of the test program was to characterize the head-loss characteristics of the CalSil debris with regard to the application of the NUREG/CR-6224 head-loss correlation to predict the head loss associated with the accumulation of debris beds containing quantities CalSil debris. The NUREG/CR-6224 correlation was extensively validated for LDFG debris, such as NUKON™ insulation debris in combination with suppression pool corrosion products, during the resolution of the BWR strainer issue. The NUREG/CR-6224 correlation is applicable to a wide variety of debris types, but its proper application requires the specification of the debris specific head-loss parameters (e.g., the specific surface area). The NUREG/CR-6224 correlation is summarized in Section 4.1.1. Considerations for applying the correlation to test data are discussed in Section 4.1.2. The application of the correlation to debris beds formed of only NUKON™ debris is discussed in Section 4.1.3. The application of the correlation to debris beds formed of NUKON™ in combination with a sand-and-concrete-dust particulate is discussed in Section 4.1.4. The application of the correlation to debris beds formed of NUKON™ in combination with CalSil is discussed in Section 4.1.5. The application of the correlation to debris beds formed of only CalSil debris is discussed in Section 4.1.6.

### 4.1.1. The NUREG/CR-6224 Head-Loss Correlation
A semi-theoretical head-loss correlation for predicting head loss through fiber beds was developed in NUREG/CR-6224 based on fundamental principals of porous media filtration and hydraulics (Zigler, 1995). The correlation previously was shown to provide an accurate characterization of head loss across LOCA-generated debris beds composed of randomly assembled fragments of fiberglass insulation (Rao, 1996). The correlation is programmed into the NRC-developed BLOCKAGE code (Shaffer, 1996). The correlation also provides a means of accounting for the effects of particulate material captured in the fiber bed.

The general equation, valid for laminar, transient, and turbulent flow regimes, is formulated as

$$\frac{dH}{dL_o} = C \left[ 3.5 S_v^2 (1-\varepsilon_m)^{1.5} \left[1 + 57(1-\varepsilon_m)^3\right] \mu U + 0.66 S_v \frac{(1-\varepsilon_m)}{\varepsilon_m} \rho_w U^2 \right] \left(\frac{dL_m}{dL_o}\right) \quad,$$

where
$C$ = 4.1528 x $10^{-5}$ (ft-$H_2O$/in.)/(lb$_m$/ft$^2$-s$^2$) [units conversion constant]
$S_v$ = specific surface area = 1.71 x $10^5$ ft$^2$/ft$^3$ for NUKON$^{TM}$
$\mu$ = dynamic viscosity (lb$_m$/s-ft)
$U$ = velocity (ft/s)
$dH$ = head loss (ft-$H_2O$)
$\rho_w$ = water density (lb$_m$/ft$^3$)
$dL_o$ = fiber bed theoretical thickness (in.)
$dL_m$ = actual bed thickness (in.).

The mixture porosity, $\varepsilon_m$, is given as

$$\varepsilon_m = 1 - (1 + \frac{\rho_f}{\rho_p}\eta)(1-\varepsilon_o)\frac{dL_o}{dL_m} \quad,$$

where
$\rho_f$ = density of an individual fiber (175 lbm/ft$^3$ for fiberglass)
$\rho_p$ = density of each individual particle
$\eta$ = ratio of the mass of particulate to mass of fiber in the bed
$\varepsilon_o$ = theoretical fiber bed porosity.

Values for $\varepsilon_o$ and $dL_m$ can be calculated as

$$\varepsilon_o = 1 - \frac{c_o}{\rho_f}$$

$$dL_m = \frac{c_o}{c} dL_o \quad ,$$

where     $c_o$ = the "as-fabricated" packing density (2.4 $lb_m/ft^3$ for NUKON[TM] fiber)
           $c$ = actual packing density ($lb_m/ft^3$).

The following correlation is used to estimate the compressibility of the debris bed:

$$c = \alpha c_o \left( \frac{dH}{dL_O} \right)^{\gamma} \quad ,$$

where         $\alpha = 1.3$
                $\gamma = 0.38$.

The homogeneous specific surface area of the bed is determined from the specific surface areas of the individual components. A debris bed likely will consist of multiple types of fibers and particulates, each with their respective specific surface area. The homogeneous-bed-specific surface area for a bed consisting of one type of fiber and one type of particulate is given by:

$$S_v = S_{vf} \left[ \frac{1 + \dfrac{\rho_f}{\rho_p} \eta \dfrac{S_{vp}}{S_{vf}}}{1 + \dfrac{\rho_f}{\rho_p} \eta} \right] \quad ,$$

where         $S_{vf}$ = the fiber specific surface area ($ft^2/ft^3$)
                $S_{vp}$ = the particulate specific surface area ($ft^2/ft^3$).

The solution of the general NUREG/CR-6224 correlation and its supporting equations requires an iterative solution.

In addition, there is a practical limit to the fiber bed compression whenever significant particulate is embedded in the fiber matrix. The particulate cannot be compressed beyond its granular density, referred to herein as the sludge density (e.g., ~65 $lbm/ft^3$ for BWR suppression pool iron oxide corrosion products). Therefore, whenever the bed density reaches the following limit, further compression ceases.

$$dL_m = dL_o \frac{c_o}{c_{sludge}} (\eta + 1) \quad ,$$

where            $c_{sludge}$ = the sludge density

When the correlation is applied to a debris bed that does not contain significant fiber (e.g., CalSil-only debris), the fiber compressibility correlation does not apply and the porosity equation must be simplified.

The bed compressibility is set to one (i.e., $dL_m/dL_o = 1$), the bed-specific surface area is that of the particulate, and the bed porosity is determined from the particulate sludge density

$$\varepsilon_m = 1 - \frac{c_{sludge}}{\rho_p} \quad ,$$

where $\rho_p$ = density of each individual particle.

### 4.1.2. Considerations for Applying of the NUREG/CR-6224 Correlation to Test Data

The NUREG/CR-6224 correlation provides a method of analytically predicting the head loss associated with a bed of debris accumulated on a strainer or sump screen. Another way to think of the correlation is that it provides a method of extrapolating limited test data into postulated accident scenario debris beds. The correlation is applied to appropriate test data to experimentally determine the debris head-loss parameters; these parameters then can be used to estimate the head loss for beds of similar debris.

The head-loss parameters that require experimental determination are the specific surface area and the sludge density specific to each type of debris and to the size distribution of the particles and perhaps the fibers. The density of individual particles can usually be estimated from the material composition. It should be emphasized that the specific surface area, if not the sludge density, is very dependent on the particle size distribution. For a spherical particle, the idealized geometric specific surface area is 6 divided by the diameter, and for a strand of fiber, it is 4 divided by the diameter. However, due to nonuniformities and interactions, only a very crude estimate of specific surface area can be made using a characteristic diameter.

The development of the NUREG/CR-6224 correlation assumed that the debris bed is uniform in thickness so that the velocity of flow through the bed is constant across the bed. The correlation applies to flat screens or to screens or strainers that have been shown to be approximated as flat screens, such as cone-shaped strainers. It was also assumed that the bed is homogeneous so that the composition and head-loss properties do not depend on the location within the bed. In reality, a debris bed could be skewed to one side or formed lumpy so that it is not uniform in thickness. A nonuniform bed will not create as high a head loss as will an ideally uniform bed. All test results inherently have some degree of nonuniformity, and the tests reported herein have varying degrees of nonuniformity, as will become apparent in the following analyses. However, the head-loss parameters should be determined from relatively uniform beds of debris.

It is possible for debris beds to form that are not homogeneous. In a BWR suppression pool, for example, the high-density corrosion products will tend to settle once pool turbulence dissipated so that more of this particulate will accumulate on the strainer earlier than later. Thus, the initial layer of debris will have a higher particulate-to-fiber mass ratio than subsequent layers. Nonhomogeneous beds can homogenize, at least in head-loss testing, as particles dislodge from the bed, transit the circuit, and deposit in the debris bed again. However, this behavior has not been adequately characterized.

The stability of the debris bed is an important consideration when analyzing this test data. It will be apparent that debris beds reoriented following changes in the pump flow. CalSil particulate is relatively fine and therefore more susceptible to movement if the bed is perturbed. In addition, larger pieces of CalSil are subject to substantial dissolution, which is both turbulence and temperature dependent, i.e., an increase in either temperature or turbulence was shown to enhance the disintegration of the CalSil. This dissolution was studied in the separate-effect debris characteristics tests [Rao, 2002a]. During testing, larger pieces of CalSil debris partially disintegrated, especially in the higher temperature tests, so that the debris bed changed either slowly or suddenly when the pump flow was altered. A relatively sudden shift from a relatively nonuniform bed to a relatively uniform bed could easily be responsible for a relatively rapid increase in head loss as the flow velocity increased only slightly.

The efficiency at which the CalSil particulate is filtered from the flow stream is also an important consideration. The quantity of CalSil in the debris bed only equates to the quantity of CalSil added to the

test loop if the filtration process is complete. If a substantial quantity of particulate remained in transit, indicated by cloudy flow, then the quantity of particulate in the bed is uncertain. Thus, it is important that a majority of the particulate is filtered from the flow. The filtration efficiency is a function of the inter-fiber spacing, which in turn, is a function of the compression of the fibrous debris bed. Complete filtration during these tests was problematic and this problem likely accounted for some of the erratic behavior encountered.

Head-loss testing of fibrous debris beds has demonstrated a compression hysteresis effect in that the fibrous debris bed did not expand to the same extent as the flow velocity was decreased as it compressed when the velocity increased. That is, the head-loss curve associated with a systematic reduction in pump flow was higher than during the systematic increase in flow.

Pressure-induced nonuniformities such as holes or tunnels have been shown to form whenever the pressure differential across the bed becomes excessive. An example is shown in Figure 3.18. Because these holes tend to relieve the pressure differential, the NUREG/CR-6224 correlation will tend to overpredict head losses under these conditions.

Temperature also affects the head loss due to its effect on the water viscosity. It also affects the water density but to a much lesser extent. The tests reported herein were conducted either with nominally room temperature water or heated water. In both cases, the temperature was somewhat transient. For room temperature water, the water temperature was heated somewhat by the pump and it equilibrated with its surroundings. The heated water was supplied by water heated at a nominal temperature of 125°F, but the water subsequently cooled due to heat transfer to the surroundings and was also heated somewhat by the pump. Therefore, a secondary effect of the temperature transient is present in the test data.

The analysis discussed in this section proceeds as follows.

- The NUKON™-only head-loss tests are compared with NUREG/CR-6224 to illustrate the capability of the correlation on UNM fiber bed testing.

- The NUKON™ with dirt particulate head-loss tests are compared to further demonstrate the correlation and to demonstrate the dependency of the head-loss prediction on the particle size distribution.

- The NUKON™ with CalSil debris head-loss tests are analyzed to estimate the characteristic head-loss parameters for CalSil.

- The CalSil-only head-loss test is analyzed to further demonstrate those parameters.

### 4.1.3. Debris Beds Formed of Only NUKON™ Debris

Tests 1a, 1a', and 1b were conducted with debris beds that consisted of only NUKON™ debris. The parameters of these tests are shown in Table 4.1. This set of tests provides data to compare the head loss at two different debris bed thicknesses (Tests 1a and 1a') and to compare the head loss at two different temperatures (Tests 1a and 1b). Test 1b was conducted three times to show test repeatability.

**Table 4.1. Fibrous-Only Debris Tests**

| Fibrous Debris | Nominal Water Temperature | |
|---|---|---|
| | 70°F | 125°F |
| 116 g (~1.72-inch) | Test 1a | Test 1b |
| 58 g (~0.86 inch) | Test 1a' | No Test |

The key parameters used in the NUREG/CR-6224 correlation, as applied to a fiber-only debris bed, include the bed cross sectional area, the water temperature, the pump flow rate, the quantity of NUKON™ debris, the specific surface area, and the densities. The test apparatus has two cross sectional areas that influence the head loss, and these are the areas of the piping and the screen support ring. The thickness of the debris bed depends on the cross sectional area of the pipe; however, due to edge effects, the thickness should use an area somewhat less than that of the pipe. The flow velocity through the bed depends on the smaller area of the screen support ring as well as the pipe. The support ring actually functioned as a thick-edged orifice, and the flow converged slightly while transiting the debris bed. The area used in this analysis was 0.7426 ft$^2$, corresponding to a diameter of 11.67 in., which is somewhat smaller than the pipe ID of 11.89 in. but larger than the support ring ID. The NUKON™ parameters were 171,000/ft for the specific surface area, 2.4 lbm/ft$^3$ for the as-manufactured density, and 175 lbm/ft$^3$ for the fiberglass density.

The comparison of the two bed thicknesses with their corresponding NUREG/CR-6224 correlation predictions is shown in Figure 4.1. The debris bed in Test 1a is ~1.72 in. thick and is twice as thick as Test 1a'. As shown, the correlation does an excellent job of predicting both Tests 1a and 1a'. In Test 1a' with a bed thickness of 0.86 in., the test head loss appeared to fall away somewhat from the trend at the higher velocities; the reason for this behavior was not readily apparent.
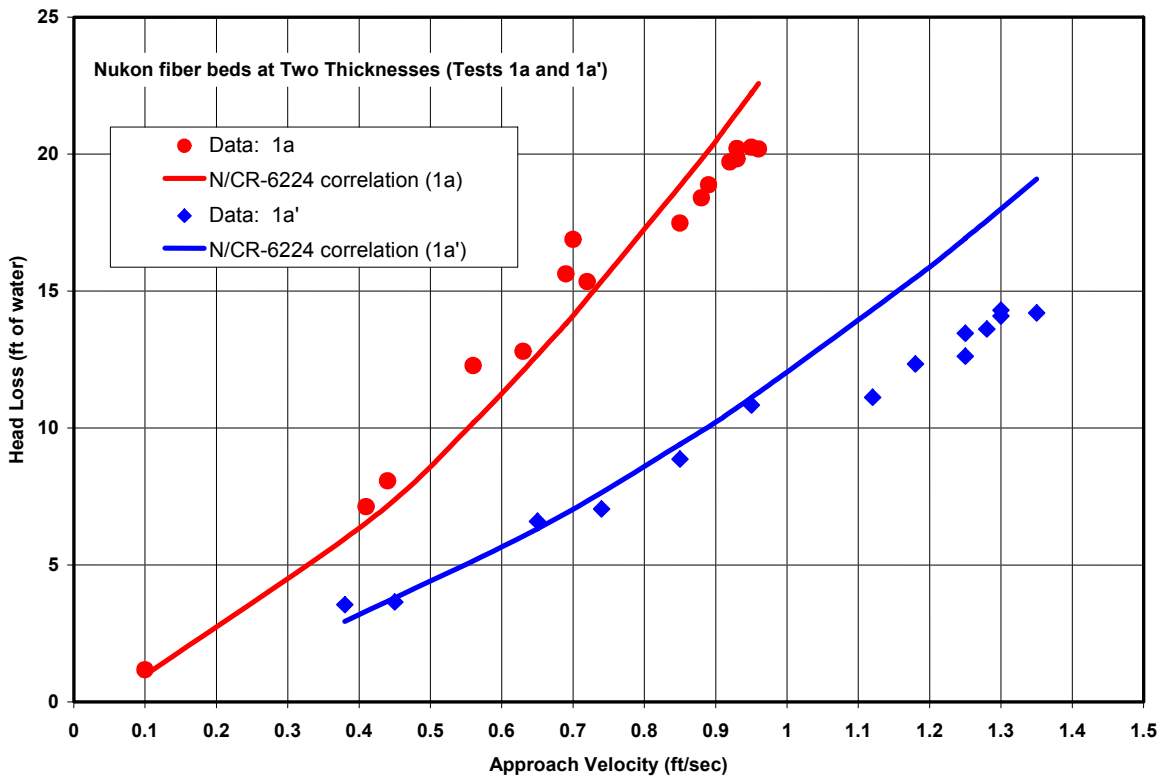


**Figure 4.1. Comparison of tests with NUREG/CR-6224 correlation at two bed thicknesses.**

The comparison of the two temperatures with their corresponding NUREG/CR-6224 correlation predictions is shown in Figure 4.2. The debris bed in Test 1a was conducted using room-temperature water, and Test 1b was conducted using heated water nominally at 125°F. As previously noted, the correlation does an excellent job of predicting Tests 1a. However, in Test 1b with its three separate trials, the correlation fell somewhat short at the higher velocities, whereas the correlation was accurate at the lower velocities. The principal effect that temperature has on the head losses is the variation in the viscosity and, to a lesser extent, the water density. Note that the test data for Test 1b tend to converge

with the data for Test 1a when the velocity approaches 1 ft/s. The viscosity of room temperature water is ~80% higher than for water at 125°F. If the water cooled significantly during the course of Test 1b, the cooling could have contributed to the observed trend.
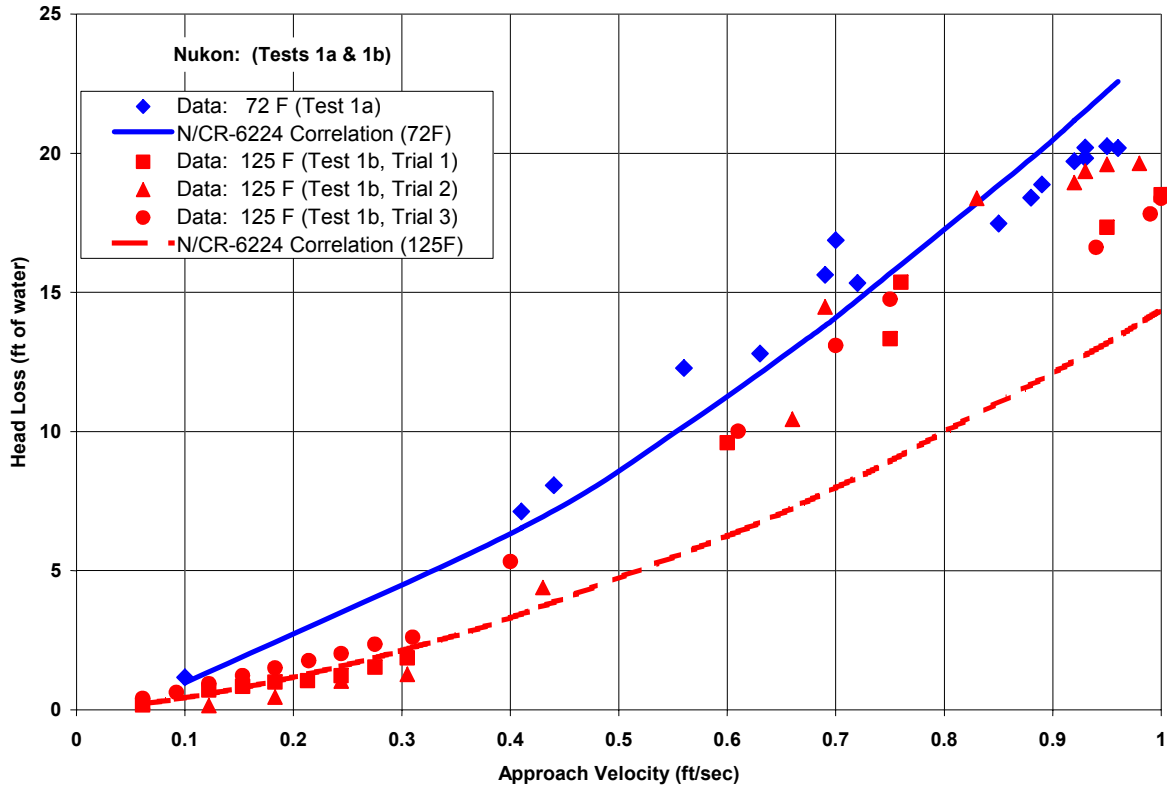


**Figure 4.2. Comparison of tests with NUREG/CR-6224 correlation at two temperatures.**

The tests reaffirm previous test conclusions that the NUREG/CR-6224 correlation does an excellent job of predicting the head loss associated with a NUKON™ fiber debris bed. Further, the head-loss parameters in use for this type of debris are valid.

### 4.1.4. Debris Beds Formed of NUKON™ and Dirt Debris

Tests 1c and 1d were conducted using dirt samples as particulate in conjunction with NUKON™ insulation debris. The parameters applied to the NUREG/CR-6224 correlation to estimate the head loss associated with these tests included the proven NUKON™ parameters. The densities of dirt were assumed to be one-half of these for iron oxide corrosion products, i.e., a particle density of 162 lbm/ft$^3$ and the sludge density of 32.5 lbm/ft$^3$. The dirt was collected from the floor of a concrete laboratory at UNM and therefore likely consisted of mostly concrete by-product and may not represent a realistic sample from the nuclear plant containment. The analyses attempted to determine the specific surface area for the dirt sample by adjusting the input value for this area in the NUREG/CR-6224 correlation until the data fit firmly beneath the correlation predictions. This procedure illustrates a method of experimentally estimating the specific surface area for a particulate sample.

The data from Tests 1c and 1d are compared with the NUREG/CR-6224 correlation in Figures 4.3 and 4.4, respectively. Specific surface areas for the particulate of 190,000/ft and 130,000/ft were used in the correlation to place correlation results above the data. A pronounced feature of the test data was that head-loss data taken as the flow velocity was reduced were substantially higher than when the velocity was increasing. This type of behavior is similar to the compression hysteresis effect where the fiber bed is

slower to decompress than to compress, but the behavior in these tests is not hysteresis. Note that as the velocity starts to decrease, the head-loss increases, which is not hysteresis and does not fit known debris bed behavior knowledge.
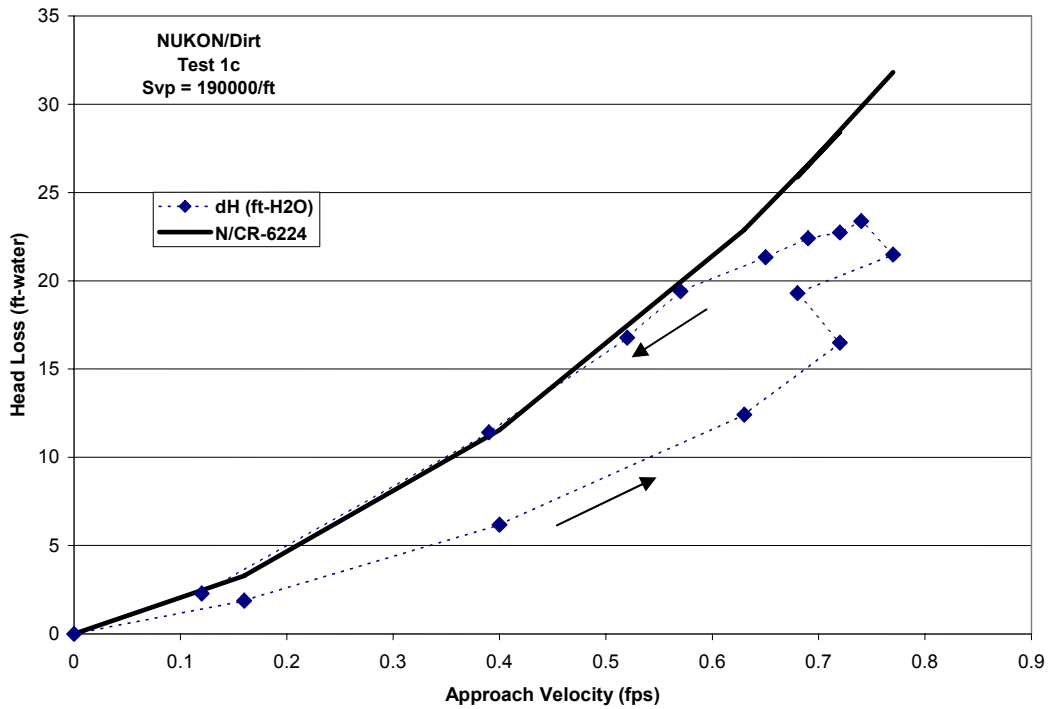


**Figure 4.3. Comparison of Test 1c with NUREG/CR-6224 correlation.**
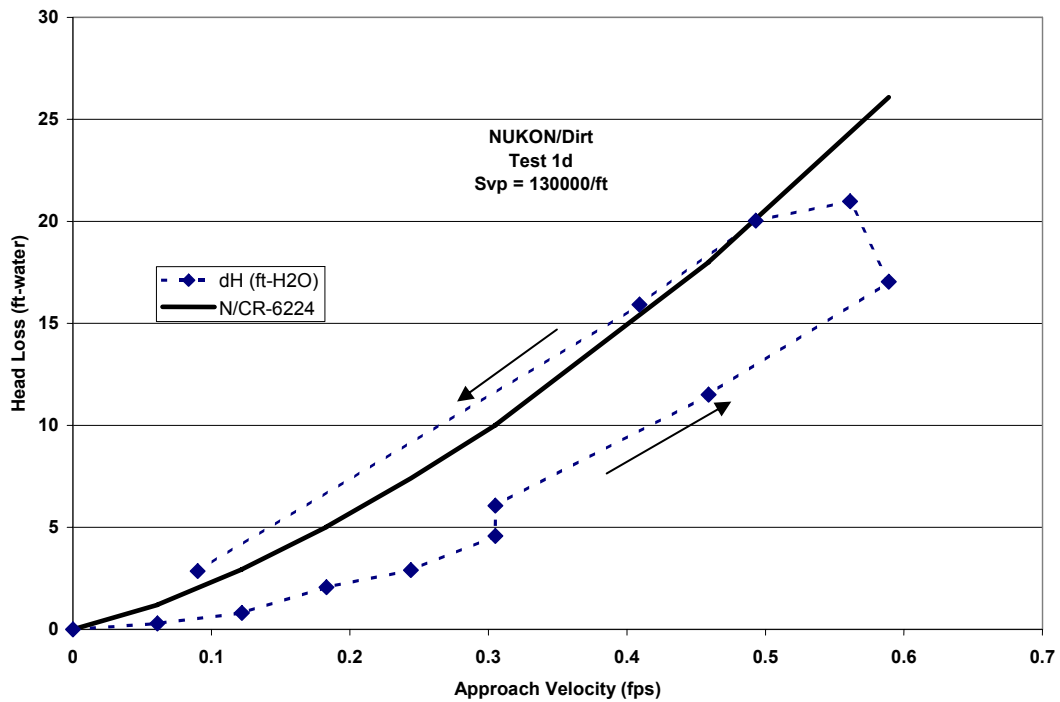


**Figure 4.4. Comparison of Test 1d with NUREG/CR-6224 correlation.**

39

The apparent explanation for head loss increasing as the velocity is decreased is that the debris bed must have shifted somehow. Apparently, the initial debris bed was relatively nonuniform, and then perhaps the reduction in flow smoothed out the bed, thereby increasing the head loss. If this is correct, then the larger head-loss data points were the most correct data to use in estimating the specific surface areas. The reasons for the difference in the specific surface area between the two tests are not clear. If the dirt samples were not carefully controlled, then perhaps the two samples had different specific surface areas. Or Test 3d with the smaller specific surface area has a relatively nonuniform debris bed relative to Test 3c, thus lower testing head losses.

### 4.1.5.  Debris Beds Formed of NUKON™ and CalSil Debris

Twelve tests were conducted that had both NUKON™ and CalSil debris (Test Series 3) where the test variables were the quantities of NUKON™ and CalSil debris and the temperature. The results of these tests were also affected by the testing difficulties discussed in Section 4.1.2, such as nonuniformities in the debris bed. Because CalSil particulate is relatively fine, debris beds with substantial quantities of CalSil are generally less stable than beds consisting of coarser debris. Each of these 12 tests is compared with the NUREG/CR-6224 correlation in an attempt to determine appropriate head-loss parameters whereby the correlation can be used to predict the head loss associated with CalSil debris beds. The order of the presentation is determined by the analytical process.

Test 3k Test 3k was conducted using heated water, nominally at 125°F, 58 g of NUKON™, and an equal mass of CalSil. In applying the NUREG/CR-6224 correlation, NUKON™ properties were applied to the fibrous debris bed and CalSil properties were applied to the particulate. Note that the very fine fibers within the CalSil insulation were treated as particulate, not as fibrous debris. The solid density of 186 lbm/ft$^3$ was assumed for both fiber and particulate in CalSil. For Test 3k, the CalSil specific surface area was adjusted until the correlation reasonably well predicted the test results. The data from Test 3k are compared with the correlation in Figure 4.5.
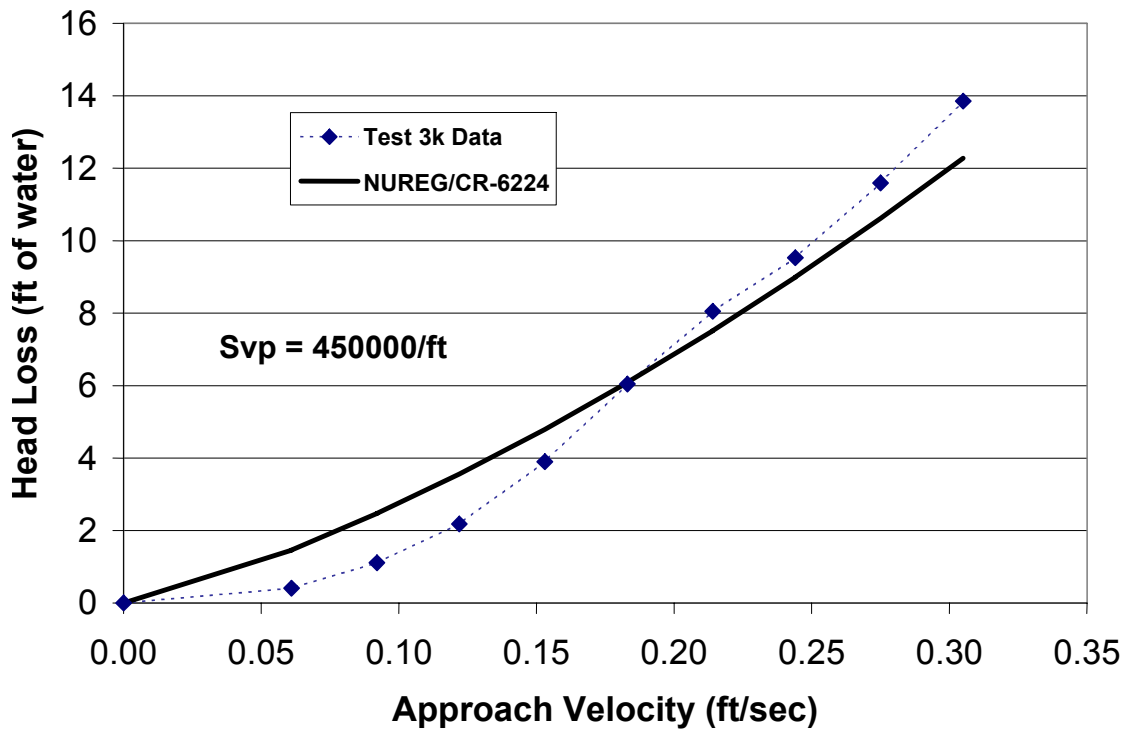


**Figure 4.5. Comparison of Test 3k with NUREG/CR-6224 correlation.**

A specific surface area of 450,000/ft was found to reasonably well (but not conservatively) predict the test data. The NUREG/CR-6224 correlation indicated that the fibrous bed continually compressed with each increase on the approach velocity, thereby indicating that the sludge compression limit was not reached so that the value of the sludge density was not needed to determine the specific surface area, i.e., the compression limit to the compressibility function, which requires the sludge density as input (described in Section 4.1.1), was not reached. Assuming the debris bed in Test 3k was relatively uniform, the specific surface area of CalSil then is ~450,000/ft or ~2.6 times that of NUKON™ fibers. However, as a caution, it should be noted that the debris bed in Test 3k was penetrated by holes, shown in Figure 3.18, which must have alleviated the head loss. Therefore, the specific surface area is likely higher than 450,000/ft. The reason that CalSil (and similar insulations) caused much higher head losses than particulates, such as suppression pool corrosion products, is its very fine particulate sizes. The fibers in CalSil are generally on the order of a couple of microns, and particles are also quite small in diameter. It is easy to see that the specific surface area for CalSil must be relatively large.

Test 3l Test 3l was conducted using heated water, nominally at 125°F, 58 g of NUKON™, and 116 g of CalSil. The application of the NUREG/CR-6224 correlation to Test 3l data was similar to that of Test 3k, except that in Test 3l, the bed compression was limited by the sludge density. Using the specific surface area determined from Test 3k data, the sludge density for CalSil was adjusted until the correlation reasonably well predicted Test 3l and that density turned out to be 18 lbm/ft$^3$. The as-fabricated density for CalSil was estimated at 14.5 lbm/ft$^3$, so this sludge density represents a compression of ~25% more than the as-fabricated density. Data from Test 3l are compared with the correlation in Figure 4.6, and a photo of the debris bed is shown in Figure 4.7. This debris bed did not have any apparent holes or uncovered screen, but the nonuniform thickness likely resulted in a lower head loss than if the bed were completely uniform.
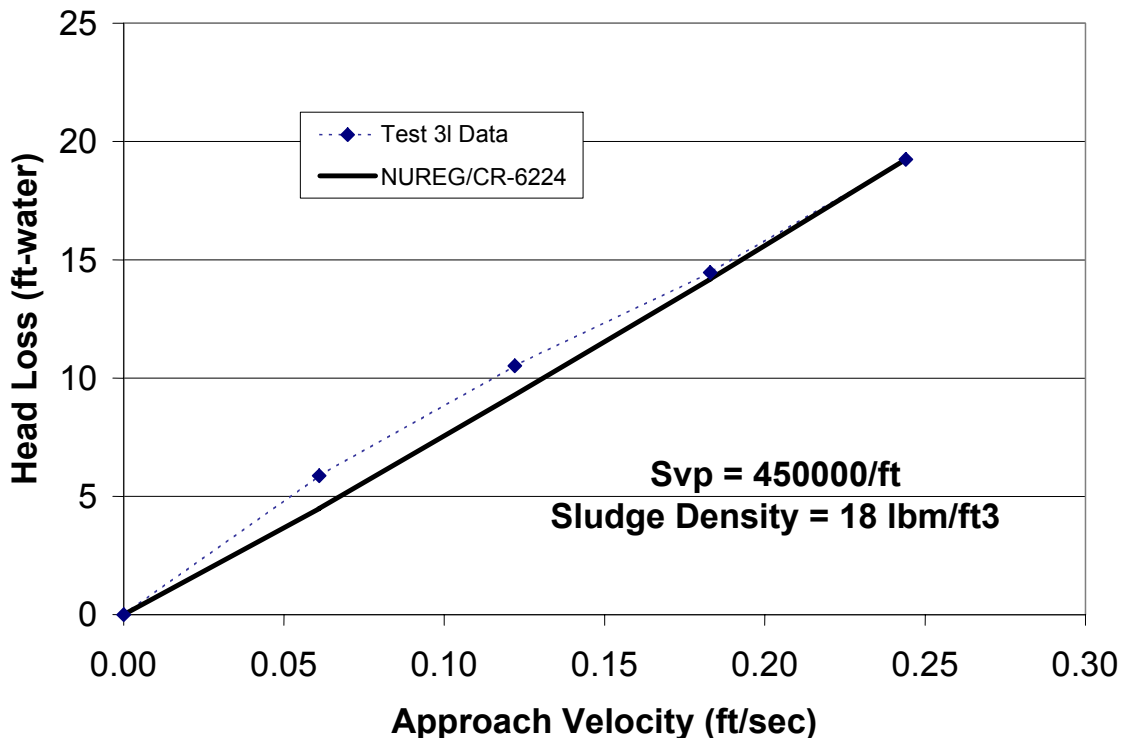


**Figure 4.6. Comparison of Test 3l with NUREG/CR-6224 correlation.**

**Figure 4.7. Photo of Test 3l debris bed.**

With these two experimentally determined head-loss parameters for CalSil, enough is known to predict CalSil head-loss behavior with the general form of the NUREG/CR-6224 correlation, i.e., no need for correction factors. However, it will be shown that a substantial uncertainty is associated with this result, i.e., the specific surface area may be substantially higher than 450,000/ft because the uniformity in Test 3k and 3l may not have been adequate. These parameters are now used to show how the correlation compares with head-loss data from other tests.

Test 3d Test 3d was conducted using room temperature water, nominally at ~70°F, 58 g of NUKON™, and 29 g of CalSil (a particulate-to-fiber mass ratio of 0.5). The application of the NUREG/ CR-6224 correlation to Test 3d data assumed a specific surface area of 450,000/ft and a sludge density of 18 lbm/ft$^3$. The comparison of Test 3d data with the correlation is shown in Figure 4.8; the comparison looks very favorable. Note that the Test 3d shows some of the compression hysteresis behavior and that the behavior is not excessive.

Test 3b and 3c Tests 3b and 3c were conducted using room-temperature water, 7.3 g of NUKON™, and 7.3 and 14.6 g of CalSil, respectively. The application of the NUREG/CR-6224 correlation to Tests 3b and 3c data assumed a specific surface area of 450,000/ft and a sludge density of 18 lbm/ft$^3$. The comparison of Tests 3b and 3c data to the correlation is shown in Figures 4.9 and 4.10, respectively. The correlation greatly exceeds the test data of these two tests because the beds were very nonuniform and significant portions of the screen were essentially uncovered. Photos of these tests are shown in Figure 3.13. These tests are of little value.

Test 3e, 3f, 3g, 3h, and 3i Tests 3e through 3i were all conducted using room-temperature water but with varying amounts of NUKON™ and CalSil debris. The comparisons for these tests are shown in Figures 4.11 through 4.15, respectively. In general, the correlation, predicted higher head losses than the data, but the data from these tests had substantial scatter caused by such factors as the bed nonuniformities already noted. During some of the tests, the debris bed must have reconfigured when the pump flow was systematically reduced, i.e., when the head loss increased significantly following a reduction in flow. If the bed were uniform, then a reduction in flow could not have increased head loss, but a bed reconfiguration

42

**Figure 4.8. Comparison of Test 3d with NUREG/CR-6224 correlation.**



**Figure 4.9. Comparison of Test 3b with NUREG/CR-6224 correlation.**

**Figure 4.10. Comparison of Test 3c with NUREG/CR-6224 correlation.**



**Figure 4.11. Comparison of Test 3e with NUREG/CR-6224 correlation.**

**Figure 4.12. Comparison of Test 3f with NUREG/CR-6224 correlation.**



**Figure 4.13. Comparison of Test 3g with NUREG/CR-6224 correlation.**
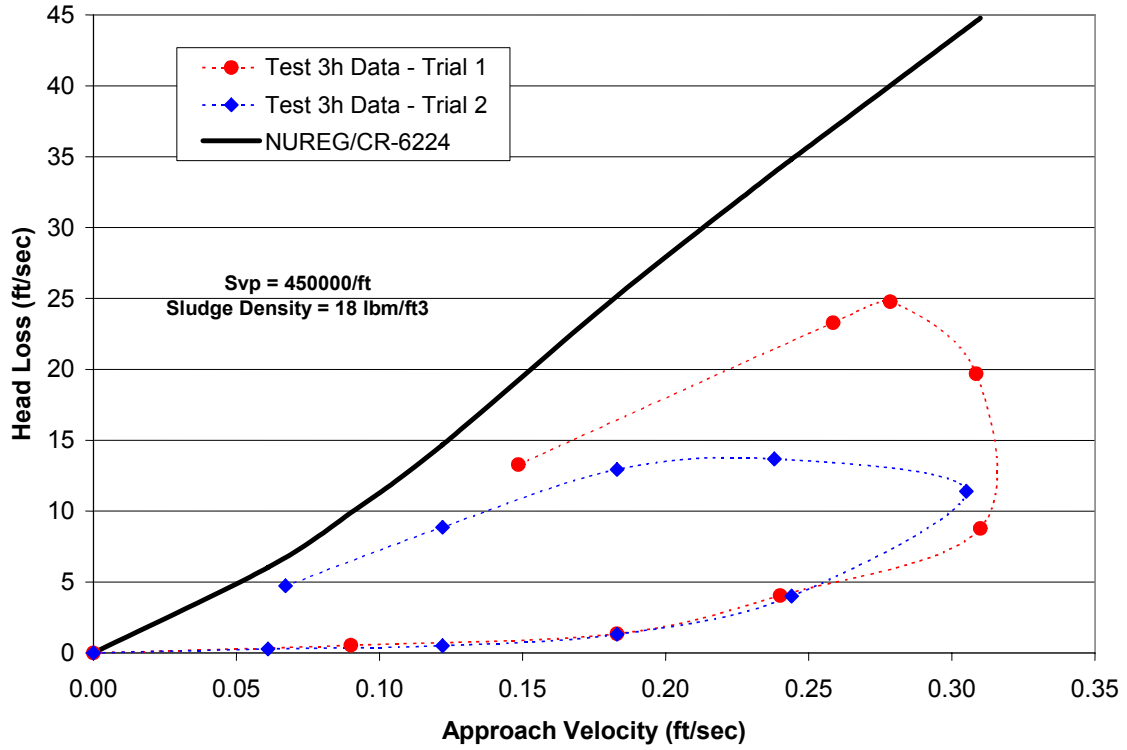
**Figure 4.14. Comparison of Test 3h with NUREG/CR-6224 correlation.**
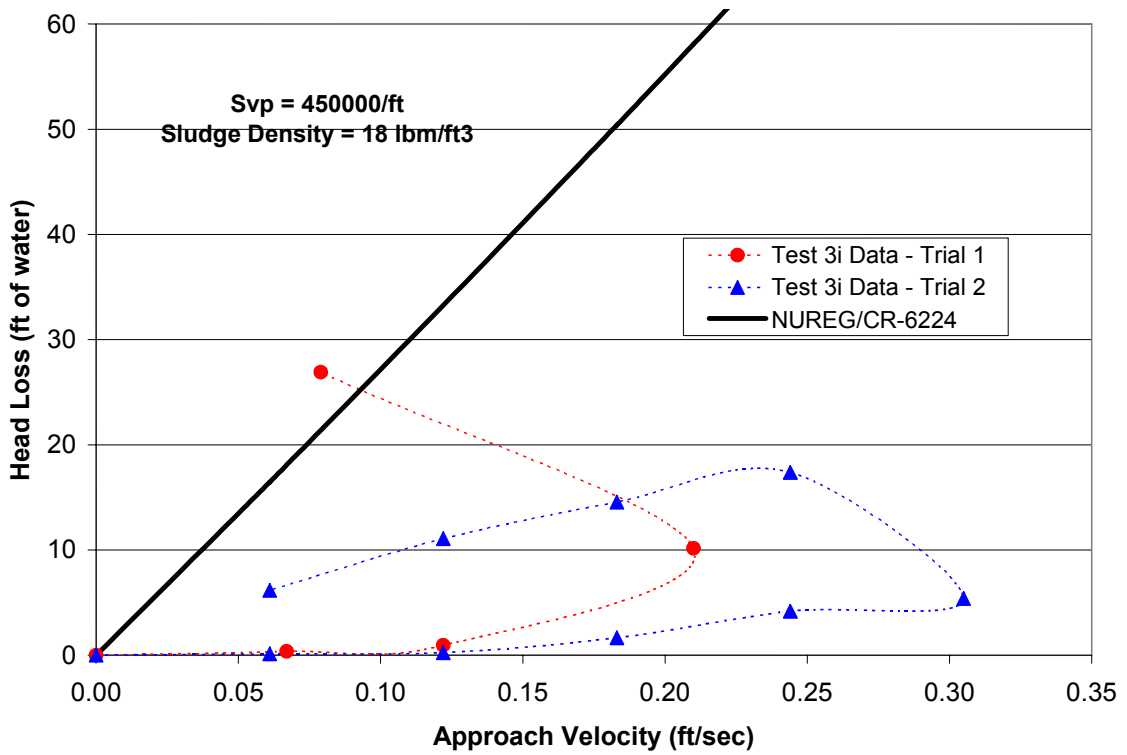


**Figure 4.15. Comparison of Test 3i with NUREG/CR-6224 correlation.**

from a relatively nonuniform to a more uniform configuration would explain this behavior. It is quite possible that lumps of CalSil debris initially located in the bed subsequently disintegrated, due to soaking and turbulence during the test, and thereafter formed a different bed configuration. In these situations, the higher head losses associated with flow reduction are more applicable than the lower head losses. Repeated tests in some cases did not reasonably replicate the original test data. Although the test data have substantial uncertainty, the correlation as configured still conservatively predicts the data.

Test 3a and 3j data from Tests 3a and 3j exceed the NUREG/CR-6224 correlation when the correlation is configured using a specific surface area of 450,000/ft; in fact, the data are better predicted using a specific surface area of 700,000/ft. The comparison of the correlation with the test data is shown in Figures 4.16 and 4.17 for Tests 3a and 3j, respectively.

These tests appear to be outliers for the other NUKON™/CalSil tests in that all the other tests were either reasonably well predicted or bounded by the correlation when the specific surface area and the sludge density are specified as 450,000/ft and 18 lbm/ft$^3$, respectively. To further complicate the issue, Test 3a was a thin-bed test and may have had some exposed screen, as shown in the photo in Figure 3.13. Two possible explanations exist for the high head losses associated with Tests 3a and 3j. First, an error occurred in each of these two tests, such as the measurement of the debris introduced into the tests or in Test 3j, the water was actually at room temperature rather than 125°F, or the pressure transducer malfunctioned. The second possible explanation is that the data in these two tests are valid, the specific surface area is actually in the neighborhood of 700,000/ft, and all the other tests suffered from a nonuniform bed, or non-homogeneous bed, or incomplete coverage of the screen. The photo of the Test 3j debris bed, shown in Figure 4.18, shows one of the better-formed debris beds from the test series, which is another indication that the specific surface area may be as high as 700,000/ft. When the CalSil debris remains in a lumpy form, a portion of the debris bed would have less CalSil than another portion, so that flow slipped around the CalSil to some extent rather than through it. Additional testing has been proposed; perhaps these tests will solve this dilemma. The additional testing should focus on creating uniform and homogeneous debris beds.
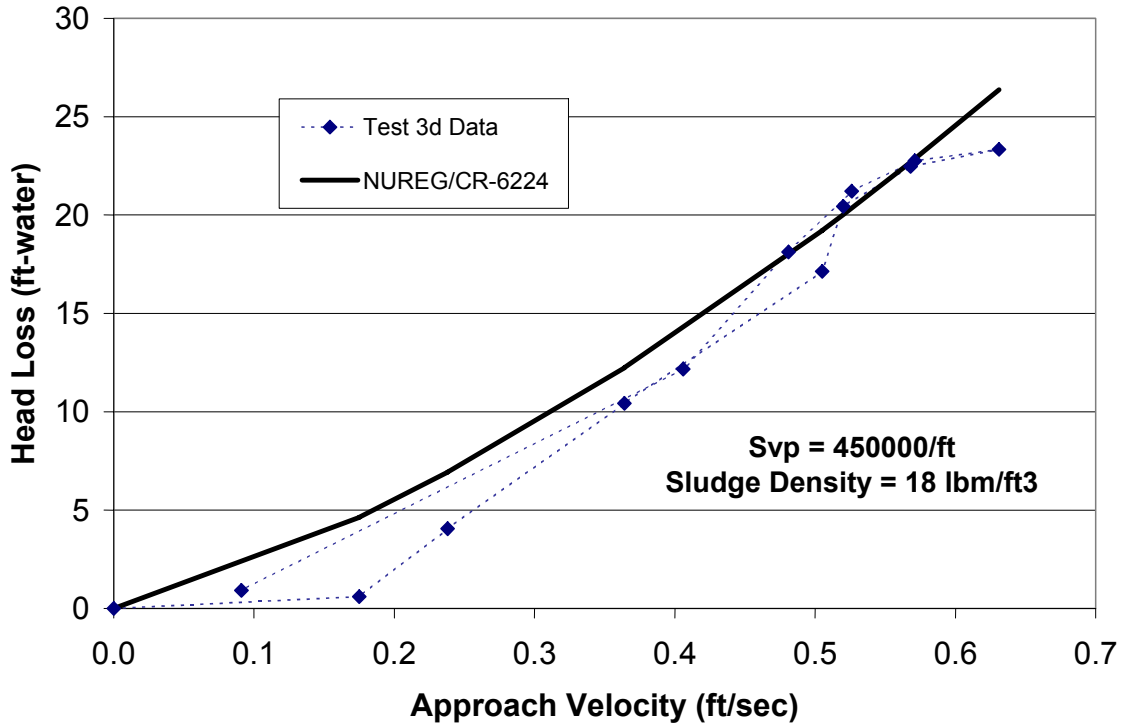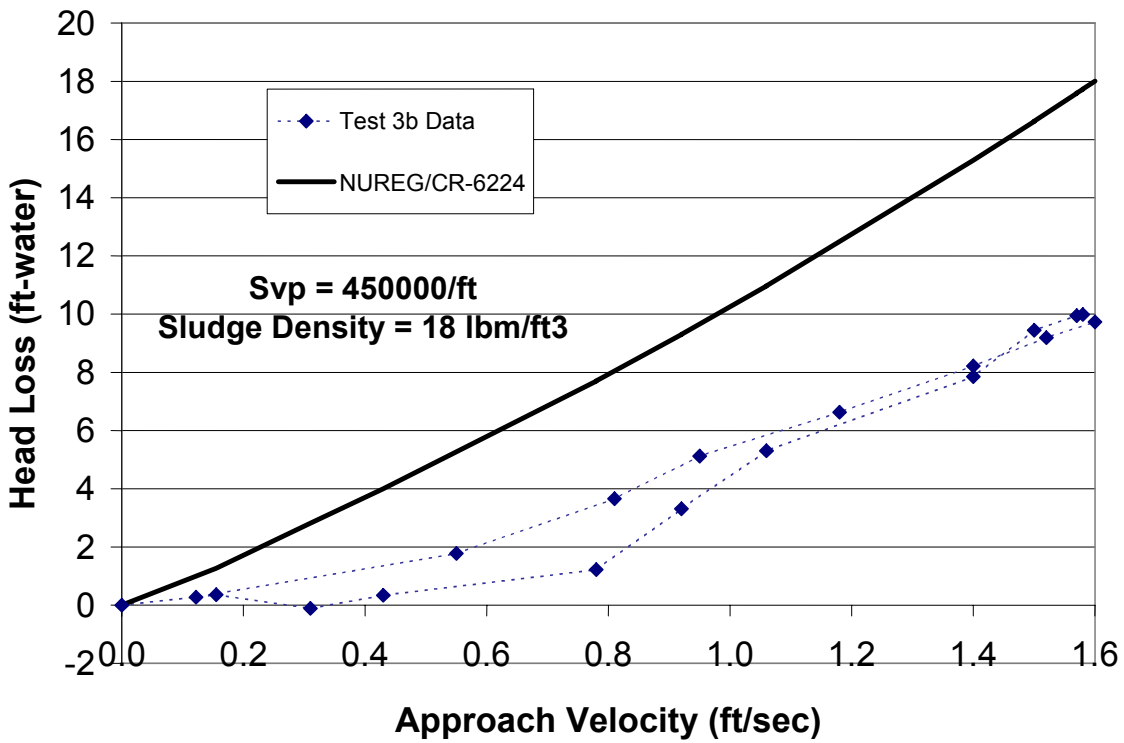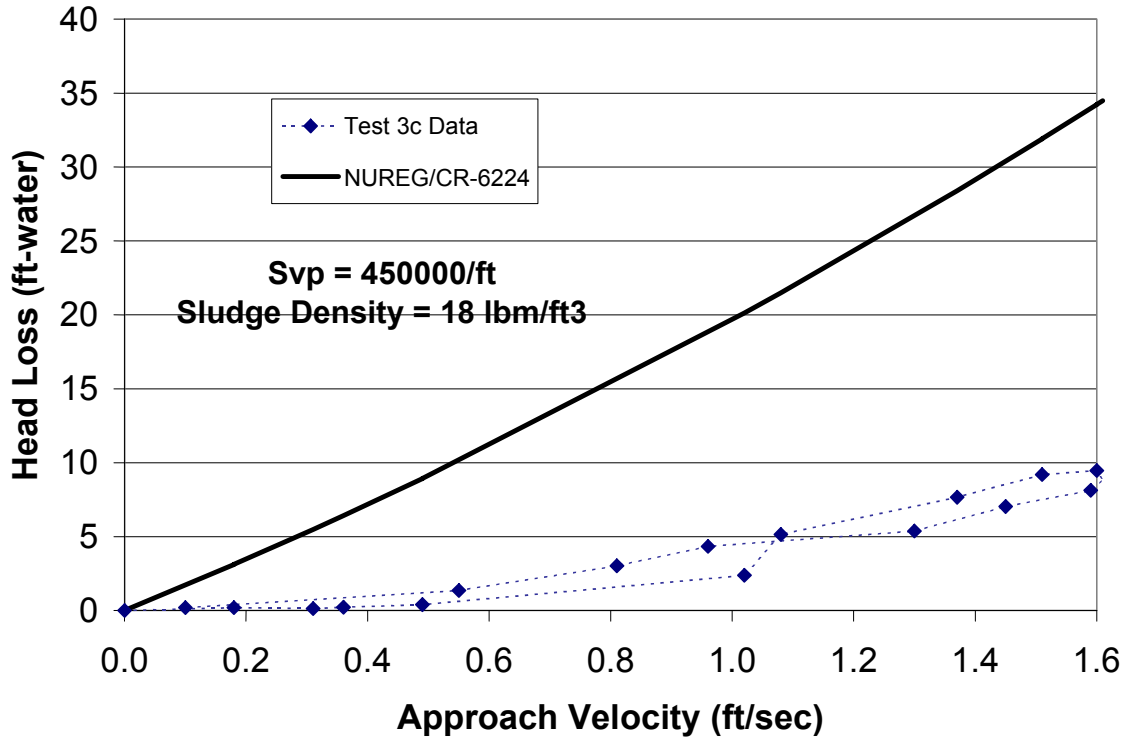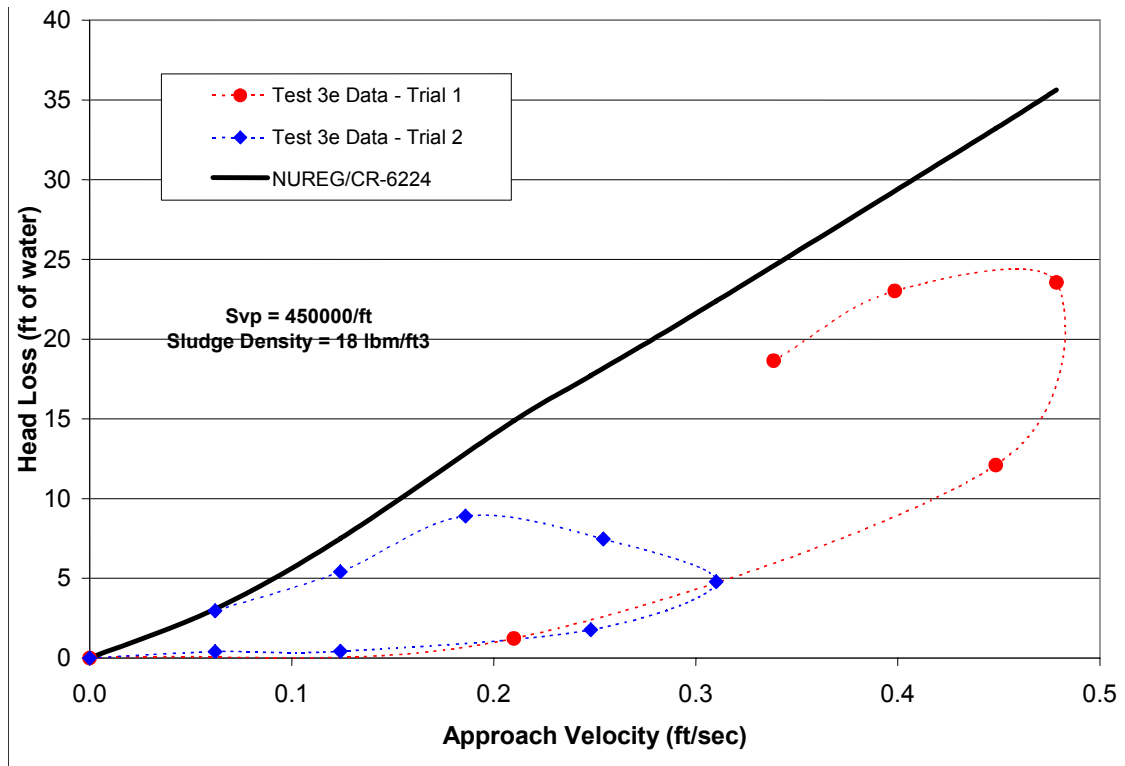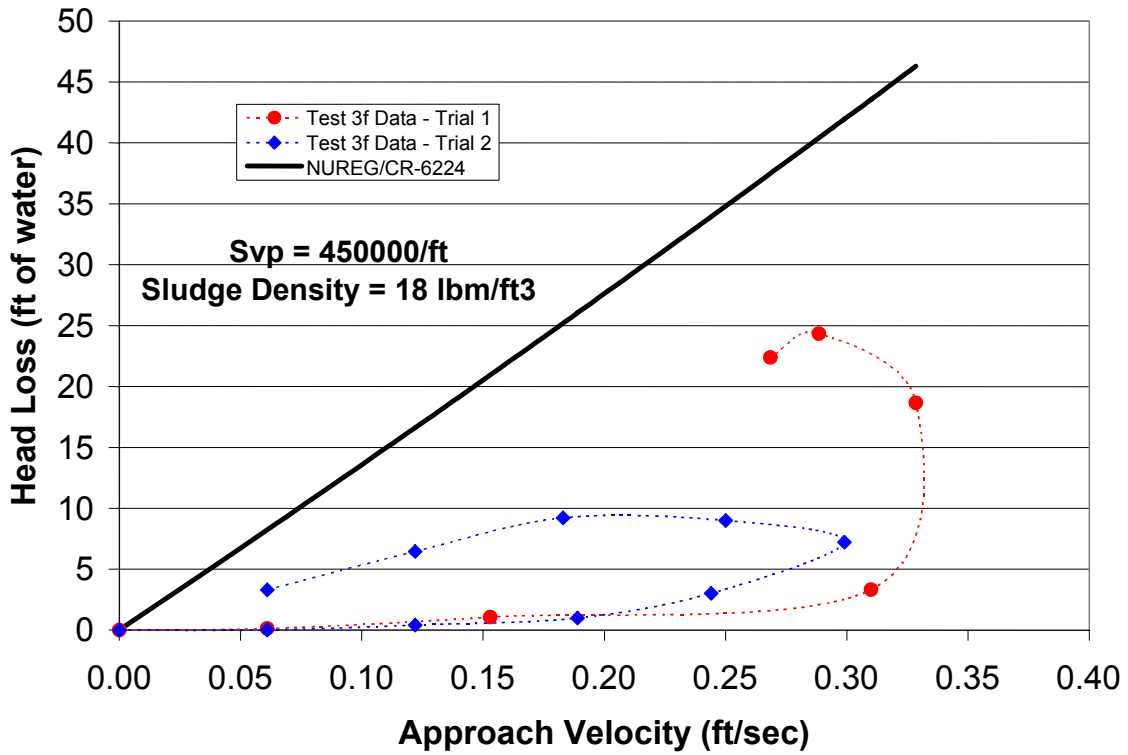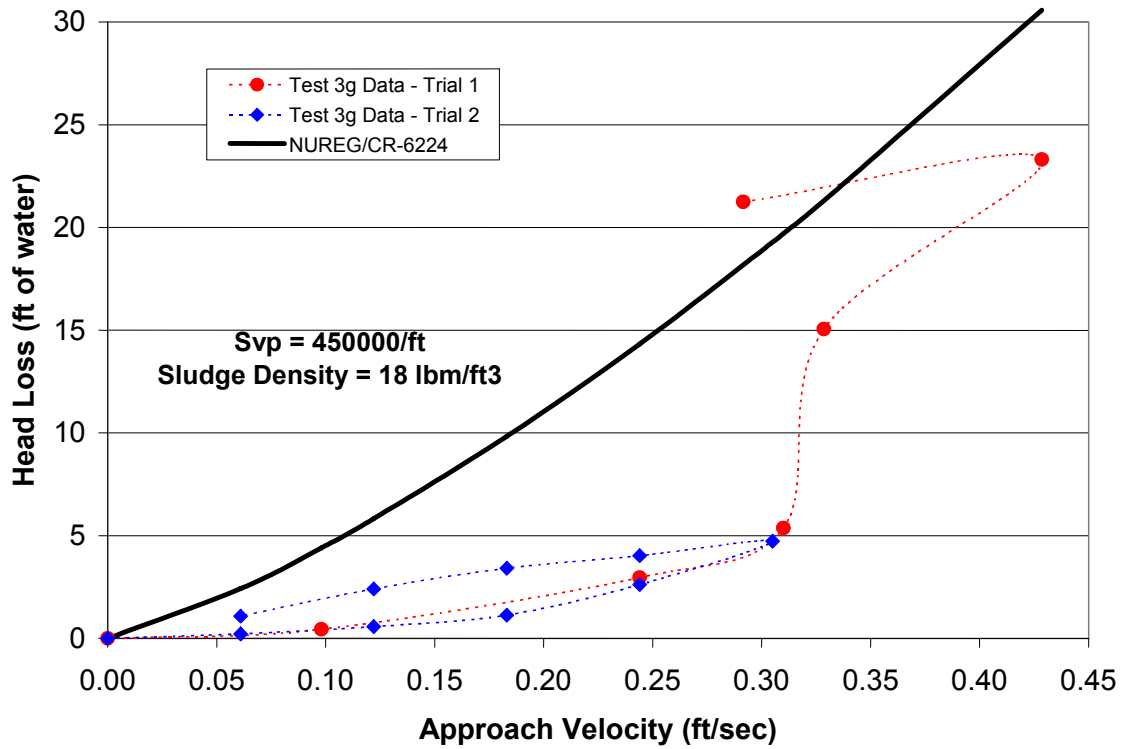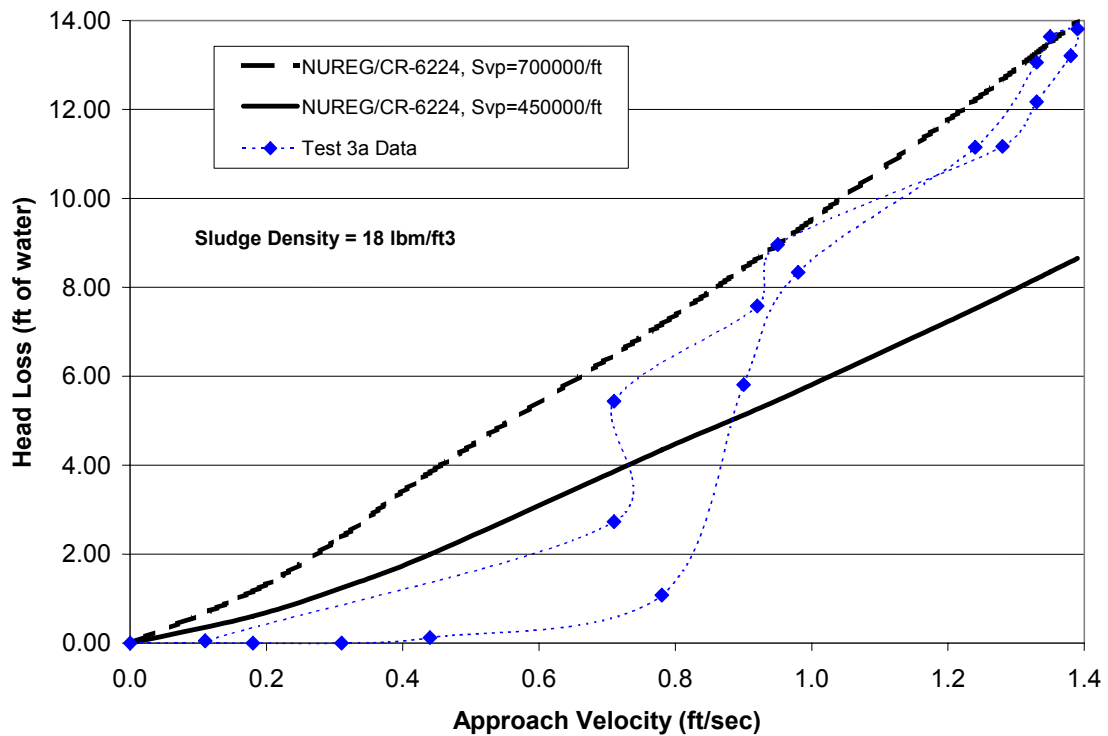


**Figure 4.16. Comparison of Test 3a with NUREG/CR-6224 correlation.**
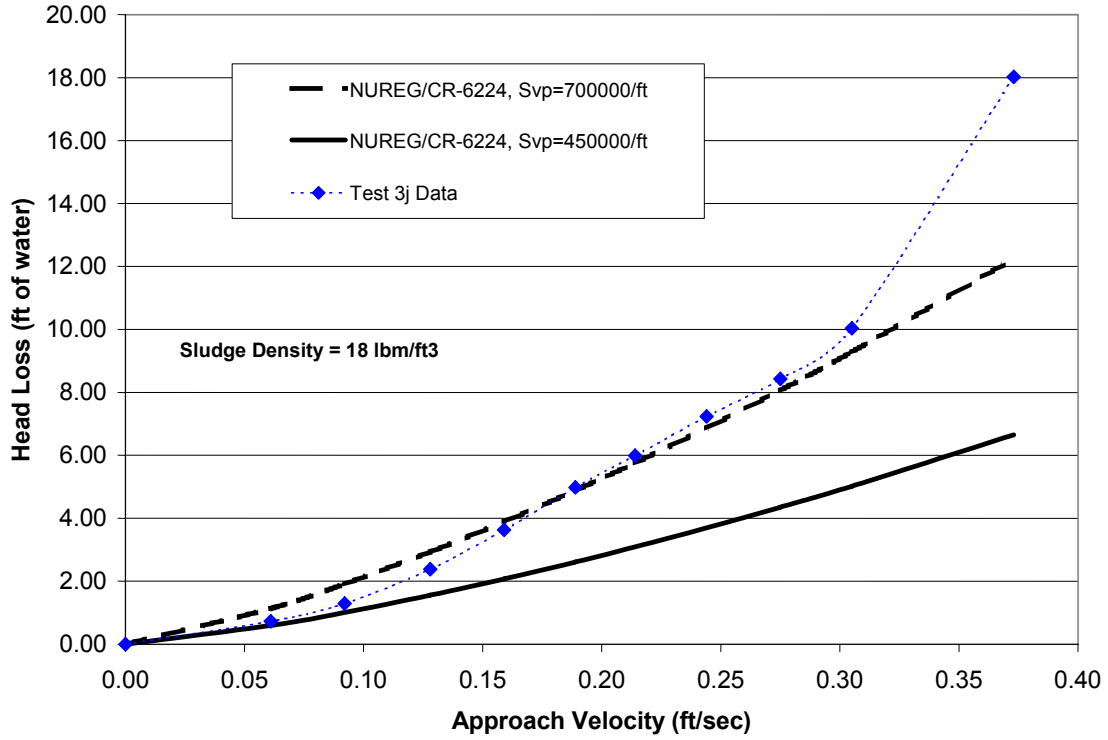
**Figure 4.17. Comparison of Test 3j with NUREG/CR-6224 correlation.**



**Figure 4.18. Photo of Test 3j debris bed.**

### 4.1.6. Debris Beds Formed of Only CalSil Debris

Six tests were conducted using only CalSil debris; those tests clearly show that CalSil debris can accumulate in a 1/8-in.-mesh screen and cause substantial head loss without the aid of another form of fiber. The test parameters included three quantities of CalSil (7.2, 58, and 116 g) both at room temperature and using heated water at the nominal temperature of 125°F. All of these debris beds were relatively thin; even the 116-g beds were only ~0.28 in. thick; therefore, substantial nonuniformities almost certainly occurred and the discrepancies noted when comparing the tests are likely due to these nonuniformities.

The best of the six tests appears to be Test 2f, where 116 g of CalSil was used (i.e., thicker bed) and heated water was used so that the CalSil more readily disintegrated (i.e., fewer lumps in the CalSil). The data from Test 2f are compared with the NUREG/CR-6224 correlation in Figure 4.19 using specific surface areas of 290,000/ft and 450,000/ft. It is likely that a portion of the screen was not covered by CalSil, much as Tests 2b and 2c show in the photos in Figure 3.9. Such gaps in coverage would explain the discrepancy in the comparison.

The other five CalSil-only tests compare substantially less well with the correlation when a specific surface area of 450,000/ft is used. The key results from the CalSil-only tests is the verification that CalSil without additional fibers will cause significant head loss on screens with meshes of 1/8 in. and certainly smaller meshes and possibly larger meshes.
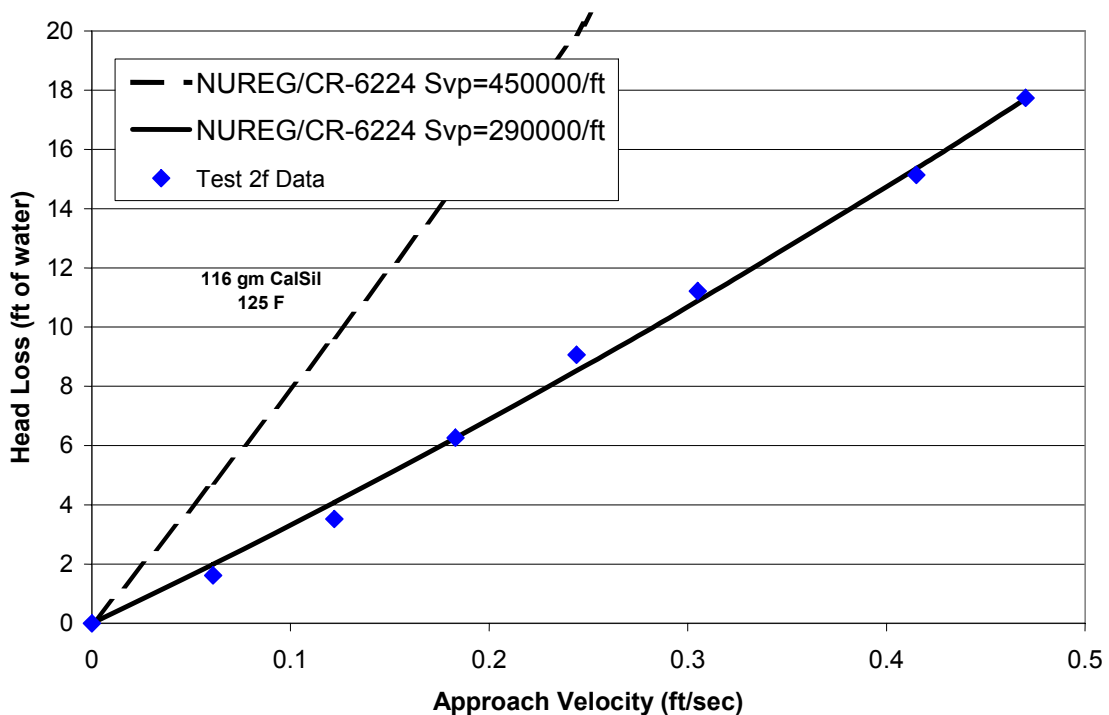


**Figure 4.19. Comparison of Test 2f with NUREG/CR-6224 correlation.**

### 4.2. Debris Beds Formed of RMI and RMI Combined with CalSil Debris

Predicting the hydraulic performance of debris beds composed of RMI and beds of mixed RMI and CalSil is also important to PWR applications. A correlation for RMI debris beds was developed by LANL based on published head-loss data for several types of RMI debris [Rao, 2003]. This correlation is compared with the UNM test data for RMI debris beds and beds of mixed RMI and CalSil. The LANL correlation takes the following form:

$$dH = \frac{1.56x10^{-5}}{K_t^2} U^2 \left( {A_{foil}} \middle/ {A_{screen}} \right) \quad ,$$

where  dH  =  head loss (in.-H$_2$O)
  K$_t$  =  interfoil gap thickness (ft)
  U  =  approach velocity (ft/s)
  A$_{foil}$  =  surface area of the RMI foils (ft$^2$)
  A$_{screen}$  =  debris screen surface area (ft$^2$).

The total surface area of the foil was estimated based on the measured debris mass used in each experiment:

A$_{foil}$ = 2 x (RMI mass) x ($\rho_{steel}$ / th)   ,

where  $\rho_{steel}$  =  488 lb/ft$^3$
  th  =  foil thickness = 2.5 mil.

The interfoil gap thickness is specific to a particular manufactured RMI design. In the current analysis, a value of 0.011 shows an excellent agreement with the data from the two RMI only debris tests, as shown in Figure 4.20. K$_t$ values for the 2.5-mil stainless-steel insulation used by US vendors range from 0.01 to 0.014 (ft), depending on the general size of the RMI debris, with the 0.01-ft value corresponding to smaller debris [Rao, 2003]. The RMI debris test data are well within the correlation parameters developed from earlier testing.
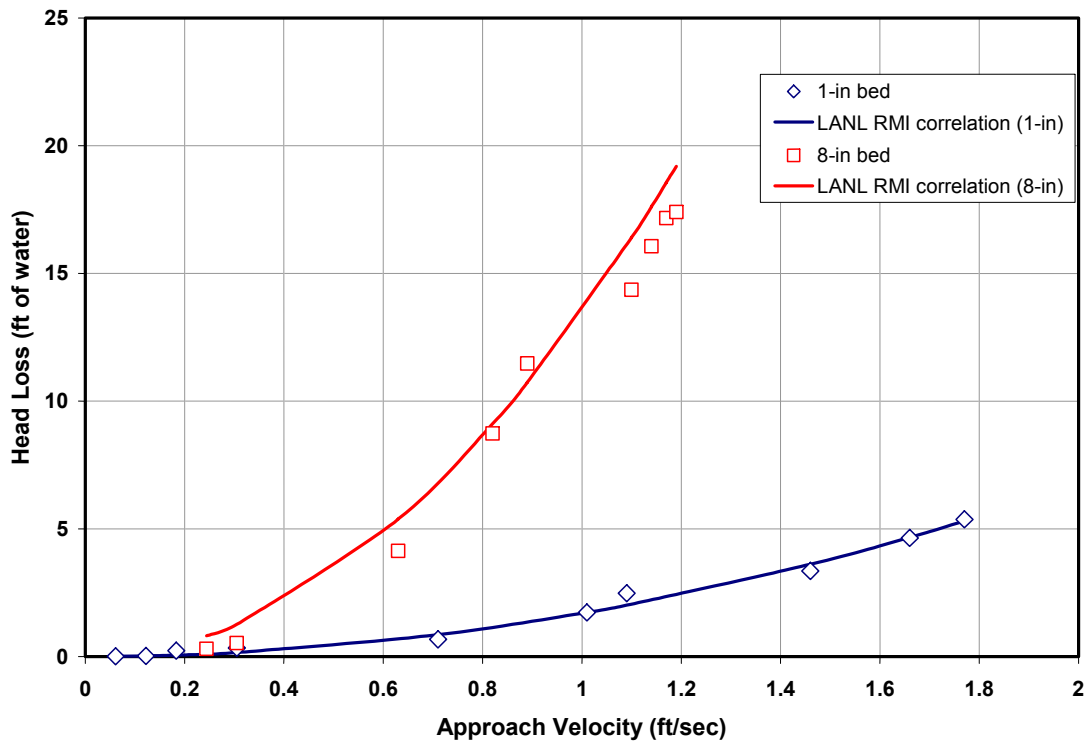


**Figure 4.20. Comparison RMI-only Tests 5a and 5b with LANL RMI correlation.**

Figures 4.21 and 4.22 compare the data for the mixed RMI/CalSil debris beds with the RMI-only debris and the correlation for the 1-in. and 8-in. debris beds, respectively. Research to date has not developed a predictive tool to estimate the head loss for a bed of RMI and CalSil debris. A realistic predictive model likely should account for the fraction of the CalSil that resides directly on the screen, thereby potentially forming an effective relative uniform layer that functions somewhat separate of the RMI. Much of the CalSil trapped within the RMI debris may be effectively removed from the actual flow through the RMI debris bed. However, it will be difficult to analytically estimate the fraction of the mixed-bed CalSil actually residing on the screen.

The method that has been used to estimate the head loss for fiberglass and RMI debris beds was to estimate the head loss for each component as though it were the only debris on the screen and then add the head losses together. Because the volume of RMI exceeds the volume of the CalSil by a wide margin, the head loss associated with the RMI is likely not significantly impacted by the CalSil unless the quantities of CalSil are excessive. The head loss associated with the CalSil would likely be overpredicted by assuming that it formed a uniform bed on the screen rather than being dispersed within the RMI (see Figure 3.24). Ordinarily, the sum of the two components should provide a conservative, or possibly overly conservative, estimate of the combined head loss.
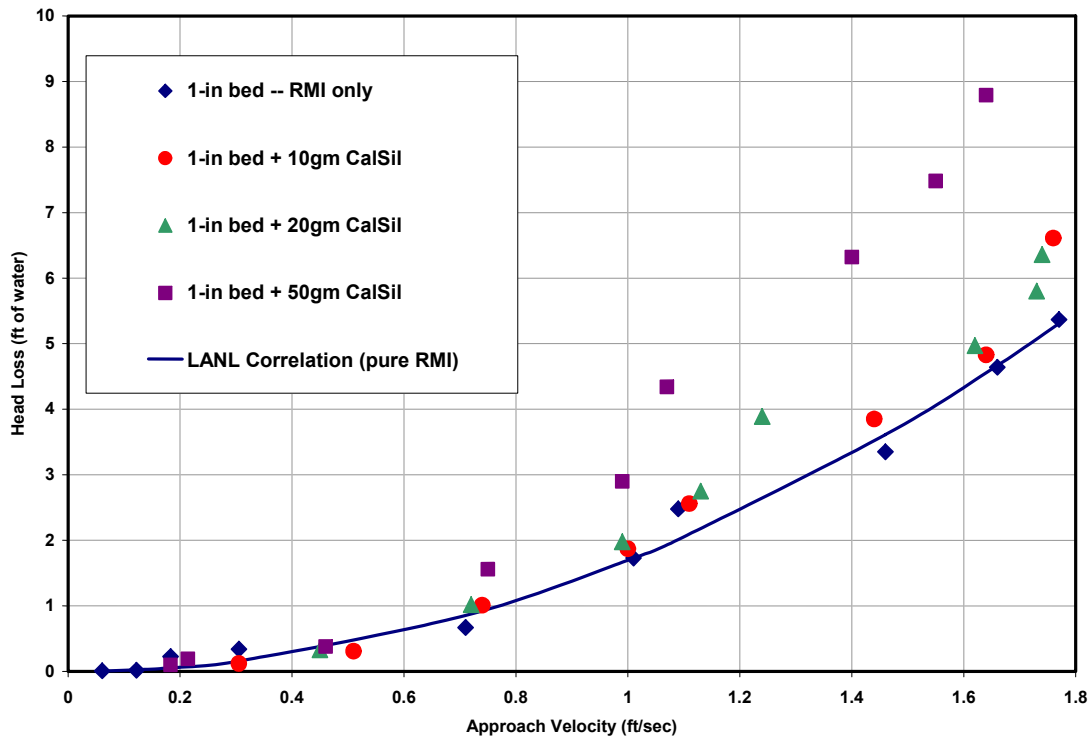


**Figure 4.21. Comparison Tests 5c, 5d, and 5e with LANL RMI correlation (1-in. RMI debris depth).**
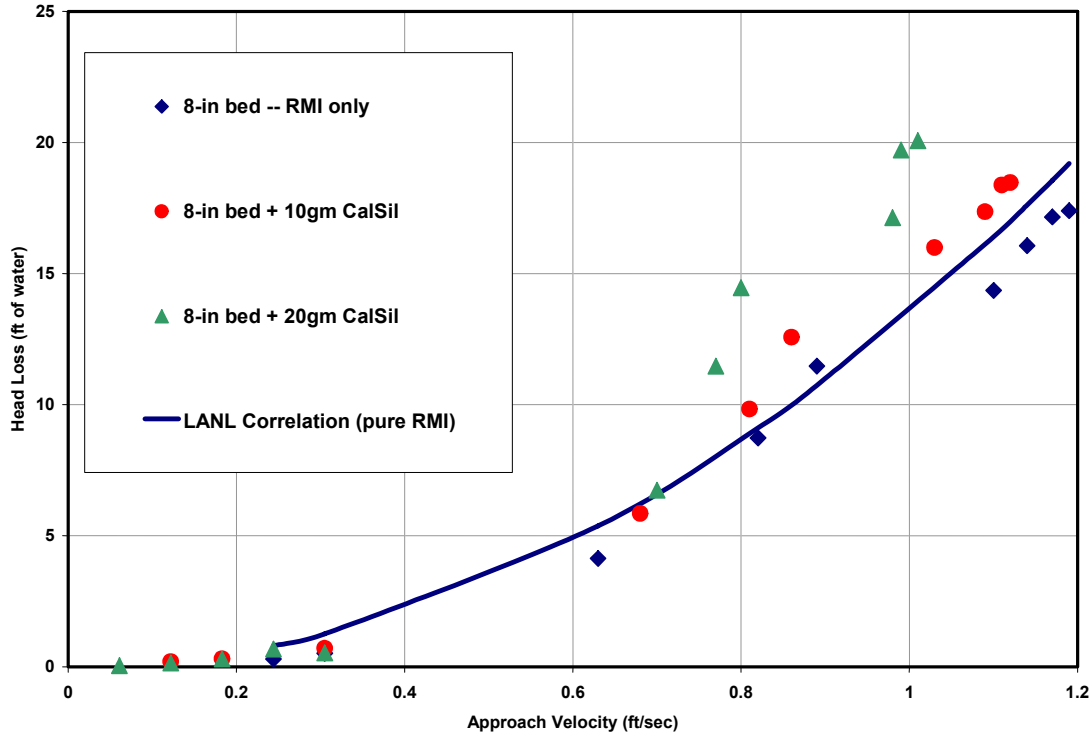
**Figure 4.22. Comparison Tests 5f and 5g with LANL RMI correlation
(8-in. RMI debris depth).**

## 5. REFINED HEAD-LOSS TESTING AND ANALYSIS

The analysis of the original series of CalSil head-loss tests identified in Table 2.2 illustrated sources of experimental error and gaps in the matrix. The results of the analysis of the original series discussed in Section 4 were inconclusive with respect to the appropriate input parameters to the NUREG/CR-6224 correlation. Thus, after modifying the experimental instrumentation, additional tests were performed to record the test data more thoroughly, and test procedures were improved to reduce the identified sources of uncertainties. The results of these additional CalSil tests have substantially improved the understanding of how the CalSil performs in a bed of fibrous debris.

### 5.1. Modifications to Experimental Apparatus and Test Procedures

The quality of each head-loss measurement depended on several parameters, including the uniformity and stability of the debris bed, the completeness of the particulate filtration, the stability of the flow, the stability of the head-loss measurement, and the minimization of air entrainment.

### 5.1.1. Instrumentation
The test instrumentation was upgraded so that time-dependent measurements of the debris-bed head loss, flow rate, and water temperature could be recorded on a computer and saved in spreadsheet format for analysis. However, the automatic recording of the flow rate was not available for the first few of these additional tests. In addition to the analytical benefits, the key advantage of the automatic recording capability was the ability to observe when quasi-steady-state conditions were achieved for each data point. The time-dependent temperature data facilitated the analytical correction for temperature drift due to continuous operational pump heating.

The data acquisition system included the Lab View 7.0 data acquisition software to store, process, save, and export the data. Along with the data acquisition software, a differential pressure transmitter, a

volumetric turbine flow meter, and a thermocouple were installed to complete the data acquisition system. The differential pressure transmitter (EW-68071-58) was supplied by Cole Parmer Industries. The sensors within the pressure transmitter allow wet/wet, wet/dry, or dry/dry connections. The volumetric turbine flow meter (A-05634-72), also supplied by Cole Parmer Industries, is a 2-in. turbine aluminum meter rated for 0 to 200 gal./min. A standard K-type unsheathed thermocouple was used without alterations because of built-in signal conditioning in the equipment. The thermocouple reading was verified with a mercury thermometer. The specification for these instruments is provided in Appendix E.

In addition, water-turbidity measurements (a measure of water clarity) were made throughout the testing. Water samples were tested to determine turbidity in Nephelometric turbidity units (NTU), which were calibrated to mass concentration of CalSil particulate. With the total water volume of the test loop measured (~76.5 gal.), the CalSil remaining in solution was estimated. The efficiency at which the NUKON™ fibers filtered the CalSil from the flow stream is an issue when testing with a fine particulate such as CalSil. The filtration efficiency was found to be a function of the compression of the fibrous bed, which affects the interfiber spacing. At low flow rates, the water generally appeared cloudy because of the CalSil that continuously passed through the bed; however, at higher velocities, the water clarity improved immensely.

### 5.1.2. Test Procedures

The primary improvements made to the test procedures involved the preparation of the debris. The debris bed in many of the original tests was not adequately uniform (e.g., Figure 3.17) and the CalSil contained lumps (e.g., Figure 3.9) that subsequently could erode, thereby altering the debris bed during the course of the tests, as well as contributing to nonuniformity. For the additional tests, the CalSil debris was prepared by pulverizing the CalSil in water until the particulate was a fine powder, thereby essentially eliminating CalSil lumps of a significant size in the debris bed, which is a likely form of CalSil debris accumulation.

The NUKON™ was first preprocessed through a common leaf shredder (as was the debris in the original test series). In the second preparation step, the shredded NUKON™ debris was processed in small batches through a household blender to further break up the debris into relatively fine debris. The fine debris was then subsequently boiled in water, as before, to eliminate air and to further break down the binding of the fibers. After the boiling process was completed, the pulverized CalSil was combined with the NUKON™ and mixed in a single bucket. The debris mixture was introduced into the test loop by slowly pouring the bucket contents into the top of the test section. The debris mixture was fine enough that it dispersed across the pipe cross section, thereby approaching the test screen relatively uniformly and subsequently producing a uniform debris bed. The revised test procedures also addressed refinements to the operation of the test loop to reduce perturbations to the flow and to retrieve the final debris bed relatively intact for subsequent drying and weighing.

### 5.2. Detailed Examination of the CalSil Insulation Debris

The CalSil insulation obtained from PCI was manufactured primarily from diatomaceous earth (DE) and lime in roughly equal portions (~90% of the total mixture). The DE is mostly silica and the lime is primarily calcium carbonate; however, miscellaneous compounds such as iron oxide were present in the DE and lime. Small quantities of fiberglass fibers and a binder were added for strength. The components were mixed, shaped, and baked, whereby the DE and lime reacted to form the CalSil in a porous crystal lattice structure that provides good insulation properties.

A series of scanning electron microscopy (SEM) photos were taken at various magnifications to provide insight into the structure of the debris. Photos showing magnification at 500 microns, 200 microns, and 20 microns are shown in Figures 5.1, 5.2, and 5.3, respectively. A scale is shown in the upper left corner of each photo; the length of the scale indicates the magnification dimension. The larger fibers measure ~10 to 15 microns across at their wider dimensions; however, the fibers do not appear circular but somewhat ribbon-like, with the narrower dimension significantly smaller than 15 microns. Smaller fibers also can be seen.

The CalSil particulate in the samples varies in dimension from sub-micron to perhaps 100 microns; however, the larger particulate seems to consist of an agglomerate of smaller particles such that the larger particulate could decompose into smaller particulate. Figure 5.3 indicates that substantial submicron particulate is possible and that the interior of the particulate contains fine voids.
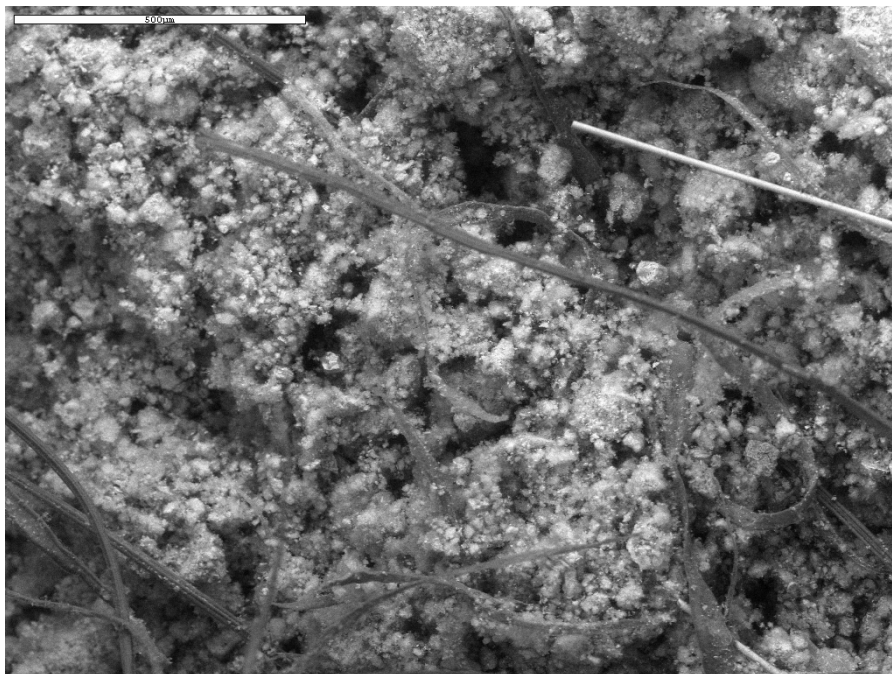


**Figure 5.1. SEM photo at a magnification of 500 microns.**
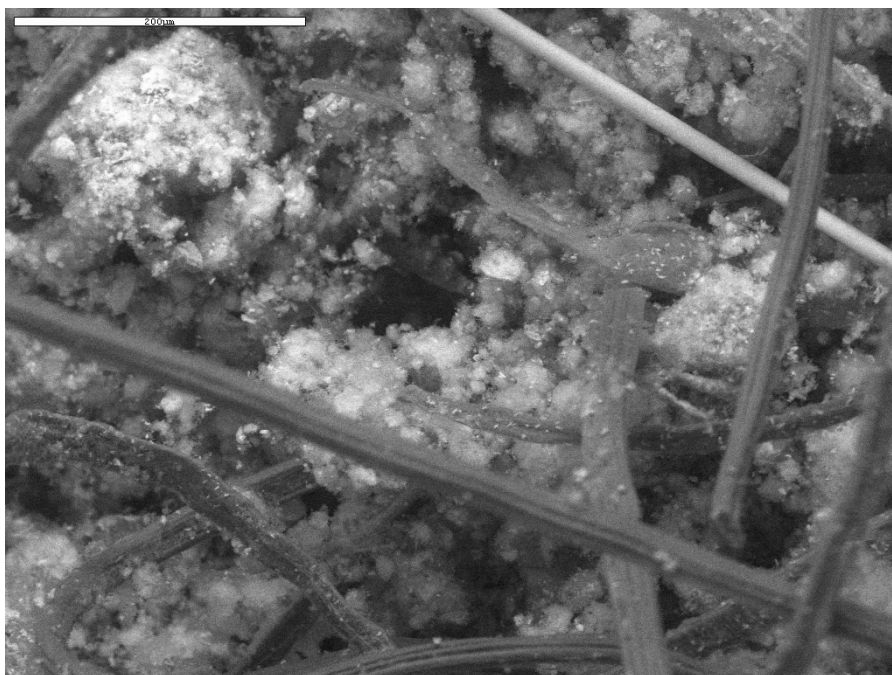


**Figure 5.2. SEM photo at a magnification of 200 microns.**
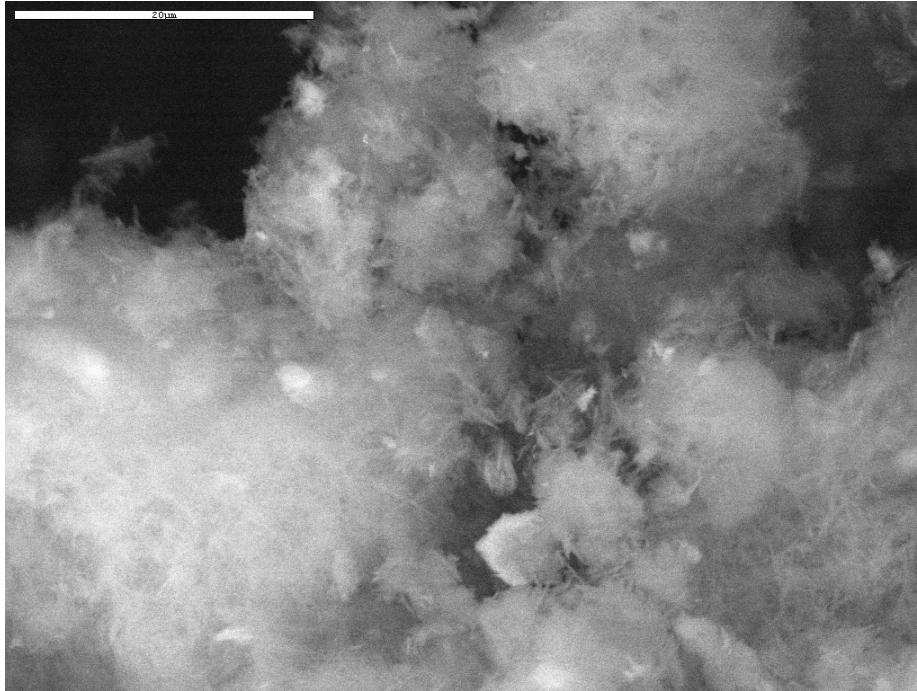
**Figure 5.3. SEM photo at a magnification of 20 microns.**

## 5.3. Particle Density Test

The properties of the CalSil that are required input to the NUREG/CR-6224 correlation include the particle density, the sludge density, and the specific surface area. The effective particle density for the particles and fibers in the CalSil debris was estimated by introducing a measured mass of CalSil debris into a beaker of water and then measuring the water displacement after sufficient time elapsed for trapped air to escape. This density was ~115 lbm/ft$^3$ and subsequently was used in the analyses. (Note that in Section 4, a density of 186 lbm/ft$^3$ was assumed.[11])

When applying the NUREG/CR-6224 correlation to debris beds containing CalSil, both the particle and fiber components of the CalSil were treated as particulate on the basis that the fibers that were integrated into the manufacture of CalSil insulation would not contribute significantly to the fiber behavior of the bed. Although it would be more appropriate to treat the CalSil fibers as bed fibers, it was necessary to treat them as particulate because the CalSil fibers cannot reasonably be separated from the particulate to determine their relative contributions and fiber-specific properties. Logic suggests that the fiber mass in the CalSil was substantially less than the mass of the NUKON™ fibers and that a portion of the CalSil fibers was significantly smaller and less significant than the NUKON™ fibers. Therefore, the CalSil fiber behavior contribution is considered insignificant relative to the NUKON™ fiber contribution.

In the same property test, the volume of CalSil debris that settled in the bottom of the beaker provided a rough estimate of the sludge density (~12 lbm/ft$^3$) when the debris was not subjected to the force of flow. The sludge density is anticipated to increase significantly under the force of flow; however, this number must be deduced from the head-loss test data. The density of the CalSil insulation, as manufactured, was estimated by the manufacturer as ~14.5 lbm/ft$^3$. To complicate the matter further, the effective sludge density of the CalSil particles, when compacted in a debris bed, may consist of a concentration of the non-fiber particulate that could exceed the sludge density measured with fibers present. Therefore, an effective sludge density was determined by deduction from the head-loss test data, i.e., a density that allowed the NUREG/CR-6224 correlation to reasonably well predict the data.

---

[11] The overestimate of the particle density resulted in an underestimate in the specific surface area.

### 5.4. Test Matrix

A total of ten additional head-loss tests were conducted in the closed-loop facility; however, two of those tests failed to produce useful data and two provided useful information but incomplete results. Six of the tests provided quality head-loss data. The parameters of these tests are shown in Table 5.1.

**Table 5.1. Test Matrix for the Additional CalSil Head-Loss Tests**

| Test | Mass* of NUKON™ Debris (g) | Mass* of CalSil Debris (g) | Relative Quality of Test |
|---|---|---|---|
| 6B | 100 | 55 | Complete and quality data |
| 6C | 12 | 6 | Quality data until the bed was disrupted by the force of flow |
| 6E | 70 | 35 | Complete and quality data |
| 6F | 40 | 20 | Complete and quality data |
| 6G | 15 | 7.5 | Water leak contributed to a loss of control |
| 6H | 15 | 7.5 | Complete and quality data |
| 6I | 55 | 27.5 | Complete and quality data |
| 6J | 18 | 9 | Pressure data were questionable |
| Data taken for Tests 6A and 6D were not useful. The CalSil-to-NUKON™ mass ratio was 0.5 for all tests except Test 6B, which was 0.55. | | | |

\* Masses introduced into the test assembly.

### 5.5. Head-Loss Test Results and Analysis

The parameters most affecting the magnitude of the head loss across the debris beds were the bed thickness and the bed porosity. The thickness of the bed depended on the quantity of debris in the bed. The porosity depended primarily on the compression of the bed, which in turn, depended on the flow velocity and the debris-bed resistance to flow. When the debris bed became sufficiently compressed that the particulate between the fibers interacted to form a CalSil sludge, further compression was limited by the density of the sludge and the porosity of the debris bed decreased significantly. This condition occurred in the thin-bed tests 6C, 6G, and 6H and possibly in 6J. In Tests 6B, 6E, 6F, and 6I, the compression was controlled by the fibrous debris throughout the test; the peak flow rates in each of these tests were not sufficient to reach the sludge density limiting condition.

Additional tests were conducted using a particulate-to-fiber mass ratio of 0.5 because the original set of head-loss tests showed that this ratio led to higher quality tests. When the higher mass ratios of 1.0 and 2.0 were used, the associated head losses sometimes tended to overpower the experimental apparatus and it was much more difficult to get the CalSil to filter adequately from the flow. In all of the tests except Test 6A, the debris-bed formation was more than adequately uniform, as illustrated by test photos. The difficulties encountered in forming the debris bed in Test 6A led to the household-blender approach to preparing the debris for the test. In all of the tests, the measurement of the water clarity (turbidity) reflected the visual observation of the water clarity as the CalSil was filtered from the flow. Overall, the turbidity measurements provided good qualitative information regarding the filtration process; however, the measurements could not be used to adequately adjust the mass of CalSil in the debris bed for the comparison of the NUREG/CR-6224 correlation to the head-loss data. The results and analyses for each of these tests are presented in the following order: 6B, 6E, 6I, 6F, 6C, 6H, 6G, and 6J. The raw data for these tests are presented in Appendix F.

### 5.5.1. Test 6B
The debris bed in Test 6B, shown in Figure 5.4, was formed very uniformly using 100 g of NUKON™ and 55 g of CalSil debris and appeared to fit the transparent pipe snugly around the edges of the bed. Leakage (debris-bed bypass flow) was not apparent. The head loss, flow, and temperature data were well behaved.
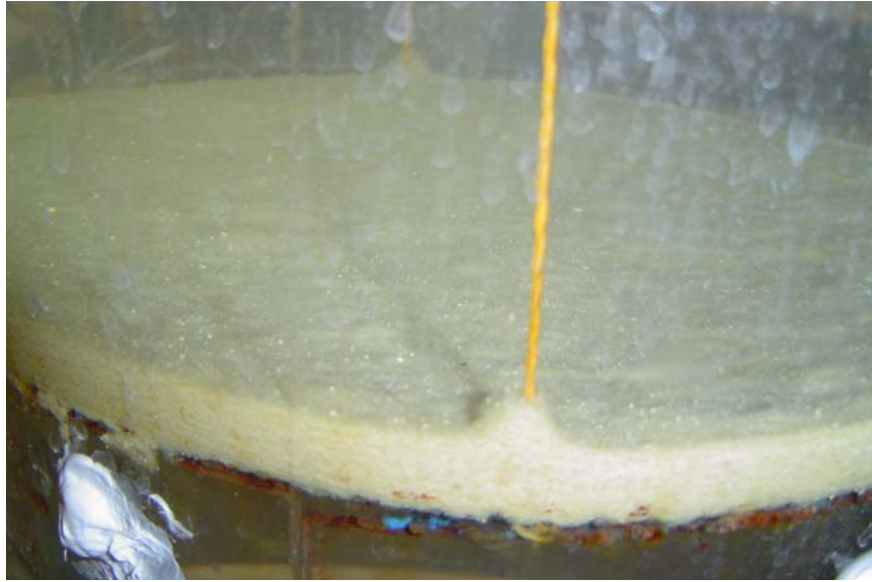
**Figure 5.4. NUKON™ and CalSil debris bed in Test 6B.**

The head-loss data for Test 6B are compared with the NUREG/CR-6224 correlation in Figure 5.5, where the CalSil specific surface area was adjusted until the correlation predicted the data point at the highest velocity tested. In this correlation prediction, the entire 55 g of CalSil was assumed to have accumulated in the debris bed, and the water temperature was the temperature at the highest velocity tested (111°F). The specific surface area that predicted the highest velocity data point was 543,000/ft. The head-loss data taken with both increasing and decreasing velocities are shown. At the highest velocity of 0.23 ft/s with an associated head loss of 20.5 ft, the limits of the apparatus had been reached because the piping had begun to vibrate sufficiently to generate a safety concern.

The turbidity measurements indicated that ~91% of the CalSil was filtered from the flow at a velocity of 0.1 ft/s and that ~99% of the CalSil was filtered at the higher velocities. Adjusting the correlation prediction to reduce the CalSil measured in solution does not correct for the differences between the prediction and the data, yet these differences appear related to the filtration efficiency in that the more compressed the fibers become with increasing velocities, the more efficient the filtration. The larger particles would be expected to be filtered out first, followed by the smaller particles. Further, the smaller particles would contribute more to the specific surface area and the head loss on a per-unit mass basis than would the larger particles. Logic suggests that if 1% of the CalSil by mass is still in solution, then something greater than 1% of the specific surface area contribution is still in solution. Thus, a significant part of the disagreement between the NUREG/CR-6224 correlation and the data was likely due to incomplete filtration of the CalSil; however, the data for this test were inconclusive regarding this point. Although the turbidity measurements provided qualitative insights into the CalSil filtration, the uncertainty of the measurements at these low mass concentrations and the nonlinearity of the specific surface area and filtration efficiency with particle size prevented the use of the turbidity measurements to correct predictions of head-loss data by simply adjusting for the CalSil still in solution. Thus, the best head-loss data points for estimating the specific surface area for CalSil are those points with the highest water clarity.
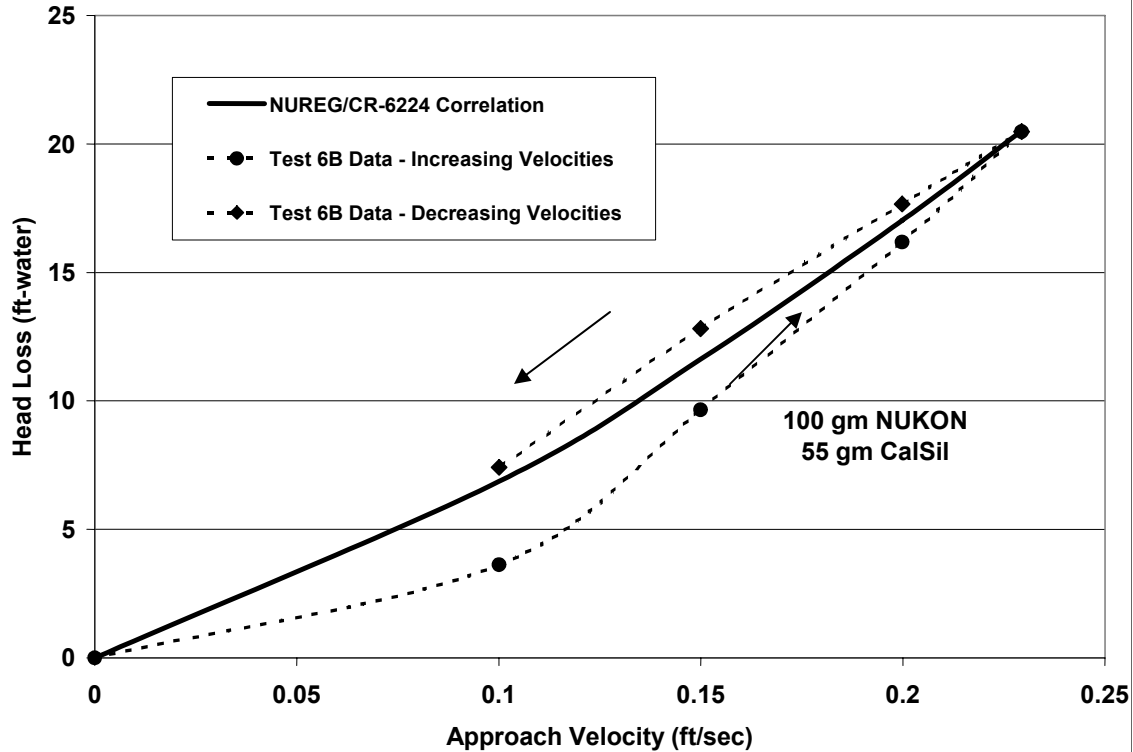
**Figure 5.5. Comparison of NUREG/CR-6224 correlation with Test 6B head-loss data.**

The debris-bed uniformity for Test 6B was adequate and the bed thickness was sufficient to measure the bed thickness at the various velocities for comparison with the NUREG/CR-6224 correlation prediction of the compression. However, exacting measurements of the bed thickness were not possible because of a slight circumferential variance and the interaction of the debris bed with the screen; i.e., some of the debris was partially forced into the screen mesh. The measured bed thickness had perhaps a 1/8-in. uncertainty for this test. Based on the as-manufactured density (2.4 lbm/ft$^3$), the thickness of this debris bed was 1.6 in. The correlation-predicted bed thicknesses are compared with the measured thickness in Figure 5.6; this comparison is reasonably good, thus adding to the confidence in applying the correlation.

The debris bed in Test 6B did not expand with decreasing velocity at the same rate as it compressed with increasing velocity, i.e., a hysteresis effect. In addition, the turbidity measurements indicated that most of the CalSil filtered from the flow remained in the bed as the velocity was decreased. Note that the correlation prediction cannot be compared with the decreasing-velocity head-loss data because the correlation would predict the expansion according to its compressibility function. To predict the decreasing-velocity data, the correlation compression must be fixed at the compression associated with the highest velocity.

### 5.5.2. Test 6E

The debris bed in Test 6E was formed very uniformly using 70 g of NUKON™ and 35 g of CalSil debris. The debris bed for this test was similar to that of Test 6B, only a little thinner; it also appeared to fit the transparent pipe snugly around the edges of the bed, leakage was not apparent, and the head loss, flow, and temperature data were well behaved. The thickness of this debris bed, based on the as-manufactured density, was 1.1 in.
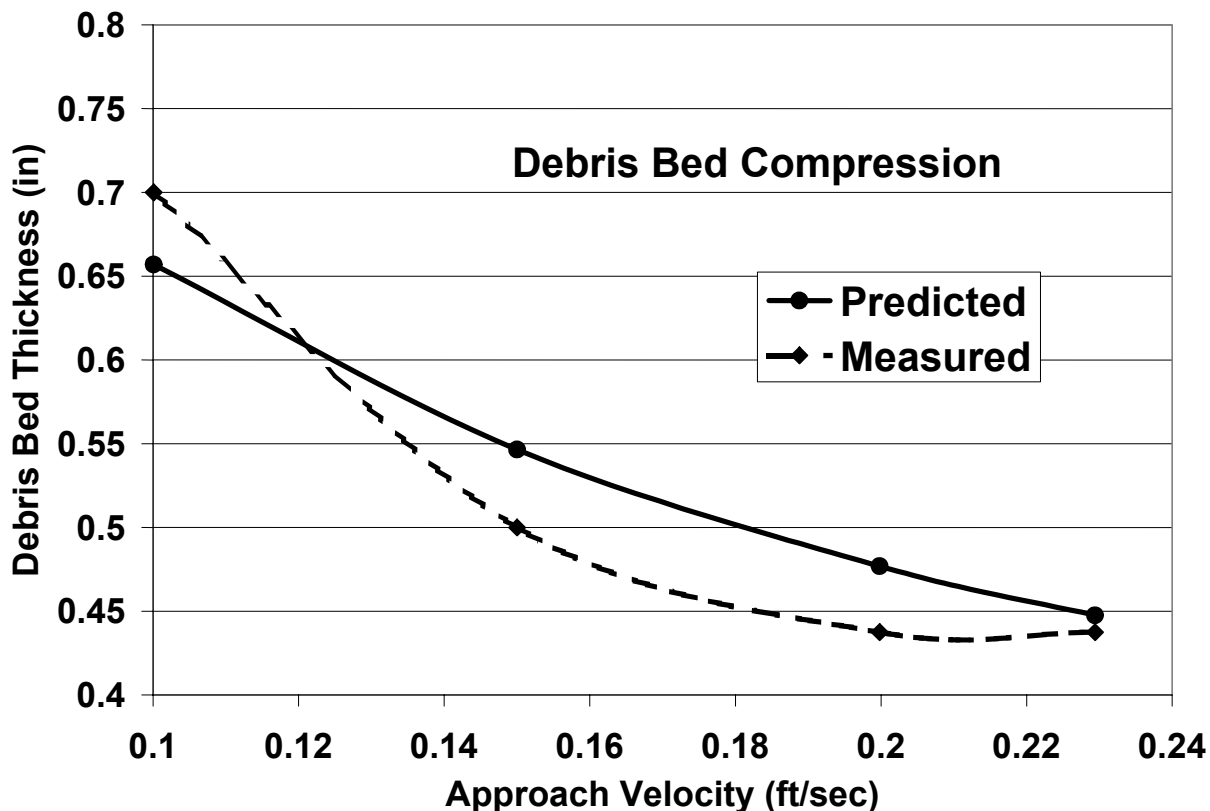
**Figure 5.6. Comparison of NUREG/CR-6224 correlation with Test 6B bed thickness.**

The head-loss data for Test 6E are compared with the NUREG/CR-6224 correlation in Figure 5.7, where the CalSil specific surface area again was adjusted until the correlation predicted the data point at the highest velocity tested. In this prediction, the entire 35 g of CalSil was assumed to have filtered from the debris bed and the water temperature for this data point was 129°F. The specific surface area that predicted the highest velocity data point was 423,000/ft. Head-loss data associated with both increasing and decreasing velocities are shown. At the highest velocity of 0.39 ft/s with the associated head loss of 14.3 ft, the flow regulation valve was fully open, with the flow passing through the small flow meter (2-in. pipe). A higher flow could have been achieved by switching to the large flow meter (6-in. pipe with less flow resistance); however, the transition would have put the integrity of the debris bed at an unnecessary risk. If the head-loss measurements had been taken at higher flow rates, a larger value for the specific surface area might have been determined.

The turbidity measurements indicated that less than 1% of the CalSil was still in solution after the approach velocities exceeded 0.2 ft/s, and the water clarity was good. The hysteresis effect for this test was much less pronounced than that of Test 6B. The turbidity measurements indicated that most of the CalSil that was filtered from the flow remained in the bed when the velocities were decreased. The measured bed thicknesses again compared well with the NUREG/CR-6224 correlation.

### 5.5.3. Test 6I
The debris bed in Test 6I was formed uniformly using 55 g of NUKON™ and 27.5 g of CalSil debris. The debris bed for this test was similar to that of Tests 6B and 6E, only thinner; it appeared sound, and no leakage was apparent. The head loss, flow, and temperature data were well behaved, except perhaps the first three head-loss measurements, which appeared to be somewhat high for no apparent reason. Based on the as-manufactured density, the thickness of this debris bed was 0.86 in.
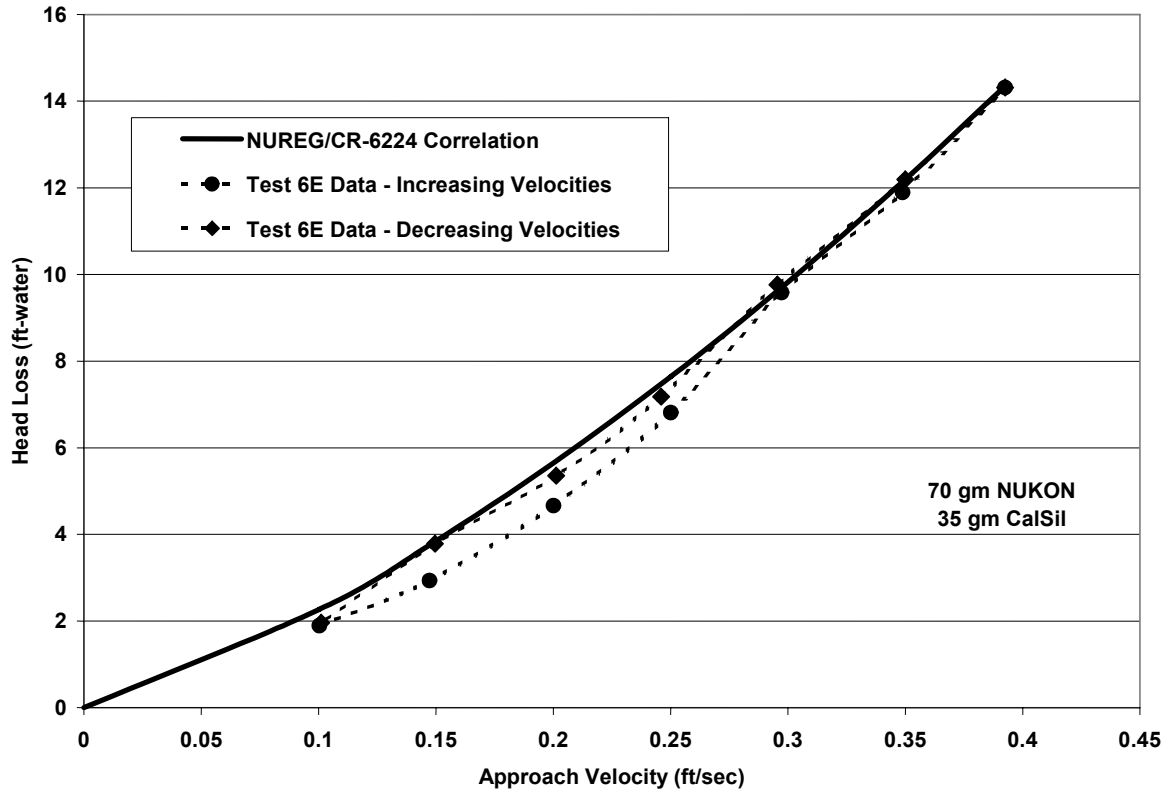
**Figure 5.7. Comparison of NUREG/CR-6224 correlation with Test 6E head-loss data.**

The head-loss data for Test 6I are compared with the NUREG/CR-6224 correlation in Figure 5.8, where the CalSil specific surface area again was adjusted until the correlation predicted the data point at the highest velocity tested. In this prediction, the entire 27.5 g of CalSil was assumed to have filtered from the debris bed, and the water temperature for this data point was 138°F. The specific surface area that predicted the highest velocity data point was 382,000/ft. The head-loss data associated with both increasing and decreasing velocities are shown. At the highest velocity of 0.46 ft/s with an associated head loss of 10.8 ft, the flow regulation valve was fully open, with the flow passing through the small flow meter (2-in. pipe).

The turbidity measurements indicated that less than 1% of the CalSil was still in solution after the approach velocities exceeded 0.3 ft/s, and the water clarity was good. The hysteresis effect was not in evidence for this test. The measured bed thicknesses compared well with the NUREG/CR-6224 correlation. The turbidity measurements indicated that most of the CalSil filtered from the flow remained in the bed when the velocities were decreased.

**Figure 5.8. Comparison of NUREG/CR-6224 correlation with Test 6I head-loss data.**

### 5.5.4. Test 6F

The debris bed in Test 6F was formed uniformly using 40 g of NUKON™ and 20 g of CalSil debris. Similar to the preceding tests, the debris bed was uniform and appeared sound, and no leakage was apparent. The head loss, flow, and temperature data were well behaved. Based on the as-manufactured density, the thickness of this debris bed was 0.63 in.

The head-loss data for Test 6F are compared with the NUREG/CR-6224 correlation in Figure 5.9, where the CalSil specific surface area again was adjusted until the correlation predicted the data point at the highest velocity tested. In this prediction, the entire 20 g of CalSil was assumed to have filtered from the debris bed, and the water temperature for this data point was 140°F. The specific surface area that predicted the highest velocity data point was 506,000/ft. The head-loss data associated with both increasing and decreasing velocities are shown. At the highest velocity of 0.44 ft/s with an associated head loss of 11.4 ft, the flow regulation valve was fully open, with the flow passing through the small flow meter (2-in. pipe).

The turbidity measurements indicated that less than 1% of the CalSil was still in solution after the approach velocities exceeded ~0.35 ft/s, and the water clarity was good. A small hysteresis effect was evident. The measured bed thicknesses compared reasonably well with the NUREG/CR-6224 correlation; however, the uncertainty in the measured thickness was now more pronounced. The turbidity measurements indicated that most of the CalSil filtered from the flow remained in the bed when the velocities were decreased.

**Figure 5.9. Comparison of NUREG/CR-6224 correlation with Test 6F head-loss data.**

### 5.5.5. Test 6C

The debris bed in Test 6C was formed uniformly using 12 g of NUKON™ and 6 g of CalSil debris. With 12 g of NUKON™, the nominal as-manufactured debris-bed thickness was only 3/16 in.; however, the bed appeared sound, no leakage was apparent, and the head loss, flow, and temperature data were reasonably well behaved. A photo of the debris bed is shown in Figure 5.10. The debris bed was disturbed slightly when the flow control transitioned from the small to the large flow meter loop, which occurred at a flow velocity of 0.5 ft/s. The disturbance then appeared to settle back into place with no apparent effect on the head-loss data. When the flow was increased beyond a velocity of 0.8, the debris bed developed sizeable holes (splits in the debris bed); therefore, any data taken at this point were not useful. The highest useful velocity was 0.81 ft/s, with an associated head loss of 9.0 ft.

The debris bed in Test 6C differed from the previous Tests 6B, 6E, 6F, and 6I in that the debris bed appeared to have compacted to the point where further compaction was limited by the sludge or granular density of the CalSil particulate. Therefore, the application of the NUREG/CR-6224 correlation to the head-loss data requires the specification of both the specific surface area and the sludge density. The head-loss data for Test 6C is compared with the NUREG/CR-6224 correlation prediction in Figure 5.11. Noting that the test head loss increased rapidly between the velocities of 0.5 and 0.58 ft/s, the compaction limiting is reasonably assumed to have occurred during this transition, which corresponds to a substantial reduction in the bed porosity and an increase in the bed filtration efficiency. In the correlation prediction shown in Figure 5.11, the sludge density was adjusted until compaction limiting was predicted between these two velocities and the CalSil specific surface area was adjusted until the correlation predicted the higher velocity data points. In this prediction, the entire 6 g of CalSil was assumed to have filtered from the debris bed, and the water temperature for this data point was 126°F. The sludge density for this prediction was 17.8 lbm/ft$^3$ and the specific surface area was 525,000/ft.

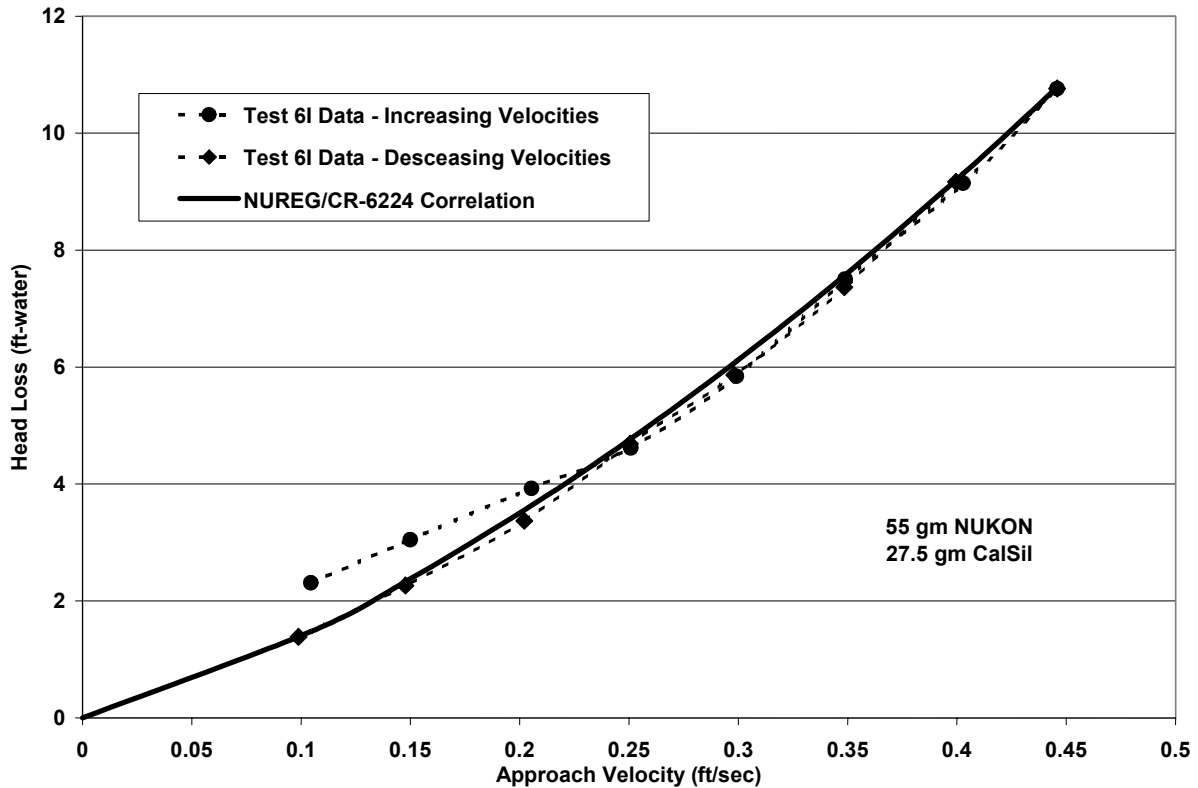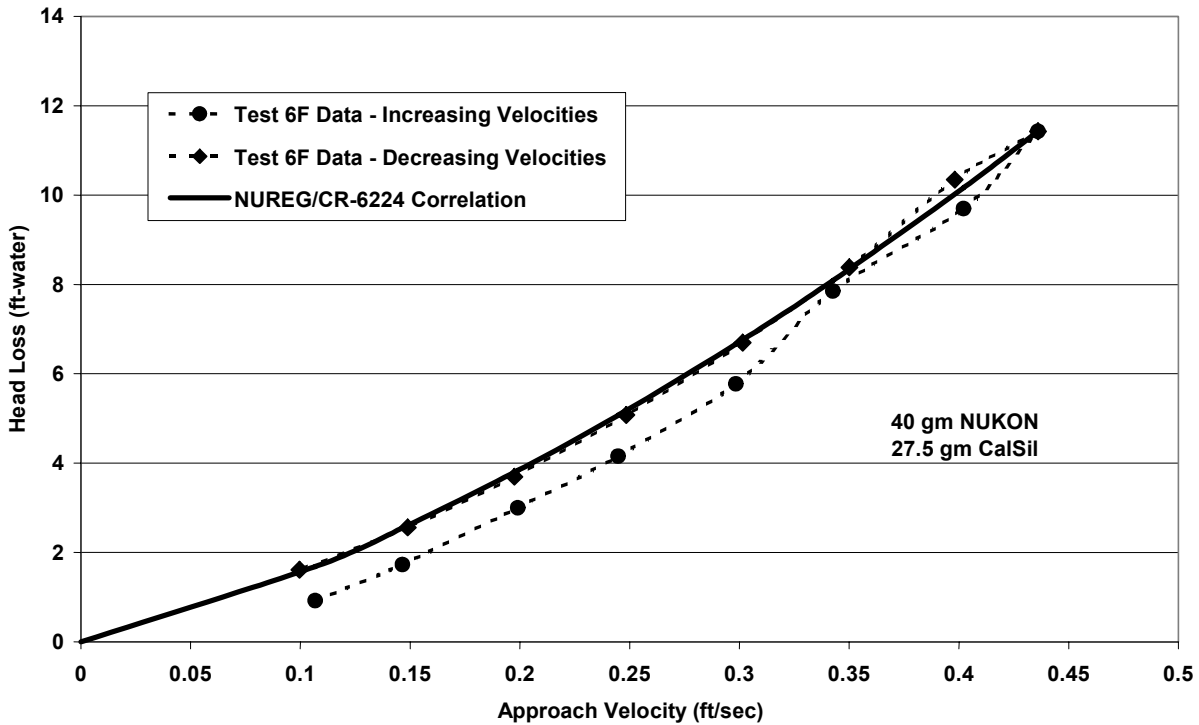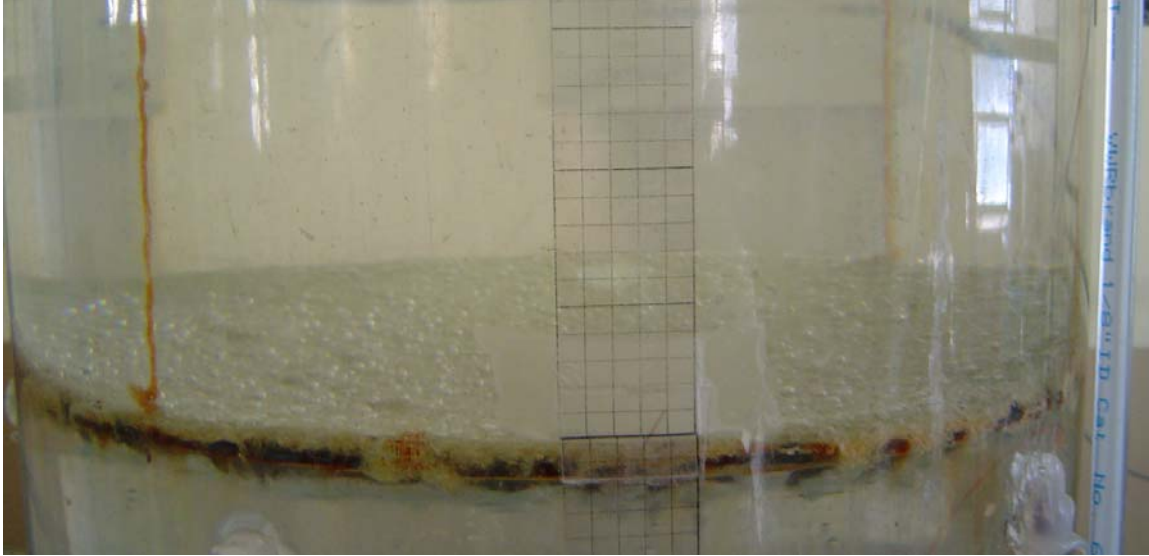Figure 5.10. NUKON<sup>TM</sup> and CalSil debris bed in Test 6C.
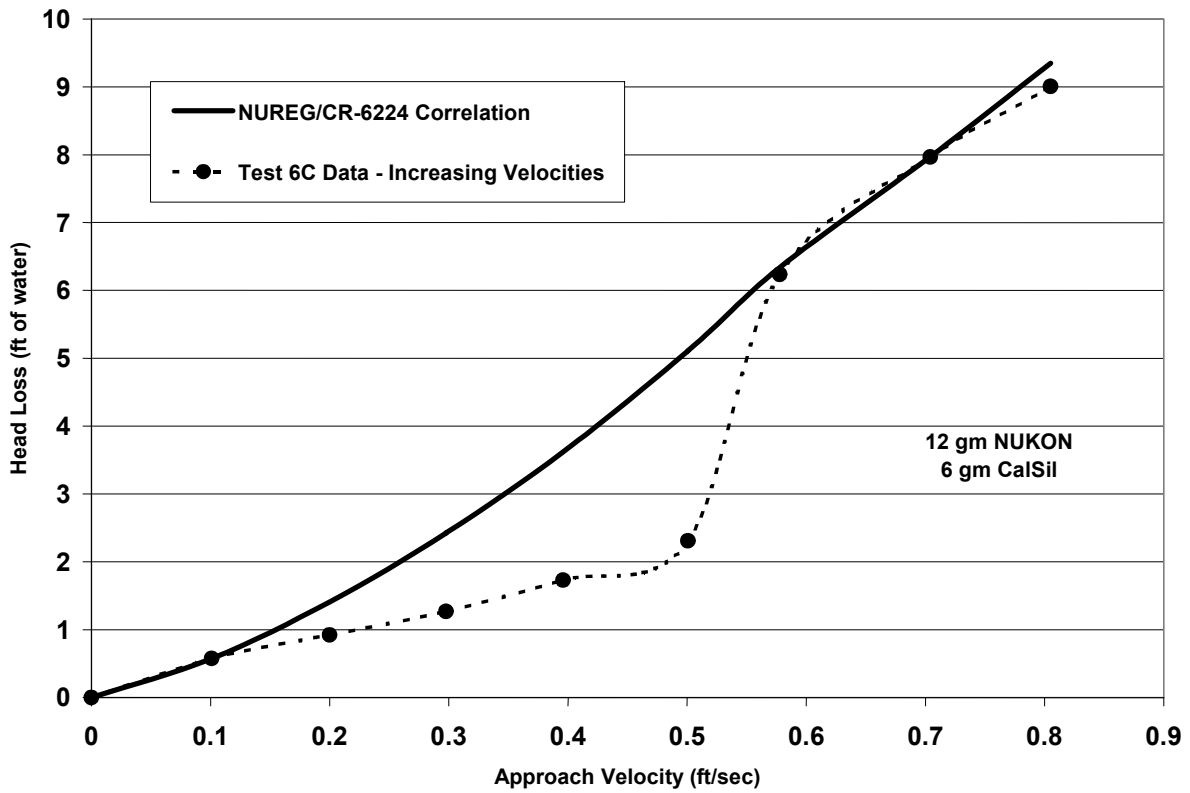


Figure 5.11. Comparison of NUREG/CR-6224 correlation with Test 6C head-loss data.

### 5.5.6. Test 6H

The debris bed in Test 6H was formed uniformly using 15 g of NUKON™ and 7.5 g of CalSil debris. With 15 g of NUKON™, the nominal as-manufactured debris-bed thickness is 0.23 in., the bed appeared sound and no leakage was apparent, and the head loss, flow, and temperature data were well behaved. A photo of the debris bed is shown in Figure 5.12.
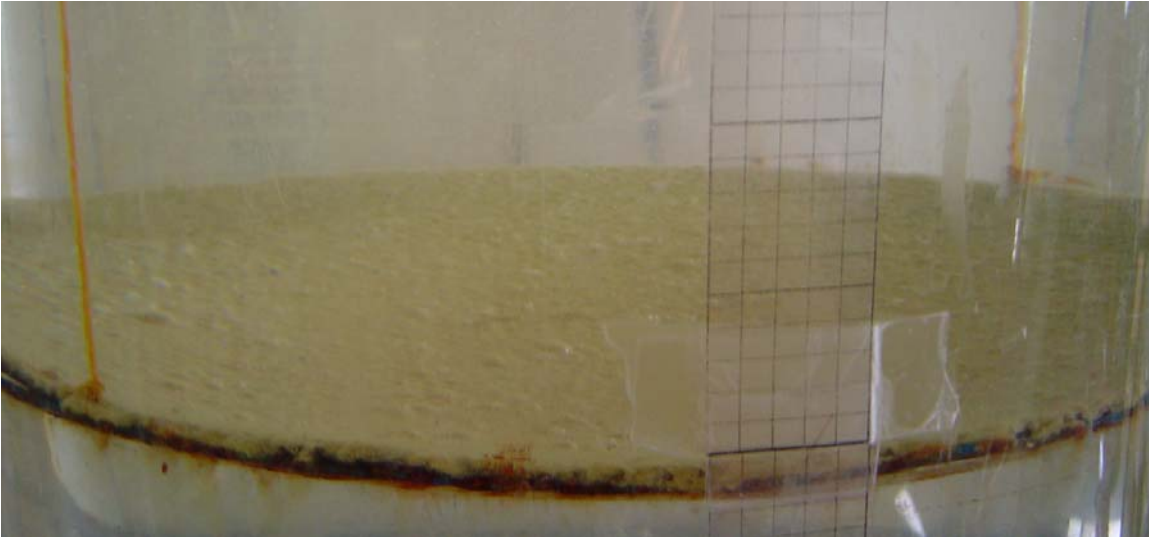


**Figure 5.12. NUKON™ and CalSil debris bed in Test 6H.**

Similar to Test 6C, the debris bed in Test 6H appeared to have compacted to the point where further compaction was limited by the sludge or granular density of the CalSil particulate. Therefore, the application of the NUREG/CR-6224 correlation to the head-loss data requires the specification of both the specific surface area and the sludge density. The head-loss data for Test 6H are compared with the NUREG/CR-6224 correlation prediction in Figure 5.13. The rapid increase in head loss between the velocities of 0.35 and 0.40 ft/s strongly indicated that the bed porosity decreased substantially because of bed compaction. With the decrease in porosity came a corresponding increase in the bed filtration rate and the entrapment of the finer particulate. Also, the bed compaction became limited during this transition, which was probably caused by the granular density of the CalSil.

In the correlation prediction shown in Figure 5.13, the sludge density and the specific surface area were adjusted until the correlation reasonably well simulated the highest head-loss data points. The sludge density for this prediction was 22 lbm/ft$^3$ and the specific surface area was 800,000/ft. In this prediction, the entire 7.5 g of CalSil was assumed to have filtered from the debris bed and the water temperature for this data point was 111°F. The head-loss data associated with both increasing and decreasing velocities are shown. At the highest velocity of 0.41 ft/s with an associated head loss of 13.0 ft, the flow regulation valve was fully open, with the flow passing through the small flow meter (2-in. pipe).

The head losses per unit thickness of bed associated with Test 6H were substantially more severe than the other tests. The high head losses occurred at a lower velocity than those of Test 6C (both of these tests were thin-bed debris-bed tests). Although the head losses associated with Test 6B were actually higher and at a lower velocity, Test 6B contained 100 g of NUKON™ in the bed compared with the 15 g for Test 6H. Test 6H is the worst-case test of the additional tests and the NUREG/CR-6224 simulation indicates the highest estimate for the specific surface area.
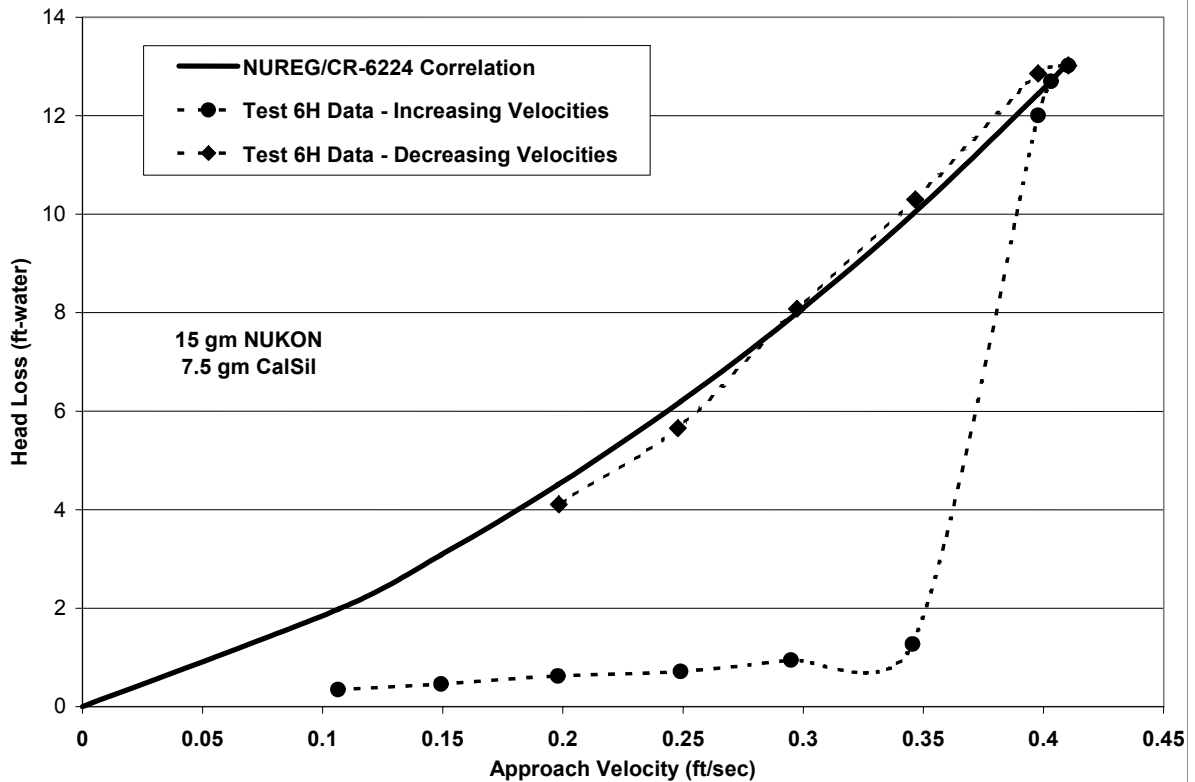
**Figure 5.13. Comparison of NUREG/CR-6224 correlation with Test 6H head-loss data.**

The relatively high head losses in Test 6H were caused either by increased filtration of the CalSil from the flow or by a significant reduction in the bed porosity due to the packing of the debris, or both. A reduced porosity would cause an increase in the filtration of the very fine particulate, thereby increasing the particulate specific surface area and head loss; however, filtration alone probably could not be responsible for the high predicted specific surface area. The compaction of the CalSil particulate beyond that predicted by the NUREG/CR-6224 correlation is also probable. Other uncertainties associated with the correlation also are embedded in the deduced specific surface area.

Observations of the tests have not shown any indication of chemical effects that might alter the debris bed particulate behavior. The debris bed in Test 6H was disturbed during the pump shutdown procedure, resulting in the fine CalSil particulate being re-entrained in the flow stream, which indicates that the particulate remained particulate.

The sludge density of 22 lbm/ft$^3$ for Test 6H is significantly higher than the 17.8 lbm/ft$^3$ deduced from Test 6C. This difference may have been due at least in part to experimental uncertainty or correlation uncertainties; however, the difference is much more likely because the CalSil is somewhat 'spongy', i.e., the particulate might still pack tighter under pressure after the particulate has compacted because of the microvoids within the small particles. Conversely, iron oxide particles, for example, would be solid enough to preclude deformation within the individual particles.

### 5.5.7. Test 6G
Test 6G was performed before Test 6H, using the same test parameters of 15 g of NUKON™ and 7.5 g of CalSil debris. The formation of the debris bed was similar to that of 6H; however, control of the test was lost after a leak occurred in the loop piping near the peak velocity tested. Because subsequent data were discarded and uncertainty was introduced into the test, the test was repeated, i.e., Test 6H. The results of

Test 6G are shown in Figure 5.14 compared with the NUREG/CR-6224 correlation prediction, based on a sludge density of 22 lbm/ft$^3$ and a specific surface area of 800,000/ft deduced from Test 6H. The comparison of Test 6G with 6H results provides good evidence of repeatability in the head-loss testing, specifically the worst-case test.
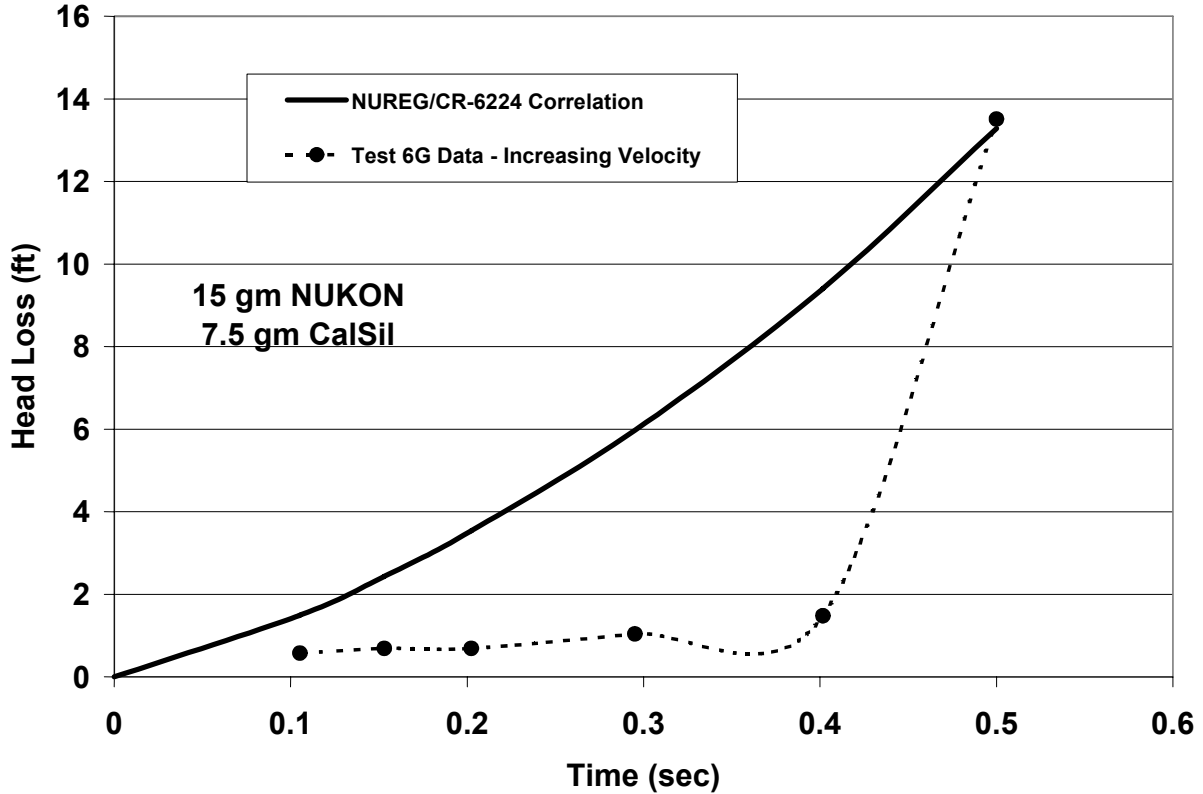


**Figure 5.14. Comparison of NUREG/CR-6224 correlation with Test 6G head-loss data.**

### 5.5.8. Test 6J

A modest increase in NUKON™ debris mass (from 12 to 15 g, with a corresponding increase in CalSil) resulted in a substantial and nonlinear increase in the head loss. An additional test was conducted to determine if yet another modest increase in debris mass would result in another increase in head loss. The debris bed in Test 6J was formed uniformly using 18 g of NUKON™ and 9 g of CalSil debris. Although the debris bed appeared to be well formed, the experimental head losses were relatively low. Either the pressure transducer was faulty or the flow velocities had to be substantially higher than the fully open regulation valve could provide using the small flow meter. In either case, there is sufficient evidence to determine that this debris bed caused lesser head loss per quantity of debris than did Test 6H; therefore, the test was successful enough to fulfill its primary purpose but was not used to estimate a specific surface area.

### 5.6. Tests from the Original Series (Tests 3a and 3j)

The reduction of data from Tests 3a and 3j of the original test series indicated a specific surface area of 700,000/ft, which was substantially higher than the areas deduced from the other original series tests. However, these deductions were based on a particle density of 186 lbm/ft$^3$, which was subsequently determined to be much too large. According to the test described in Section 5.3, the particle density was nearer 115 lbm/ft$^3$. Revisions to the analysis of Tests 3a and 3j are shown in Figures 5.15 and 5.16, respectively.
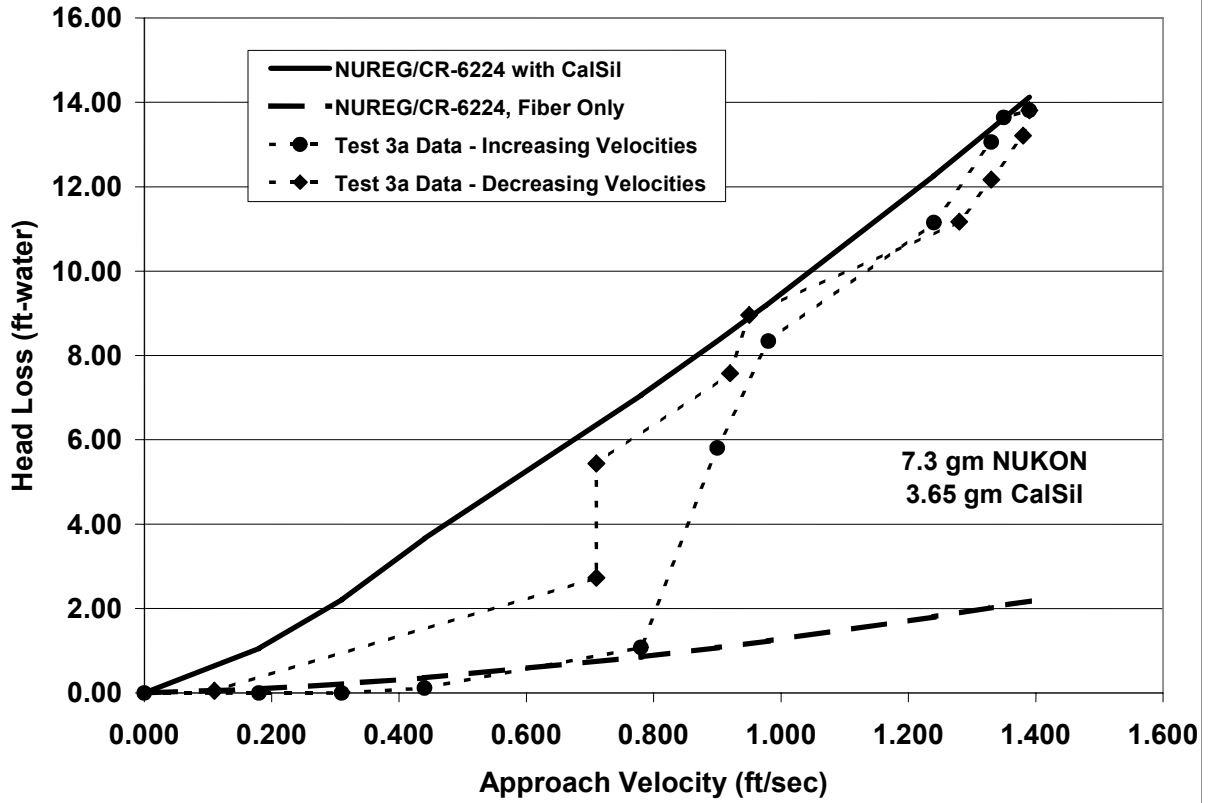
**Figure 5.15. Comparison of NUREG/CR-6224 correlation with Test 3a head-loss data.**
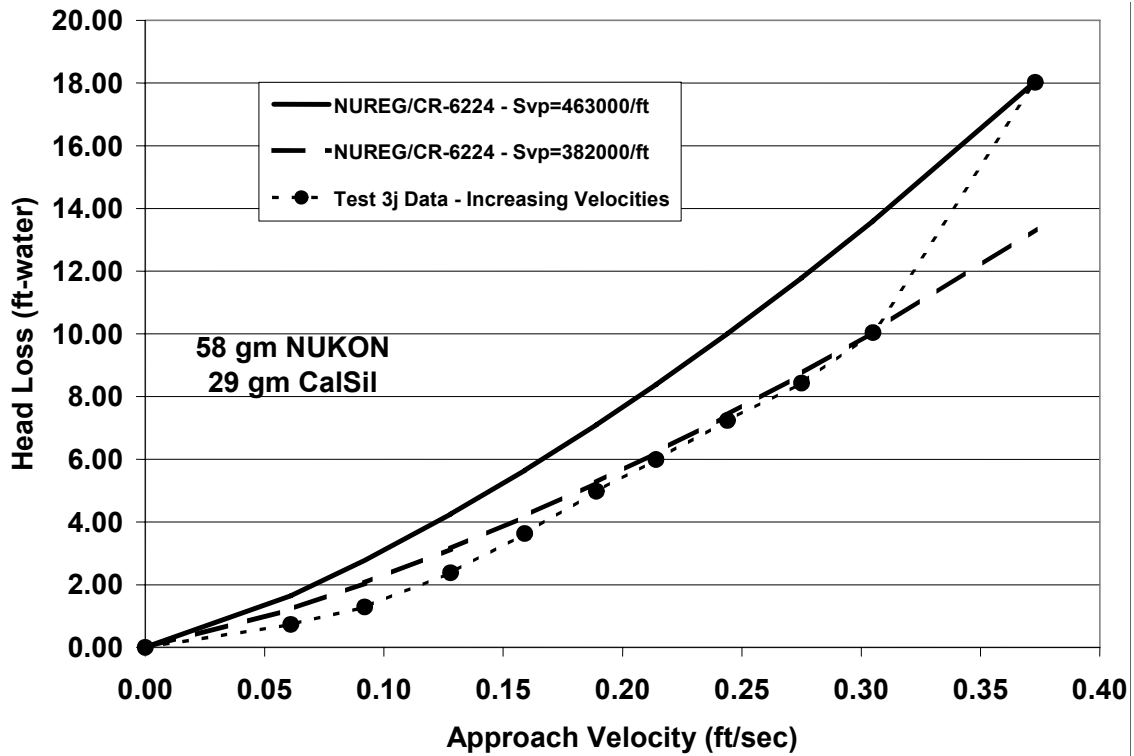


**Figure 5.16. Comparison of NUREG/CR-6224 correlation with Test 3j head-loss data.**

Using a particle density of 115 lbm/ft$^3$ and a sludge density of 17.8 lbm/ft$^3$ resulted in estimated specific surface areas of 490,000/ft and 463,000/ft for Tests 3a and 3j, respectively. For Test 3j, a specific surface area of 382,000/ft fits all of the data points except the last point (highest velocity), and this area agrees well with Test 6I. Note that Tests 3j and 6I had nearly the same quantities of debris.

The remaining tests of the original series are predicted conservatively using the parameters for the refined tests, i.e., all of the head-loss data fit below the respective NUREG/CR-6224 correlation prediction—sometimes well below because those tests had ill-formed debris beds or some other test problem.

## 5.7. Test Comparisons

The analysis of these tests has provided a range of specific surface areas (382,000 to 880,000/ft) and a range of sludge densities (17.8 to 22 lbm/ft$^3$). The specific surface areas are compared in Figure 5.17 according to their respective bed thickness (based on the as-manufactured density) when the sludge density was specified as 17.8 lbm/ft3 and the particulate-to-mass ratio was ~0.5. The reasons for the variation include the filtration efficiencies, the particulate compaction, and other uncertainties in the application of the NUREG/CR-6224 correlation.
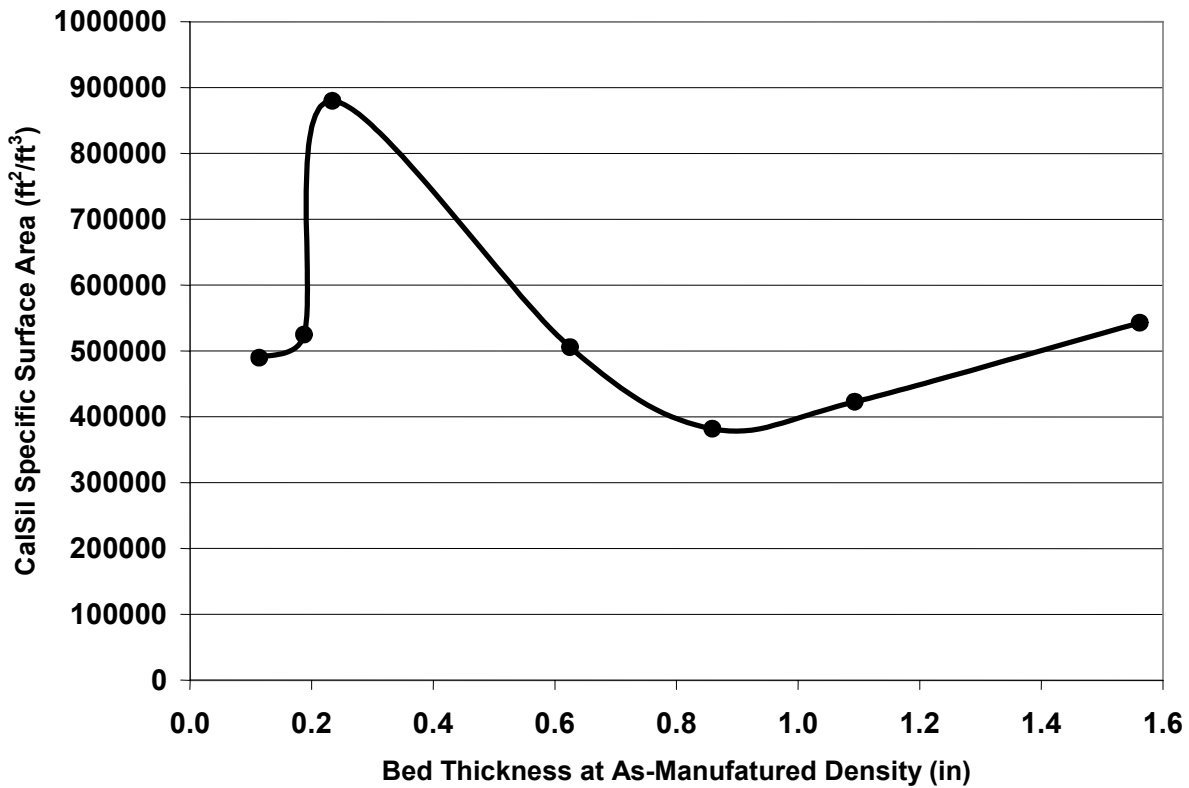


Figure 5.17. Comparison of deduced specific surface areas.

The primary variation was Test 6H, which predicted a specific surface area of 880,000/ft with a sludge density of 17.8 lbm/ft$^3$ or an area of 800,000/ft with a sludge density of 22 lbm/ft$^3$. In Test 6H, it was apparent that the bed compaction was being limited by the particulate in the bed and that the granular particulate was causing the reduced bed porosity. The phenomenon causing the high head loss was not entirely obvious. First, the bed filtration efficiency would increase, causing more of the very fine particulate to be entrapped in the bed. Second, it seems likely that CalSil particles themselves might have

deformed due to interior microvoids that make the debris somewhat 'spongy', which likely explains the range of sludge densities. Perhaps when the particulate becomes compacted, the water flows through smaller voids when the pressure differences are sufficient, thereby making more surface area effectively available. Post-test SEM photos illustrated the bunching of the CalSil particulate where the particulate seemed to deform to fill inter-particulate spacing, for which an example is shown in Figure 5.18. The exact phenomena may not ever become completely understood, but conservative parameters for the correlation can be specified. In effect, all of the uncertainties associated with the prediction of the CalSil head loss are subsumed into the specific surface area. As previously noted, no indication exists of a chemistry effect contributing to the head loss; however, these data do not necessarily prove that chemistry did not take place. When a debris bed was disturbed, the particulate tended to escape the debris bed and reenter the flow stream. It should be understood that a bed of any thickness would be compacted to a granular bed if the force of flow and the particulate-to-fiber mass were sufficient; however, for a thick bed, that force could be quite high (well beyond the UNM test apparatus capability).

The issue of filtration efficiency improving as the bed compacts is further demonstrated by the turbidity measurements. In Figure 5.19, the turbidity measurements for Tests 6C and 6H are compared as a function of the debris-bed porosity, as predicted by the NUREG/CR-6224 correlation as applied to those tests, respectively. As the debris-bed compactions became particulate limited, the water clarity improved due to increased filtration. This figure should be viewed qualitatively because the predicted bed porosities have substantial associated uncertainty.
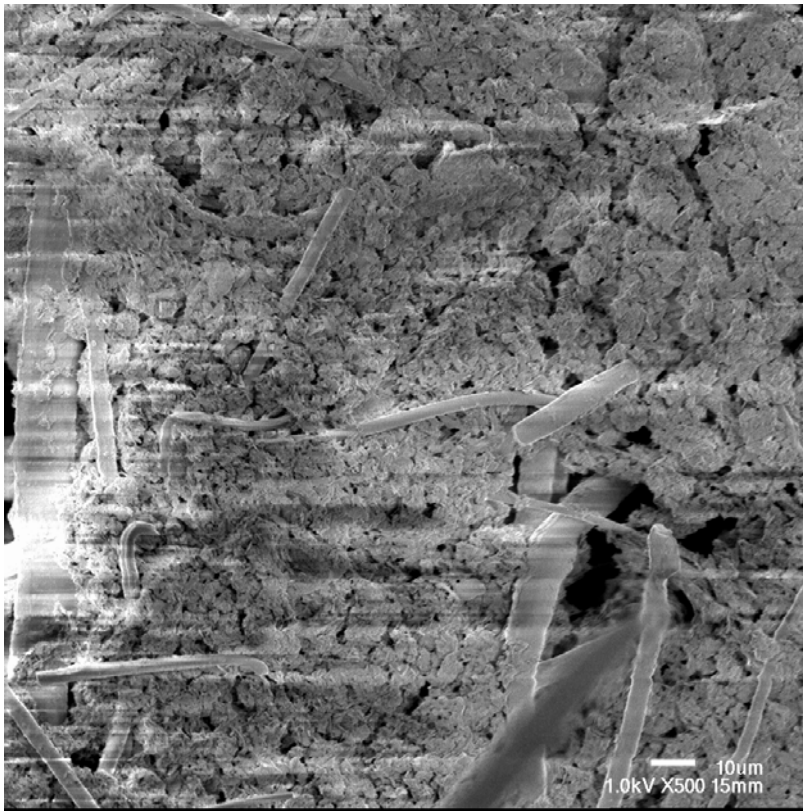


**Figure 5.18. Typical Post-Test SEM Photo**
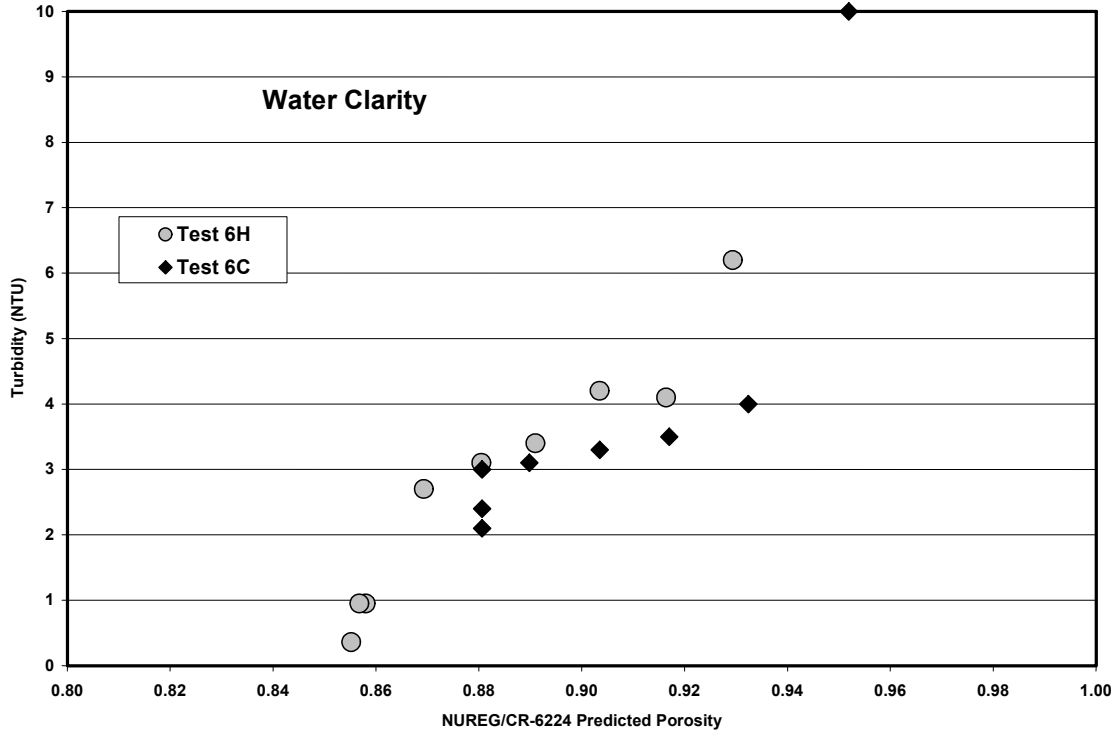
**Figure 5.19. Comparison of turbidity measurements for thin-bed Tests 6H and 6C.**

The quality of several of the original series of tests was compromised by nonuniform debris beds, incomplete filtration, debris beds disturbed by flow fluctuations, and debris-bed deformation due to relatively high pressure differentials. High pressure differentials have formed bore holes through the debris bed, allowing portions of the flow to bypass the debris; in a thin-bed test, the debris bed became totally disrupted. However, the application of the NUREG/CR-6224 correlation, based on parameters determined from the quality tests, will conservatively predict the head losses of the lesser quality tests.

The refined tests were conducted at a particulate-to-fiber mass ratio of ~0.5. The head-loss testing at a higher mass ratio in the original series seemed somewhat problematic because (1) it was difficult to filter enough of the particulate so that the CalSil mass in the debris was accurately known and (2) debris-bed deformation became much more likely at higher head losses. If more CalSil were added to any of the refined tests, the head losses would increase and the debris bed could become particulate-compaction limited at lower flow rates.

## 5.8. Recommendation of Conservative Parameters for the NUREG/CR-6224 Correlation

The recommended parameters for the NUREG/CR-6224 correlation, shown in Table 5.2, depend on whether the thin-bed debris configuration is a potential concern. If the potential for a thin-bed debris configuration exists, then the application of the correlation must consider the higher specific surface area deduced from the tests where the high thin-bed head losses were encountered, specifically Tests 6G and 6H.

The thin-bed CalSil tests are very realistic potential debris accumulation and are reproducible (i.e., the tests are not experimental outliers). Only a small quantity of fibers (or perhaps none) and fine CalSil particulate, which tends to remain in suspension, is needed to form a very uniform debris bed. The difficulties in forming a uniform debris bed during testing were associated with the preparation of the NUKON™ debris—difficulties which were resolved for the latter tests. The recommended specific surface area of 880,000/ft is 10% higher than the experimentally deduced area for Test 6H, to prudently

incorporate a 10% to 20% safety factor to account for (1) experimental uncertainties, such as instrumentation error; (2) an incomplete examination of the experimental test parameter space; and (3) the variance in the manufacture of calcium silicate insulation. The actual value of this safety factor depends on the approach velocity, i.e., whether the first or second term of the correlation dominates the head-loss prediction. The use of the 22-lbm/ft$^3$ sludge density as input to the correlation prevents the correlation from prematurely estimating compaction limiting.

**Table 5.2. Recommended Conservative CalSil NUREG/CR-6224 Correlation Parameters**

| | Recommended Head Loss Parameters | |
|---|---|---|
| **Correlation Parameter** | **Thin-Bed Configuration** | **Mixed-Bed Configuration** |
| Particle Density | 115 lbm/ft$^3$ | 115 lbm/ft$^3$ |
| Particulate Sludge Density | 22 lbm/ft$^3$ | 22 lbm/ft$^3$ |
| Particulate Specific Surface Area | 880,000 ft$^2$/ft$^3$ | 600,000 ft$^2$/ft$^3$ |

The sump screen conditions, where it can be reasonably justified that the thin-bed configuration cannot form, include (1) the advanced strainer designs, where test data has strongly indicated that thin-bed configurations would not form because of complex surface design; and (2) flow conditions insufficient for the required debris bed formation, which can be substantiated by applicable test data. Examples of the advanced strainer design include the stacked-disk strainers, where it has been generally accepted, based on testing of prototypical strainers, that a thin-bed configuration will not form under potential debris loadings. An example of insufficient flow conditions is sump conditions that include a maximum approach velocity of less than 0.1 ft/s and particulate-to-fiber mass ratios of less than 0.5—conditions for which a thin bed was not achieved in the CalSil head-loss tests because the filtration efficiency apparently was not sufficient to remove enough of the fine CalSil from the flow to form a granular debris bed. Beyond these conditions, either a thin bed was formed or the tests did not cover that part of the parameter space; thus, it is not known if a thin bed can form. Extreme care must be exercised in justifying that a thin bed cannot form.

Note that the range in the experimentally determined values for the specific surface area was due to many factors. In the tests conducted during the first phase, testing difficulties such as debris-bed nonuniformities essentially disqualified many of those tests. In addition, a particulate density of 186 lbm/ft$^3$ was assumed to evaluate the test results rather than the experimentally determined 115-lbm/ft$^3$ value used in the latter tests. Because the value of the deduced surface area depended on the value of the particle density, the earlier assumed density predicted lower values for the areas, in addition to the experimental error. It is also important to note that the specific surface area for CalSil is not a fixed value as it is for hard materials such as BWR corrosion products. Rather, the CalSil particles are somewhat "spongy," with interior voids so that when compressed, the particulate deforms to fill interparticle spaces, thus forcing water through smaller and smaller interior voids and increasing the effective specific surface area; at least, this is the working theory that appears to fit the experimental results.

The bottom line is as follows:

- Strainers/screens where thin-bed accumulation is a real potential should be evaluated regarding the head loss for thin-bed formation (i.e., 880,000/ft) unless it can be clearly shown by comparison with the test data that the approach velocities are much too low to create the thin bed due to the inability to filter the Calsil from the flow (fiber-type dependent).

- Complex strainers/screens (e.g., stacked disk strainers) that have been reasonably shown to be incapable of forming a thin bed can use a lesser value for the specific surface area (i.e., 600,000/ft).

- These specific surface areas must be used in conjunction with the particulate density of 115 lbm/ft$^3$, i.e., the two parameters are interdependent in the correlation.

- Caution must be exercised when applying these recommendations to CalSil that is produced by another manufacturer or by another manufacturing process. Macroscopic and microscopic examinations should be compared between the CalSil in question and the CalSil tested to evaluate the applicability of the recommendations to the CalSil in question.

## 6. CONCLUSIONS

Significant findings from these experiments are the following.

1. Debris accumulation on a simulated (vertical) PWR sump screen was examined for several different types of LOCA-generated debris, including shredded fiberglass, crushed CalSil, mixtures of NUKON™ and CalSil, and crumpled stainless-steel foils from the interior of the RMI. With the exception of RMI foils, debris was observed to accumulate on the screen in a relatively uniform manner for conditions in which the local fluid velocity was significantly greater than the bulk transport velocity of debris fragments. The RMI foils accumulated primarily near the bottom of the screen; however, continuous hydraulic forces gradually caused late-arriving foils to "climb" over the pile of debris that accumulated earlier. Over time, this created a "bottom-skewed" profile in which most of the screen surface (1 ft in height) was covered with debris; however, roughly one-half of the total RMI debris remained stationary at the bottom of the screen.

2. Head-loss measurements were made in a new closed-loop test facility at UNM. Before conducting experiments with debris containing CalSil, qualification tests were run to measure the head loss caused by debris that has been examined in prior studies (in other test facilities). In particular, tests were performed to measure head loss caused by shredded NUKON™ fiber and mixtures of NUKON™ fiber and a sand-and-concrete-dust particulate. Measurements were compared with predictions of the head loss using the NUREG/CR-6224 correlation with excellent agreement.

3. The application of the NUREG/CR-6224 head-loss correlation to a bed of debris requires certain parameters (e.g., specific surface area) as input to the correlation. These parameters have been determined for NUKON™ insulation debris and for some other materials, such as BWR suppression pool corrosion products, but not for many types of insulation and particulate debris typically found in PWR containments; in particular, these parameters have not previously been determined for CalSil. The determination of these parameters is experimental, and one method is to numerically vary the parameter in the correlation while simulating an appropriate test until the correlation results reasonably predict the data. The analysis of the results described herein show that the specific surface area for CalSil is quite large, which should be expected due to the fine nature of its components, as shown in Scanning Electron Microscopy (SEM) photos taken of the debris tested. The analyses herein strongly indicate that the high specific surface area of CalSil is responsible for the high head losses it is known to generate. For perspective, the generally accepted value for the specific surface area of NUKON™ is 171,000/ft; while the experimentally determined values for CalSil are roughly 3-5 times this value. The leading term of the NUREG/CR-6224 correlation depends on the square of this number, and the second term is linear with the specific surface area. Testing difficulties have included the establishment of reasonably uniform and homogeneous debris beds under conditions where nearly the entire test quantity of CalSil is filtered from the flow stream and the accurate measurement of debris bed head losses, flow rates, temperatures, and water clarity but these challenges were successfully handled in a second group of tests. Recommendations for the input parameters to the NUREG/CR-6224 correlation were developed to ensure conservative simulation of head loss associated with fibrous debris beds that contain the PCI brand of CalSil insulation debris. The recommendations focus on the prediction of thin-bed behavior where the debris has been

72

compacted until further compaction is limited by the CalSil particulate. The recommendations are: 1) 115 lbm/ft$^3$ for the particle density, 22 lbm/ft$^3$ for the sludge density, and 880,000 ft$^2$/ft$^3$ for the specific surface area. This specific surface area includes a 10 to 20% safety factor to cover uncertainties.

4.  Tests conducted using only CalSil fragments to form the debris bed clearly demonstrated that CalSil debris can accumulate on a 1/8-in. mesh screen and cause substantial head loss without the aid of another form of fiber to hold it in place. Further, it was clearly demonstrated that CalSil creates substantially higher head losses than does a comparable quantity of LDFG. Experimentally, it was found even more difficult to form a truly uniform bed of CalSil debris than it was to form a NUKON™/CalSil bed. The thickest beds of CalSil formed in these tests were ~1/4-in. thick (on average) so that the fragments of CalSil formed lumps and unevenness in the bed and small portions of the screen were not covered by the CalSil, thereby forming a bypass. The analysis, however, strongly indicates that once the CalSil head-loss parameters have been adequately determined, the form of the NUREG/CR-6224 correlation where the correlation is modified to simulate a granular bed (without significant fiber) will perform well for a uniform CalSil debris bed.

5.  Measured head losses for mixtures of CalSil and RMI were higher than those measured for the base RMI debris. Head loss doubled in magnitude when 75 g of CalSil per ft$^2$ of screen area was added to a 1-in. bed of crumpled RMI foils; significantly less CalSil (~30 g per ft$^2$ of screen area) doubled the head loss across an 8-in. bed of RMI foils. The LANL correlation for characterizing head loss in RMI debris beds was shown to provide an excellent prediction of data measured for baseline test conditions involving 1-in. and 8-in. debris beds of pure stainless-steel RMI.

## 7.    REFERENCES

Brocard, 1983   D. N. Brocard, "Buoyancy, Transport and Head Loss of Fibrous Reactor Insulation," NUREG/CR-2982, SAND82-7205, Rev. 1, Alden Research Laboratory, July 1983.

BWROG, 1996   BWR Owners' Group, "Utility Resolution Guidance (URG) for ECCS Suction Strainer Blockage," November 1996.

Rao, 1996   D. V. Rao and F. J. Souto, "Experimental Study of Head Loss and Filtration for LOCA Debris," NUREG/CR-6367, SEA 95-554-06-A:8, Science and Engineering Associates, Inc., February 1996.

Rao, 2002a   D. V. Rao, B. C. Letellier, A.K. Maji, and B. Marshall, "GSI-191: Separate-Effects Characterization of Debris Transport in Water," NUREG/CR-6772, LA-UR-01-6882, Los Alamos National Laboratory, August 2002.

Rao, 2002b   D. V. Rao, B. C. Letellier, C. Shaffer, S. Ashbaugh, L. S. Bartlein, "GSI-191: Technical Assessment: Parametric Evaluations for Pressurized Water Reactor Recirculation Sump Performance," NUREG/CR-6762, LA-UR-01-4083, (4 Vols.), Los Alamos National Laboratory, August 2002.

Rao, 2002c   D. V. Rao, C. Shaffer, B. C. Letellier, A. K. Maji, L. Bartlein, "GSI-191: Integrated Debris-Transport Tests in Water Using Simulated Containment Floor Geometries," NUREG/CR-6773, LA-UR-02-6786, Los Alamos National Laboratory, December 2002.

Rao, 2003   D. V. Rao, C. Shaffer, M. T. Leonard, and K. W. Ross, "Knowledge Base for the Effect of Debris on Pressurized Water Reactor Emergency Core Cooling Sump Performance," NUREG/CR-6808, LA-UR-03-0880, February 2003.

Shaffer, 1996   NUREG/CR-6371, C. Shaffer, W. Bernahl, J. Brideau, and D. V. Rao, "BLOCKAGE 2.5 Reference Manual," SEA96-3104-A:4, December 1996.

Wilde, 1993    J. Wilde, "Strainer Test with Fiber Insulation and Reactor Tank Insulation. Results from the Small Model," Vattenfall Development Corporation, Sweden, June 1993.

Zigler, 1999    G. Zigler, and F. Souto, "Characterization of ECCS Suction Strainer Head Loss due to Mixed Fibrous and Calcium Silicate Insulation Debris," ITS Corporation, May 1999.

**APPENDIX A: DETAILED TEST FACILITY DESCRIPTIONS**

**A.1.    Large-Flume Test Apparatus**

The debris-accumulation tests were conducted in a large flume located in the Open-Channel Hydraulics Laboratory at the Civil Engineering Department of the University of New Mexico (UNM). The large flume was not designed or modified to replicate (1) fluid flow or debris transport characteristics on the floor of a PWR containment or (2) the geometric configuration of particular recirculation sump designs. Rather, it was used to generate data on the behavior of transportable forms of LOCA-generated debris in the immediate proximity of a vertical screen under a variety of flow conditions. The specific design requirements of the large-flume apparatus were as follows:

- The internal geometry and pumping power of the flume was to be sufficient for measuring debris accumulation for flow velocities spanning the range of 0.5 ft/s to 2.0 ft/s.

- The screen on which debris was to accumulate was to resemble the basic configuration of a fully submerged, vertical 1/8-in.-mesh sump screen.

- The width of the simulated sump screen was to be sufficiently wide, relative to the size of debris being tested, to minimize the effects of walls or other obstacles on the accumulation pattern.

- The flume geometry and physical features had to provide the experimenter with the ability to visually observe debris transport and accumulation on the screen.

These basic requirements led to the following design and operating features of the flume.

Flume Configuration
The basic configuration of the large flume is illustrated in Figure A.1. The flume consists of an open-top box 20 ft long, 3 ft wide, and 4 ft high. The water inlet and flow conditioning occurs in the first 4 ft of the flume. In the central portion of the flume (i.e., the 10-ft length between the flow straightener and the test screen), the active width of the flume was reduced from 3 ft to 1 ft by installing 1-in.-thick plywood walls. This converging section of the flume was necessary to allow tests to be conducted with volume-average approach velocities at the screen above 1 ft/s.

The walls of the 2-ft linear section of the flume immediately upstream of the screen are constructed of 1/2-in.-thick, transparent Plexiglas™, allowing experimenters to observe the behavior of transported debris as it accumulates on the screen. The floor of the flume is covered with 1/16-in.-thick treated plywood and covered with an epoxy coating. The entire flume assembly rests atop a table ~2.5 ft above the floor of the UNM Laboratory. The elevated position of the flume allows pumps, valves, piping, and other components of the hydraulic flow loop to be located below the flume itself and above a 360-ft$^3$ water reservoir under the laboratory floor. The reservoir is the primary resource for filling the flume with water to begin an experiment.

Downstream of the debris screen, an exit tunnel (1 ft x 1 ft square in cross section) was mated to the end of the linear portion of the flume to simulate a submerged recirculation sump enclosure and attached suction piping. The tunnel is sealed from other upstream portions of the flume, except for a 1-ft x 1-ft entrance doorway, through which all water flowing through the flume must pass to reach the exit drain at the opposite end of the tunnel. A 1/8-in.-mesh screen covers the entire cross section of the doorway, simulating flow conditions at the surface of a fully submerged recirculation sump. A steel reinforcing mat (with large openings) was mounted immediately behind the 1/8-in.-mesh screen to provide structural strength to the screen.

A photograph of the debris screen and its supporting reinforcing mesh is shown in Figure A.2. Photographs of the linear section of the flume upstream of the screen and the exit tunnel downstream of the flume are shown in Figure A.3.
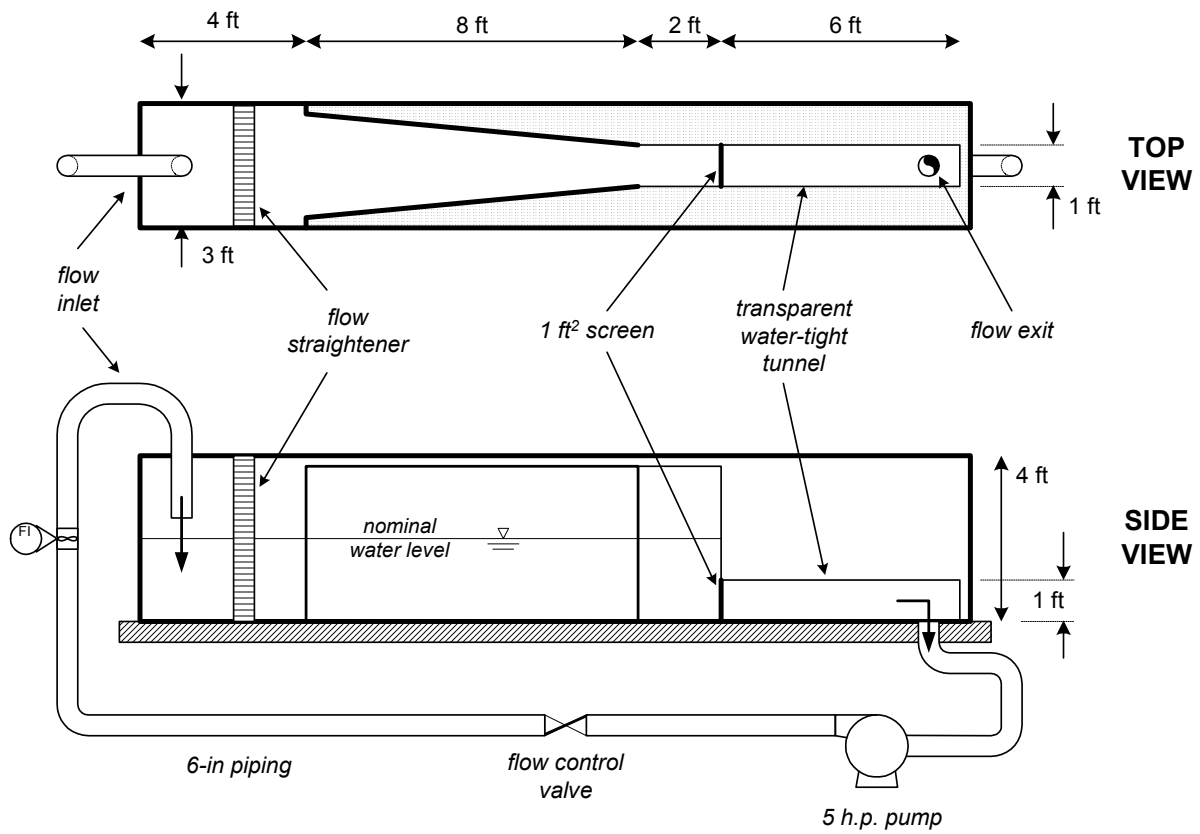
**Figure A.1. Flume configuration.**



**Figure A.2. Debris screen at entrance to flume exit tunnel (large, diamond-shaped mat behind screen is for structural reinforcement only).**

Direction of flow



End of converging section of flume    Vertical debris screen    Exit tunnel    *SIDE VIEW*



Direction of flow

*TOP VIEW*
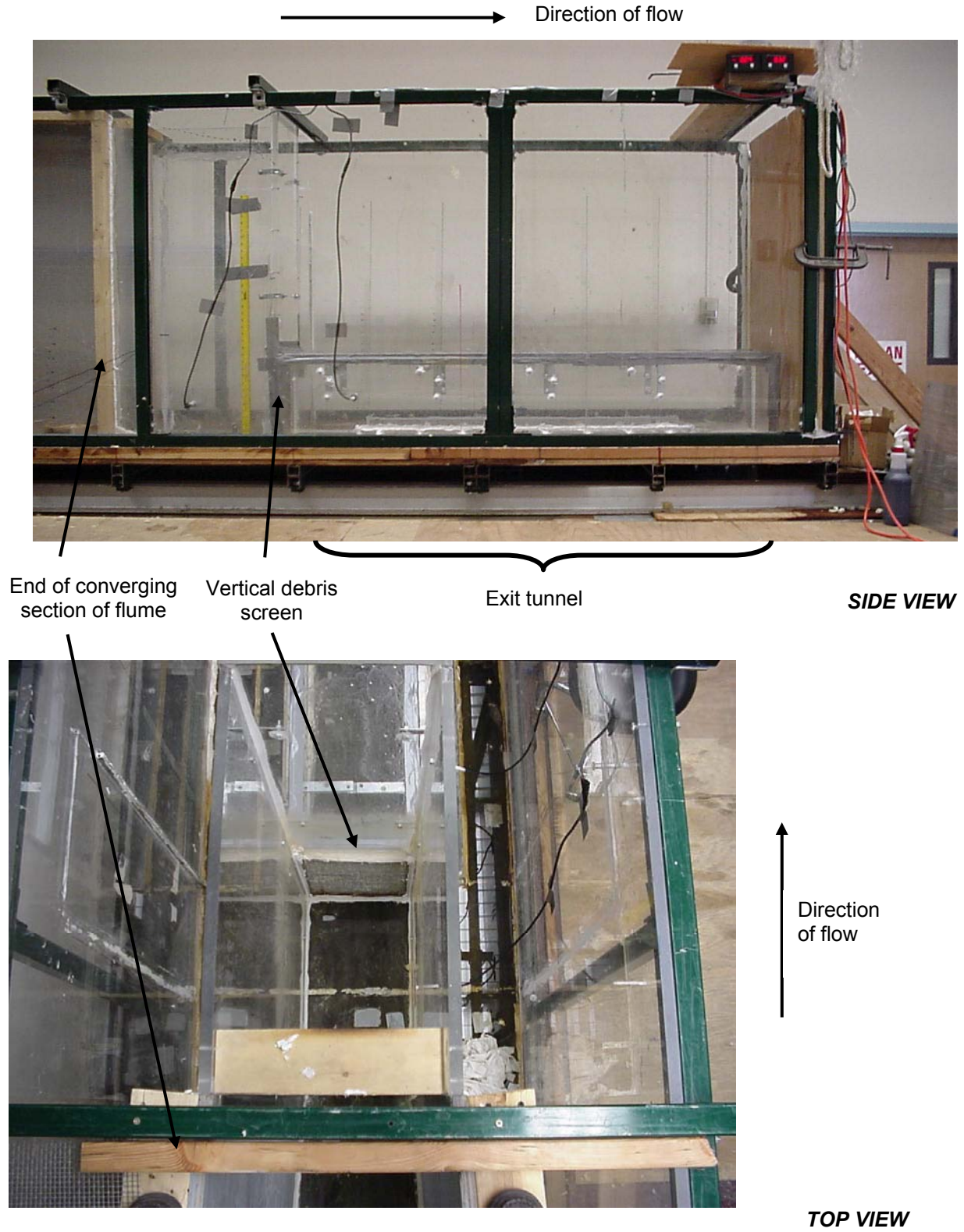
**Figure A.3. Flume arrangement from end of converging section through the flow exit tunnel.**

Inlet Flow Conditioning

The effects of local levels of turbulence on debris transport were examined in earlier experiments conducted in the large flume test facility [Rao, 2002]. These effects were not reexamined in the current test program. As in previous tests, water entering the flume from the recirculation piping was allowed to fall into the flume through a downward-facing discharge pipe. Large-scale turbulence was limited by forcing the water to pass through metal frame flow straighteners before entering the converging section of the flume. A photograph and illustration of the flow straighteners are shown in Figure A.4. A photograph showing the effectiveness of this device in reducing the level of large-scale turbulence in the flume is shown in Figure A.5. This manner of flow conditioning is identical to that described by Rao et al. [Rao, 2002] as "Configuration B" in the study of debris transport.



Flow Straightener
Sheet Metal
15 pieces, 4'x1'
1$\overline{1}$ pieces, 3'x1'
6" slots 3"c/c
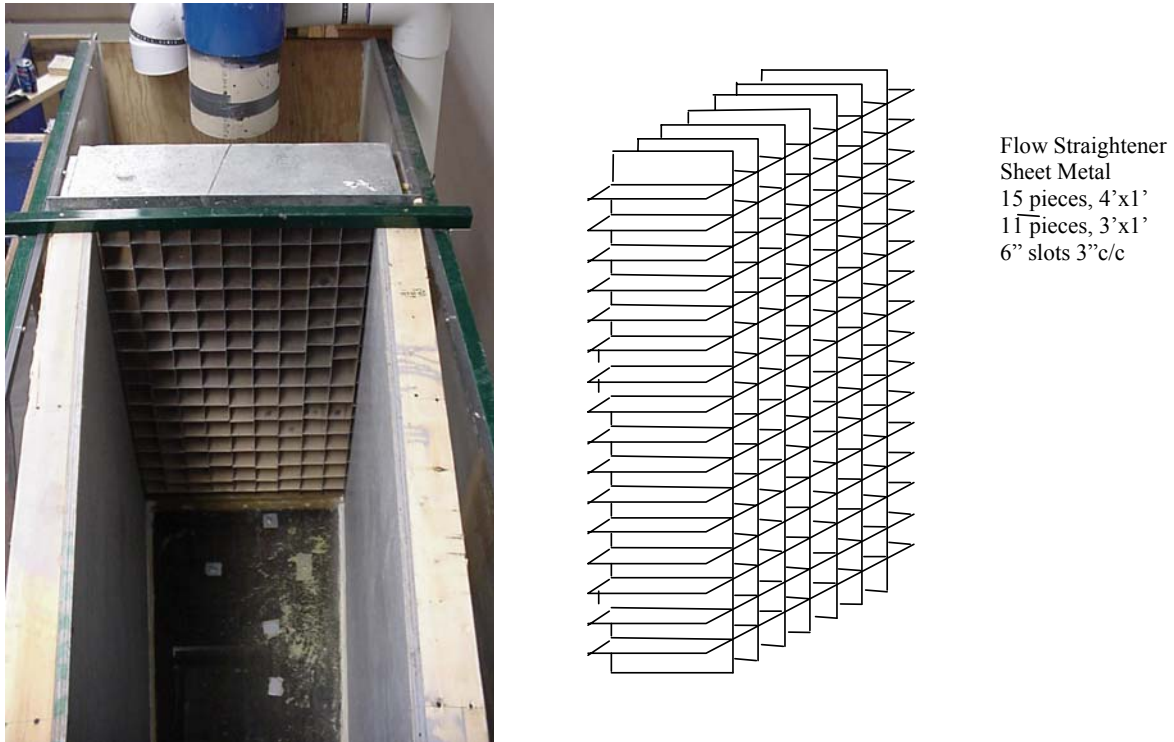
**Figure A.4.  Flow inlet section of flume (left) including flow straightener (detail at right) and walls of converging channel.**

Flume Flow Control

The flume is initially filled with water by operating a variable speed centrifugal pump capable of transferring water from the laboratory water reservoir at a maximum rate of 2200 gal./min. Water from the test apparatus drained back into the sump, which was located below the laboratory main floor. Once the proper amount of water is added to the flume (i.e., the nominal water depth is 18 in. in the experiments conducted here), the large-volume fill pump is isolated and the flume is operated in recirculation mode.

In recirculation mode, water flow through the flume is maintained by operating a 5-hp recirculation pump located in a closed loop that draws suction from a 10-in. line connected to the floor of the sump at the far end of the enclosed exit tunnel and discharges back into the inlet area. The closed recirculation flow loop is illustrated in Figure A.1. A photograph of portions of the recirculation line is shown in Figure A.6.
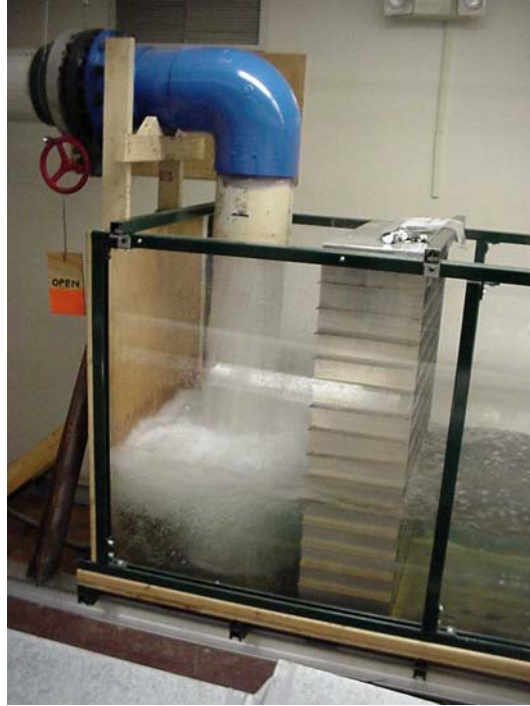
**Figure A.5. Flume inlet flow conditioning.**



Direction of flow into the flume

Butterfly flow control valve

Flow inlet end wall of the flume

Hoffer turbine flow meter
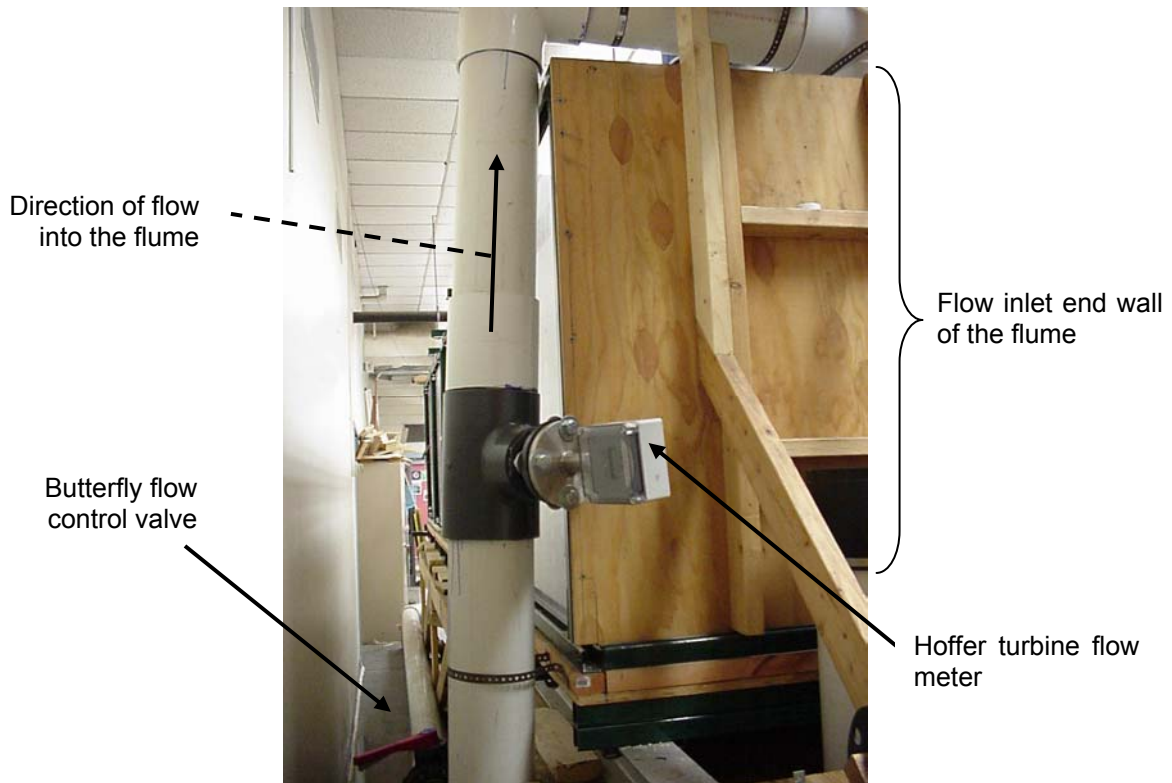
**Figure A.6. Large flume recirculation loop components.**

The flow rate through the flume during each experiment was controlled by adjusting the position of a butterfly valve located downstream of the recirculation pump. During each of the flume experiments, the valve control arm was adjusted to a predetermined location corresponding to a desired flow rate. The control arm location required to produce a particular flow rate was identified by cross calibration with flow rate measurements made in the recirculation loop piping using a Hoffer turbine flow meter. The factory calibration of the Hoffer flow meter was, in turn, verified by performing an independent integral flow measurement test, as described in Appendix D.

## A.2.    Closed-Loop Head-Loss Test Facility

Experiments to measure head loss across debris-laden screen were conducted in a new facility constructed and operated by the Civil Engineering Department at UNM. This test apparatus closely resembles the head-loss test loop used in earlier experiments conducted at Alden Research Laboratory (ARL) for the NRC [Rao, 1996]. Like the ARL test loop, the UNM test apparatus was designed as a closed hydraulic loop with a vertical test section and horizontal debris filtration and capture screen. Specific design objectives of the UNM head-loss test apparatus were as follows.

- Geometric similitude with the ARL test loop was desired to facilitate comparison and collective analysis of data collected in both facilities. Accordingly, the vertical test section is constructed with a 12-in. (nominal)-diameter pipe.

- The walls of the vertical test section had to be transparent, allowing the physical condition of the debris bed to be observed while head-loss measurements are recorded.

- Head loss had to be measured with a water flow rate spanning the range of 0.2 to 2.0 ft/s.

These basic requirements led to the following design and operating features of the closed-loop test facility.

Facility Configuration
An illustration of the configuration and major components of the UNM closed-loop test facility is shown in Figure A.7. A photograph of the test facility is shown in Figure A.8. As indicated above, the primary section of the experimental apparatus is a vertically oriented, 12-in.-diameter PVC pipe. A fixed, horizontal screen is mounted approximately mid-height within this pipe, in the center of a transparent test section.

Due to physical constraints of the Laboratory in which the facility was constructed, the maximum overall height of the test loop is limited to roughly 11 ft. With the debris screen to be positioned approximately mid-height of this length, the closed hydraulic loop was configured in a manner that provides approximately four pipe diameters (4 ft) of linear approach distance upstream of the debris screen and the same length downstream of the screen.

The debris screen is a 1/8-in. rectangular mesh, similar to those used in most PWR recirculation sump screens. Although some plants have screens with different mesh sizes, only a 1/8-in. screen was examined in the current tests. Steel webbing with 1-in. (nominal) diamond-shaped openings was installed below (underneath) the 1/8-in. debris screen to provide structural reinforcement to the screen and thereby prevent the screen from collapsing when subjected to the high differential pressure. Photographs of the debris screen and underlying steel reinforcing webbing are shown in Figure A.9.

Although the main test section of the loop is constructed of 12-in. (nominal) PVC pipe, the return flow loop was considerably smaller in diameter, facilitating flow measurement instrumentation. The return flow circuit is designed to allow accurate flow measurements to be made over a wide range of values. An inner loop was constructed of 6-in. (nominal)-diameter PVC pipe, which was equipped with a Hoffer turbine flow meter (the same flow meter calibrated for use in the large flume). This loop was used for experiments in
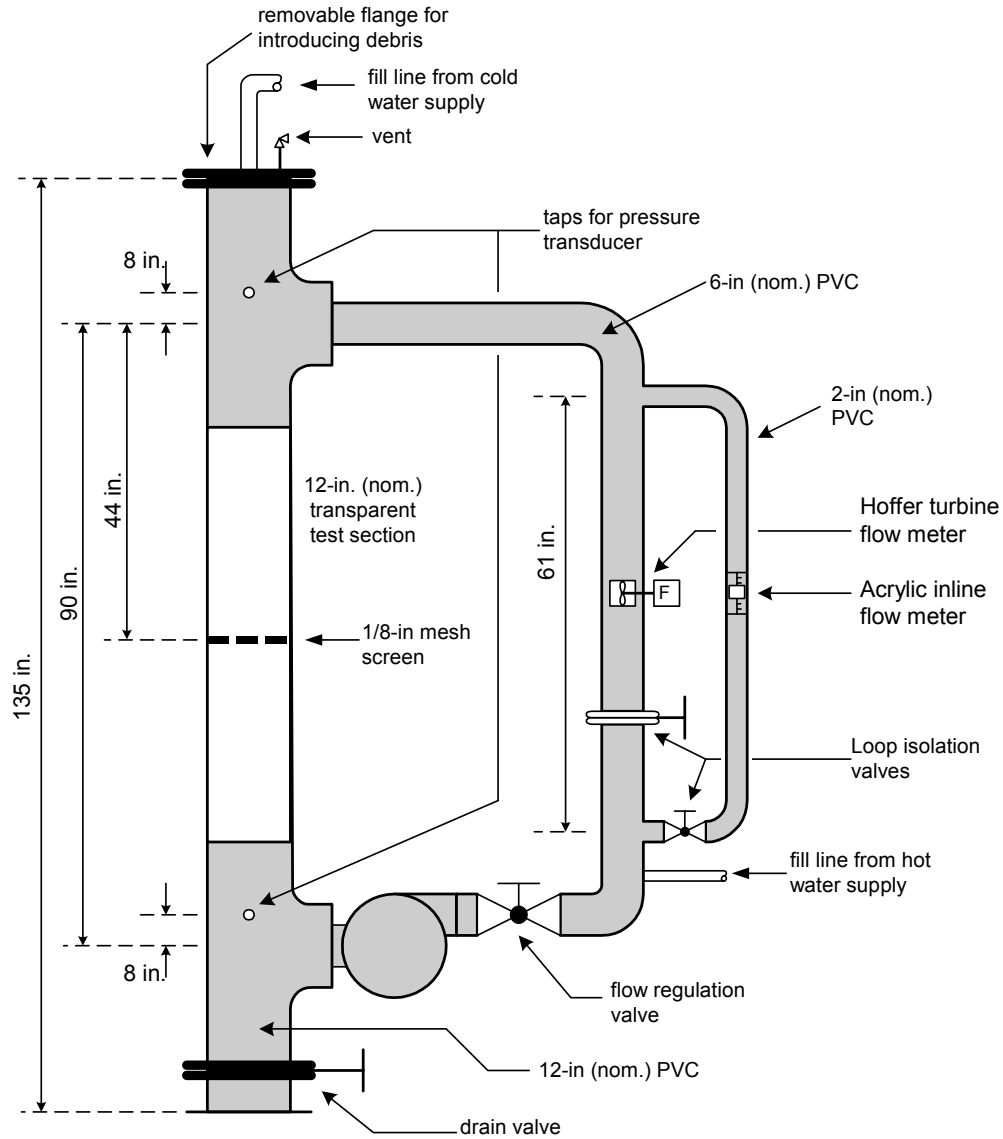
**Figure A.7. Configuration and major dimensions of the UNM closed-loop head-loss test facility.**

which the bulk flow rate through the closed loop was greater than 100 gal./min (i.e., the lower end of the calibration range for the Hoffer flow meter). For experiments involving bulk flow rates less than 100 gal./min, a smaller (2-in.-diameter), parallel flow loop was used. This alternative flow loop was equipped with an Acrylic in-line flow meter, which provides accurate flow measurements between 20 and 100 gal./min. Appendix D provides information on the calibration of these instruments.

Only one of these return loops operates at one time; switching flow from the larger (inner) loop to the smaller (outer) loop is accomplished by changing the position of isolation valves located at the entrance to each loop. A photograph of the intersection of these two lines and their isolation valves is shown in Figure A.10.

**Figure A.8. UNM closed-loop head-loss test facility.**
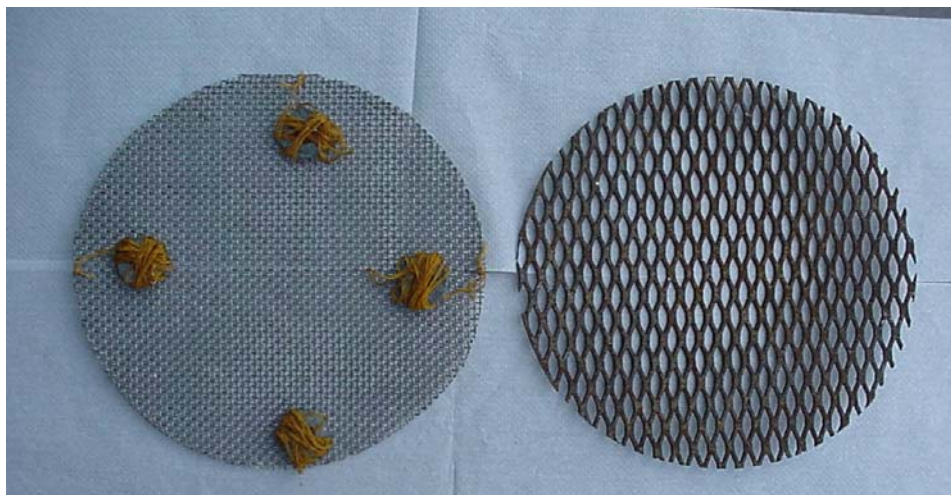


**Figure A.9. 1/8-in. mesh 11.5-in.-diameter debris screen (left) and supporting steel reinforcement (right).**

**Figure A.10. Intersection of the bases of the 6-in. inner recirculation loop
and the 2-in. outer recirculation loop.**

The correlation between bulk flow, measured with one of these devices, and approach velocity at the debris screen was developed based on the principles of continuity and the geometry of the hydraulic loop. That is, the bulk volumetric flow through the test section (Q) can be translated to screen approach velocity as

$$Q \text{ [gal./min]} = v(\text{approach}) \text{ [ft/s]} * \pi\, r^2 * \text{[units conversion factor]} \quad .$$

For the UNM test facility, this relationship works out to

$$v(\text{approach}) \text{ [ft/s]} = 0.003 * Q \text{ [gal./min]} \quad .$$

Closed-Loop Flow Control

Flow control within the closed hydraulic loop is accomplished in much the same way as in the large flume. The flume is initially filled with water, either from a laboratory tap water source or from one of two residential hot water heaters (depending on experiment requirements for water temperature). Once the loop is full of water, the fill supplies are isolated and the hydraulic loop is operated in recirculation mode.

In recirculation mode, water flow through the loop is maintained by operating a 5-hp recirculation pump located adjacent to the exit of the vertical test section. A photograph of the pump and its connection to the base of the vertical test section is shown in Figure A.11.

The flow rate through the flume during each experiment was controlled by adjusting the position of a butterfly valve located downstream of the recirculation pump. The location of this valve (relative to the recirculation pump) is shown in Figure A.12. During each of the head-loss experiments, the position of the valve could be adjusted until the desired flow rate was achieved. Flow rate instruments were located immediately above the location of the flow control valve. The flow meters are installed approximately mid-height in the return legs of the recirculation loops, as shown in the center portion of the photograph in Figure A.8.

**Figure A.11. 5-hp motor at the base of the vertical test section of the hydraulic loop.**



**Figure A.12. Flow control valve adjacent to the loop pump.**

## A.3.    References

Rao, 1996          D. V. Rao and F. J. Souto, "Experimental Study of Head Loss and Filtration for LOCA Debris," NUREG/CR-6367, SEA 95-554-06-A:8, Science and Engineering Associates, Inc., prepared for US Nuclear Regulatory Commission, February 1996.

## APPENDIX B: RAW TEST DATA

### B.1.　Exploratory Tests

A total of 13 exploratory experiments of debris accumulation were conducted in the large flume. Recorded results of these tests are listed below. Three distinct geometric patterns of debris accumulation were observed in these tests:

- Category I:　Debris was distributed uniformly across the surface of the screen;

- Category II: Debris collected in a triangular, or bottom-skewed pattern, with more debris collected toward the bottom of the screen than on the top; and

- Category III: Debris accumulated mostly entirely on flume floor where it intersected the lower edge of the screen, effectively forming a short "curb."

The pattern that most accurately describes the observations from each test is noted below.

Rough head-loss measurements also were made in some of these tests using standard, static pressure gauges (analog, needle indicators) mounted to the side walls of the flume up- and down-stream of the screen. Results of these measurements led to the replacement of the analog gauges with digital pressure transducers in the final tests.

**Table B.1. Exploratory Test Results**

| | Debris Type | Accumulation Pattern | Head Loss | | |
|---|---|---|---|---|---|
| | | | Time (min) | Reading | Comments |
| Test A | NUKON$^{TM}$ (101g); Q = 100 gal./min; V = 0.22 ft/s | Between that of Category II and Category III | 0 5 | 0 0 | No head loss was observed for 5 min. |
| Test B | NUKON$^{TM}$ (101g); Q = 225 gal./min; V = 0.5 ft/s | Category II | 0 1 | 0 1 in.-Hg | Head loss was constant afterward. |
| Test C | NUKON$^{TM}$ (101g); Q = 410 gal./min; V = 0.9 ft/s | Category II | 0 5 | 0 2.5 in.-Hg | 101 g of NUKON$^{TM}$ was added in three equal steps. The bed did get somewhat compressed, but there was no change in shape. Fiber accumulated on the screen in the shape of Category I after the first step of debris addition. The shape changed to Category III after the third step. Head loss after the first step was small and changed to moderate after the third step. A significant quantity of air bubbles was observed to collect along the top surface of the exit tunnel. The source of these bubbles was not clear. |
| Test D | NUKON$^{TM}$ (10.1g); Q = 220 gal./min; V =0.5 ft/s | Between that of Category II and Category III | 0 5 | 0 0 | No measurable pressure drop across the screen. |

**Table B.1. Exploratory Test Results (continued)**

| | Debris Type | Accumulation Pattern | Head Loss | | |
|---|---|---|---|---|---|
| | | | Time (min) | Reading | Comments |
| Test E | CalSil (101 g);<br>Q = 220 gal./min;<br>V = 0.5 ft/s | Category II | 0<br>5 | 0<br>0 | Very small particles went into suspension. Larger particles and clumps stayed on the floor and accumulated at the floor level near the screen (shape of Category II). Some particles got trapped on the screen at different elevations, with more toward the bottom of the screen than at the top. |
| Test F | CalSil (101 g);<br>Q = 410 gal./min;<br>V = 0.9 ft/s | Between that of Category II and Category III | 0<br>10 | 0<br>0.5 in.-Hg | |
| Test G | CalSil (50.5 g) + NUKON$^{TM}$ (101g);<br>Q = 410 gal./min;<br>V = 0.9 ft/s | Between that of Category II and Category III | 0<br>5<br>12 | 0<br>0<br>1.0 in.-Hg | No measurable pressure drop across the screen. |
| Test H | CalSil (101 g) + NUKON$^{TM}$ (101g);<br>Q = 210 gal./min;<br>V = 0.5 ft/s | Between that of Category II and Category III | 1<br>3<br>5<br>10 | 1.0 in.-Hg<br>2.0 in.-Hg<br>3.0 in.-Hg<br>3.5 in.-Hg | The test was terminated after 10 min due to the presence of excessive air in the tunnel. A stable condition could not be reached. The accumulation of debris (which was harder to see in the murky water) appeared to be that of Category II, as shown in Figure B.1. |
| Test I | CalSil (202 g) + NUKON$^{TM}$ (101g);<br>Q = 210 gal./min;<br>V = 0.5 ft/s | Between that of Category II and Category III | | | Pressure difference across the debris bed was noted as (1) upstream = 2 psi and (2) downstream = –2 in.-Hg (vacuum). The recirculation pump was kept running for 10 min, during which time the downstream reading changed to –3 in-Hg. A large air pocket began to form along the top surface of the exit tunnel, as shown in Figure B.2. The primary source of the air was entrainment through a small gap between the top surface of the screen and the top of the exit tunnel doorway. This line did not appear to be completely sealed, allowing a significant volume of water (and entrained air) to bypass the screen. |
| Test J | Steel RMI (101.5 g);<br>Q = 410 gal./min;<br>V = 0.9 ft/s (without the flow straightener) | | | | Initially, 101.5 g of RMI was added in the circulating water and a pressure difference across the screen was noted. Most of the RMI collected at the bottom of the screen with enough openings among themselves (as with Category III). As a result, no noticeable pressure difference was seen. Figure B.3 illustrates the debris accumulation in the flume and screen.<br><br>Five min after the addition of the first 101.5 g, another 101.5 g of RMI was added, and no pressure difference was observed. When the diffuser was incorporated, not much change was noticed regarding the accumulation of the RMI. Photographs are shown in Figure B.4. |

**Table B.1. Exploratory Test Results (continued)**

| | Debris Type | Accumulation Pattern | Head Loss | | |
|---|---|---|---|---|---|
| | | | Time (min) | Reading | Comments |
| Test K | Large blocks (4 in. x 4 in. x 1 in.) of unshredded NUKON$^{TM}$ fiber blanket; Q = 410 gal./min; V = 0.9 ft/s | | | | Large blocks of NUKON$^{TM}$ fiber mat were cut from an intact blanket of material. Each piece weighed 11.5 g before the tests (dry). The cut blocks were presoaked in warm water and submerged in the flume as they transported downstream toward the screen. Pieces were added one at a time and the accumulation pattern noted. Photographs were taken, as shown in Figure B.5. |
| | | | | | The "debris" initially collected near the base of the screen and accumulated as a random stack of distorted blocks. As more pieces arrived, the fraction of the screen surface area covered by the blocks increased. Pieces arriving later "tumbled" up the face of pieces already attached to the surface of the screen. With 6 pieces, the overall accumulation pattern resembled Category II. As the total number of blocks increased to 9 and then 12, the pattern shifted toward Category I (with a small gap near the top surface of the screen). |
| | | | | | As the blocks accumulated, head loss across the screen increased. As in Test I, a gap along the top surface of the screen became very apparent and a large air pocket formed along the top surface of the exit tunnel. |
| Test L | NUKON$^{TM}$ (101 g); Q= 225 gal./min; V=0.5 ft/s | Category I (very uniform) | 0 5 | 0 ~0.5 in.-Hg | This experiment repeated Test B after the gap between the top surface of the screen and the exit tunnel was sealed. |
| Test M | NUKON$^{TM}$ (101 g prepared, only 25 g added to flume); Q = 410 gal./min; V = 0.9 ft/s | Category I | 0 5 | 0 2.5 in.-Hg | This experiment repeated the conditions in Test C after the top edge of the screen was completely sealed to the exit tunnel entrance doorway. |
| | | | | | The extent to which the gap along the top edge of the debris screen affected results of earlier exploratory tests was examined in this re-test. As before, NUKON™ fragments were added to the flume in several installments. |
| | | | | | The test was stopped after adding the first 25 g of NUKON$^{TM}$ because of the excessive amount of air in the exit tunnel. In this instance, however, the source of air was infiltration through cracks formed in the corners of the Plexiglas$^{TM}$ exit tunnel. The high head losses measured in Tests I and K resulted in structural damage to the glued corners of the tunnel, requiring repair and reinforcement. Unlike Test C, the accumulation on the bed was very uniform (Category I). |

| Initial appearance from right side | Initial appearance from left side | Long-term profile |

**Figure B.1: The debris did not cover the entire width of the screen and left ~2 in. of space relatively open on one side, in addition to the 3 in. of opening at the top.**



Air pocket forming at top of exit tunnel
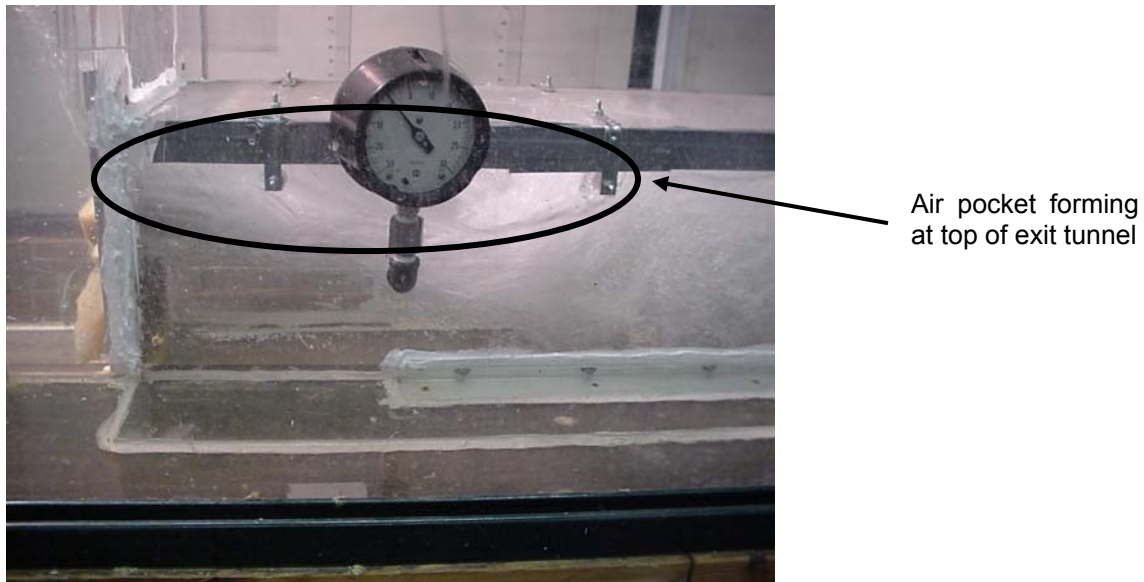
**Figure B.2. Formation of air pocket at top of exit tunnel**
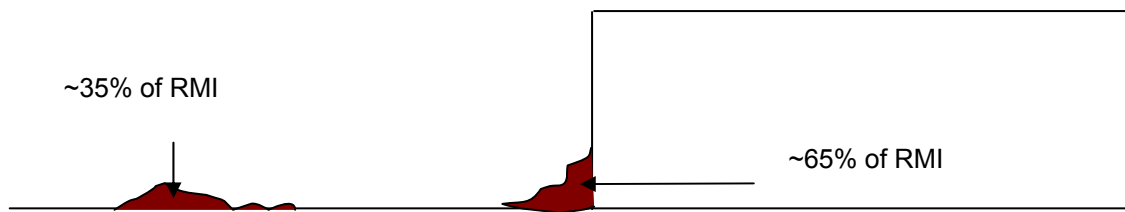
**Figure B.3. Debris accumulation in the flume and screen.**

~35% of RMI

~65% of RMI



**Figure B.4.  RMI  foil  configuration  after  the  initial  101.5  g  was  added  (left),  then several min later when a second 101.5 g was added (right).**

6 pieces (view from left)　　　6 pieces (view from right)　　　9 pieces
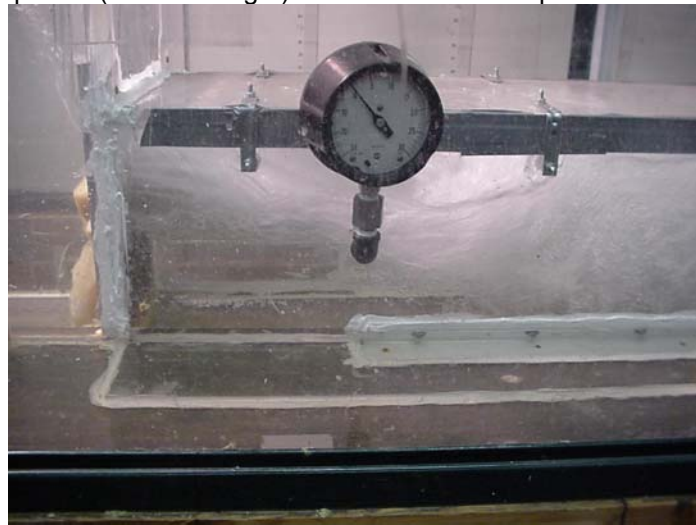


12 pieces　　　Air pocket formed downstream of screen after 12 pieces collected

**Figure B.5.　Accumulation patterns of progressively greater numbers of 4-in. x 4-in. x 1-in. pieces of intact NUKON™ fiber blanket.**

## B.2. Head-Loss Test Data

Raw data gathered in the closed-loop head-loss test facility are summarized below.

| TEST 1(a) 116 g NUKON™ (70°F) | | TEST 1(a') 58 g NUKON™ (70°F) | |
|---|---|---|---|
| Velocity (ft/s) | Head Loss (ft-$H_2O$) | Velocity (ft/s) | Head Loss (ft-$H_2O$) |
| 0.1 | 1.17 | 0.38 | 3.55 |
| 0.41 | 7.13 | 0.65 | 6.59 |
| 0.56 | 12.28 | 0.85 | 8.87 |
| 0.69 | 15.63 | 0.95 | 10.84 |
| 0.7 | 16.88 | 1.18 | 12.34 |
| 0.88 | 18.4 | 1.25 | 13.46 |
| 0.92 | 19.71 | 1.3 | 14.09 |
| 0.95 | 20.25 | 1.35 | 14.2 |
| 0.96 | 20.19 | 1.3 | 14.3 |
| 0.93 | 20.2 | 1.28 | 13.61 |
| 0.93 | 19.83 | 1.25 | 12.62 |
| 0.89 | 18.88 | 1.12 | 11.12 |
| 0.85 | 17.48 | 0.74 | 7.04 |
| 0.72 | 15.34 | 0.45 | 3.65 |
| 0.63 | 12.8 | | |
| 0.44 | 8.07 | | |

| TEST 1(b) Trial 1 116 g NUKON™ (125°F) | | TEST 1(b) Trial 2 116 g NUKON™ (125°F) | | TEST 1(b) Trial 3 116 g NUKON™ (125°F) | |
|---|---|---|---|---|---|
| Velocity (ft/s) | Head Loss (ft-$H_2O$) | Velocity (ft/s) | Head Loss (ft-$H_2O$) | Velocity (ft/s) | Head Loss (ft-$H_2O$) |
| 0.061 | 0.18 | 0.061 | 0.28 | 0.061 | 0.41 |
| 0.122 | 0.71 | 0.122 | 0.16 | 0.092 | 0.63 |
| 0.153 | 0.85 | 0.183 | 0.47 | 0.122 | 0.94 |
| 0.183 | 1.0 | 0.244 | 1.04 | 0.153 | 1.23 |
| 0.213 | 1.05 | 0.304 | 1.28 | 0.183 | 1.51 |
| 0.244 | 1.23 | 0.43 | 4.4 | 0.214 | 1.77 |
| 0.275 | 1.54 | 0.66 | 10.44 | 0.244 | 2.02 |
| 0.305 | 1.87 | 0.69 | 14.48 | 0.275 | 2.36 |
| 0.6 | 9.6 | 0.83 | 18.38 | 0.31 | 2.61 |
| 0.75 | 13.34 | 0.92 | 18.95 | 0.4 | 5.33 |
| 0.76 | 15.37 | 0.93 | 19.35 | 0.61 | 10.01 |
| 0.95 | 17.34 | 0.95 | 19.6 | 0.7 | 13.09 |
| | | | | 0.75 | 14.76 |
| | | | | 0.94 | 16.62 |
| | | | | 0.99 | 17.82 |
| | | | | 1.0 | 18.38 |

| TEST 1(c) 58 g NUKON™ with 58 g concrete dirt/dust (70°F) | | TEST 1(d) 116 g NUKON™ with 116 g concrete dirt/dust (70°F) | |
|---|---|---|---|
| Velocity (ft/s) | Head Loss (ft-H$_2$O) | Velocity (ft/s) | Head Loss (ft-H$_2$O) |
| 0.16 | 1.88 | 0.061 | 0.29 |
| 0.4 | 6.18 | 0.122 | 0.81 |
| 0.63 | 12.41 | 0.183 | 2.06 |
| 0.72 | 16.49 | 0.244 | 2.9 |
| 0.68 | 19.3 | 0.305 | 4.58 |
| 0.77 | 21.49 | 0.305 | 6.06 |
| 0.74 | 22.34 | 0.459 | 11.51 |
| 0.74 | 22.87 | 0.589 | 17.04 |
| 0.74 | 23.07 | 0.561 | 20.99 |
| 0.74 | 23.38 | 0.493 | 20.04 |
| 0.72 | 22.74 | 0.409 | 15.92 |
| 0.69 | 22.41 | 0.09 | 2.85 |
| 0.65 | 21.34 | | |
| 0.57 | 19.41 | | |
| 0.52 | 16.78 | | |
| 0.39 | 11.41 | | |
| 0.12 | 2.28 | | |
| | | | |

| TEST 2(a) 7.2 g CalSil (70°F) | | TEST 2(b) 58 g CalSil (70°F) | | TEST 2(c) 116 g CalSil (70°F) | |
|---|---|---|---|---|---|
| Velocity (ft/s) | Head Loss (ft-H$_2$O) | Velocity (ft/s) | Head Loss (ft-H$_2$O) | Velocity (ft/s) | Head Loss (ft-H$_2$O) |
| 0.06 | 0 | 0.19 | 0.07 | 0 | 0 |
| 0.15 | 0.05 | 0.31 | 0.61 | 0.19 | 1.58 |
| 0.31 | 0.04 | 0.41 | 1.71 | 0.31 | 2.8 |
| 0.5 | 0.08 | 0.7 | 3.46 | 0.58 | 11.68 |
| 0.82 | 0.36 | 0.93 | 5.21 | 0.74 | 14.94 |
| 1.1 | 0.52 | 1.05 | 6.43 | 0.75 | 16.61 |
| 1.16 | 0.41 | 1.4 | 7.4 | 0.95 | 18.39 |
| 1.58 | 1.23 | 1.55 | 7.87 | 0.99 | 18.82 |
| 1.81 | 1.36 | 1.63 | 8.07 | 1.08 | 18.99 |
| 1.94 | 1.45 | 1.64 | 7.71 | 1.07 | 18.49 |
| 1.96 | 1.75 | 1.69 | 7.33 | 1.03 | 17.27 |
| 1.8 | 1.33 | 1.63 | 6.88 | 0.92 | 15.8 |
| 1.59 | 0.88 | 1.45 | 5.65 | 0.82 | 13.45 |
| 1.18 | 0.68 | 1.05 | 4.42 | 0.63 | 10.09 |
| 1.12 | 0.45 | 0.98 | 3.68 | 0.44 | 4.35 |
| 0.84 | 0.32 | 0.85 | 2.63 | | |
| 0.54 | 0.09 | 0.54 | 1.1 | | |
| 0.18 | 0.07 | | | | |

| TEST 2(d) 7.2 g CalSil (125°F) | | TEST 2(e) 58 g CalSil (125°F) | | TEST 2(f) 116 g CalSil (125°F) | |
|---|---|---|---|---|---|
| Velocity (ft/s) | Head Loss (ft-H$_2$O) | Velocity (ft/s) | Head Loss (ft-H$_2$O) | Velocity (ft/s) | Head Loss (ft-H$_2$O) |
| 0.122 | 0.11 | 0.153 | 0.08 | 0.061 | 1.62 |
| 0.244 | 0.27 | 0.183 | 0.17 | 0.122 | 3.52 |
| 0.78 | 0.35 | 0.214 | 0.15 | 0.183 | 6.27 |
| 1.22 | 0.48 | 0.244 | 0.14 | 0.244 | 9.07 |
| 1.87 | 0.89 | 0.275 | 0.23 | 0.305 | 11.22 |
| 1.95 | 0.99 | 0.305 | 0.22 | 0.415 | 15.14 |
| | | 0.497 | 0.85 | 0.47 | 17.74 |
| | | 0.76 | 3.21 | | |
| | | 0.93 | 3.73 | | |
| | | 1.07 | 4.56 | | |
| | | 1.45 | 4.88 | | |
| | | 1.63 | 5.48 | | |
| | | 1.77 | 4.61 | | |

| TEST 3(a) 7.3 g NUKON™ 3.65 g CalSil (70°F) | | TEST 3(b) 7.3 g NUKON™ 7.3 g CalSil (70°F) | | TEST 3(c) 7.3 g NUKON™ 14.6 g CalSil (70°F) | |
|---|---|---|---|---|---|
| Velocity (ft/s) | Head Loss (ft-H$_2$O) | Velocity (ft/s) | Head Loss (ft-H$_2$O) | Velocity (ft/s) | Head Loss (ft-H$_2$O) |
| 0.18 | 0.0 | 0.155 | 0.36 | 0.18 | 0.19 |
| 0.31 | 0.0 | 0.31 | 0.0 | 0.31 | 0.14 |
| 0.44 | 0.12 | 0.43 | 0.34 | 0.36 | 0.22 |
| 0.78 | 1.08 | 0.78 | 1.22 | 0.49 | 0.4 |
| 0.9 | 5.81 | 0.92 | 3.31 | 1.02 | 2.38 |
| 0.98 | 8.34 | 1.06 | 5.3 | 1.08 | 5.14 |
| 1.24 | 11.15 | 1.4 | 7.85 | 1.37 | 7.66 |
| 1.33 | 13.06 | 1.5 | 9.45 | 1.51 | 9.19 |
| 1.35 | 13.64 | 1.57 | 9.95 | 1.6 | 9.47 |
| 1.39 | 13.81 | 1.58 | 9.99 | 1.61 | 8.84 |
| 1.38 | 13.21 | 1.6 | 9.73 | 1.61 | 8.86 |
| 1.33 | 12.17 | 1.52 | 9.19 | 1.59 | 8.13 |
| 1.28 | 11.17 | 1.4 | 8.22 | 1.45 | 7.03 |
| 0.95 | 8.96 | 1.18 | 6.63 | 1.3 | 5.38 |
| 0.92 | 7.58 | 0.95 | 5.12 | 0.96 | 4.33 |
| 0.71 | 5.44 | 0.81 | 3.66 | 0.81 | 3.03 |
| 0.71 | 2.73 | 0.55 | 1.78 | 0.55 | 1.36 |
| 0.11 | 0.05 | 0.122 | 0.28 | 0.1 | 0.19 |

| TEST 3(d) 58 g NUKON™ 29 g CalSil (70°F) | | TEST 3(e) 58 g NUKON™ 58 g CalSil (70°F) | | TEST 3(f) 58 g NUKON™ 116 g CalSil (70°F) | |
|---|---|---|---|---|---|
| Velocity (ft/s) | Head Loss (ft-H$_2$O) | Velocity (ft/s) | Head Loss (ft-H$_2$O) | Velocity (ft/s) | Head Loss (ft-H$_2$O) |
| 0.175 | 0.61 | 0.21 | 1.23 | 0.061 | 0.14 |
| 0.238 | 4.06 | 0.4485 | 12.1 | 0.153 | 1.06 |
| 0.364 | 10.43 | 0.4785 | 23.55 | 0.31 | 3.32 |
| 0.505 | 17.14 | 0.3985 | 23.02 | 0.3585 | 18.66 |
| 0.52 | 20.45 | 0.3385 | 18.65 | 0.2885 | 24.35 |
| 0.568 | 22.47 | | | 0.2685 | 22.38 |
| 0.631 | 23.34 | | | 0.2635 | 7.44 |
| 0.571 | 22.76 | | | | |
| 0.526 | 21.22 | TEST 3(e) Repeat | | TEST 3(f) Repeat | |
| 0.481 | 18.12 | 0.062 | 0.4 | 0.061 | 0.02 |
| 0.406 | 12.17 | 0.124 | 0.43 | 0.122 | 0.41 |
| 0.091 | 0.92 | 0.248 | 1.78 | 0.189 | 0.99 |
| | | 0.31 | 4.79 | 0.244 | 3.03 |
| | | 0.2542 | 7.46 | 0.299 | 7.23 |
| | | 0.186 | 8.91 | 0.25 | 9 |
| | | 0.124 | 5.41 | 0.183 | 9.22 |
| | | 0.062 | 2.97 | 0.122 | 6.46 |
| | | | | 0.061 | 3.31 |

| TEST (g) 116 g NUKON™ 58 g CalSil (70°F) | | TEST 3(h) 116 g NUKON™ 116 g CalSil (70°F) | | TEST 3(i) 116 g NUKON™ 232 g CalSil (70°F) | |
|---|---|---|---|---|---|
| Velocity (ft/s) | Head Loss (ft-H$_2$O) | Velocity (ft/s) | Head Loss (ft-H$_2$O) | Velocity (ft/s) | Head Loss (ft-H$_2$O) |
| 0.098 | 0.44 | 0.09 | 0.54 | 0.067 | 0.36 |
| 0.244 | 2.96 | 0.18 | 1.36 | 0.122 | 0.95 |
| 0.31 | 5.37 | 0.24 | 4.05 | 0.21 | 10.16 |
| 0.3285 | 15.05 | 0.31 | 8.78 | 0.079 | 22.67 |
| 0.4285 | 21.79 | 0.3085 | 19.7 | 0.079 | 26.91 |
| 0.4285 | 23.31 | 0.2785 | 24.78 | | |
| 0.2915 | 21.25 | 0.2585 | 23.29 | | |
| | | 0.1485 | 13.28 | | |
| TEST 3(g) Repeat | | TEST 3(h) Repeat | | TEST 3(i) Repeat | |
| 0.061 | 0.22 | 0.061 | 0.29 | 0.061 | 0.14 |
| 0.122 | 0.57 | 0.122 | 0.51 | 0.122 | 0.25 |
| 0.183 | 1.13 | 0.183 | 1.31 | 0.183 | 1.66 |
| 0.244 | 2.62 | 0.244 | 4 | 0.244 | 4.18 |
| 0.305 | 4.73 | 0.305 | 11.4 | 0.305 | 5.39 |
| 0.244 | 4.02 | 0.238 | 13.68 | 0.244 | 17.38 |
| 0.183 | 3.41 | 0.183 | 12.94 | 0.183 | 14.56 |
| 0.122 | 2.41 | 0.122 | 8.86 | 0.122 | 11.08 |
| 0.061 | 1.08 | | | | |
| 0.061 | 1.08 | | | | |
| 0.061 | 1.08 | | | | |

| TEST 3(j)<br>58 g NUKON™<br>29 g CalSil (125°F) | |
|---|---|
| Velocity (ft/s) | Head Loss (ft-H$_2$O) |
| 0.061 | 0.73 |
| 0.092 | 1.29 |
| 0.128 | 2.38 |
| 0.159 | 3.63 |
| 0.189 | 4.98 |
| 0.214 | 5.99 |
| 0.244 | 7.24 |
| 0.275 | 8.43 |
| 0.305 | 10.04 |
| 0.373 | 18.02 |

| TEST 3(k)<br>58 g NUKON™<br>58 g CalSil (125°F) | |
|---|---|
| Velocity (ft/s) | Head Loss (ft-H$_2$O) |
| 0.061 | 0.41 |
| 0.092 | 1.11 |
| 0.122 | 2.18 |
| 0.153 | 3.9 |
| 0.183 | 6.04 |
| 0.214 | 8.05 |
| 0.244 | 9.53 |
| 0.275 | 11.59 |
| 0.305 | 13.85 |

| TEST 3(l)<br>58 g NUKON™<br>116 g CalSil (125°F) | |
|---|---|
| Velocity (ft/s) | Head Loss (ft-H$_2$O) |
| 0.061 | 5.88 |
| 0.122 | 10.52 |
| 0.183 | 14.47 |
| 0.244 | 19.25 |

| TEST 5(a)<br>1-in.-Deep Bed<br>Stainless-Steel RMI (70°F) | |
|---|---|
| Velocity (ft/s) | Head Loss (ft-H$_2$O) |
| 0.061 | 0.01 |
| 0.122 | 0.02 |
| 0.183 | 0.23 |
| 0.305 | 0.34 |
| 0.71 | 0.67 |
| 1.01 | 1.73 |
| 1.09 | 2.48 |
| 1.46 | 3.35 |
| 1.66 | 4.64 |
| 1.77 | 5.37 |

| TEST 5(b)<br>8-in.-Deep Bed<br>Stainless-Steel RMI (70°F) | |
|---|---|
| Velocity (ft/s) | Head Loss (ft-H$_2$O) |
| 0.244 | 0.3 |
| 0.305 | 0.52 |
| 0.63 | 4.14 |
| 0.82 | 8.73 |
| 0.89 | 11.47 |
| 1.1 | 14.36 |
| 1.14 | 16.06 |
| 1.17 | 17.16 |
| 1.19 | 17.4 |

| TEST 5(c) 1-in.-Deep Bed Stainless-Steel RMI + 10 g CalSil (70°F) | | TEST 3(d) 1-in.-Deep Bed Stainless-Steel RMI + 20 g CalSil (70°F) | | TEST 3(e) 1-in.-Deep Bed Stainless-Steel RMI + 50 g CalSil (70°F) | |
|---|---|---|---|---|---|
| Velocity (ft/s) | Head Loss (ft-$H_2O$) | Velocity (ft/s) | Head Loss (ft-$H_2O$) | Velocity (ft/s) | Head Loss (ft-$H_2O$) |
| 0.305 | 0.12 | 0.45 | 0.33 | 0.183 | 0.1 |
| 0.51 | 0.31 | 0.72 | 1.02 | 0.214 | 0.19 |
| 0.74 | 1.01 | 0.99 | 1.98 | 0.46 | 0.38 |
| 1 | 1.87 | 1.13 | 2.75 | 0.75 | 1.56 |
| 1.11 | 2.56 | 1.24 | 3.89 | 0.99 | 2.9 |
| 1.44 | 3.85 | 1.62 | 4.97 | 1.07 | 4.34 |
| 1.64 | 4.83 | 1.73 | 5.8 | 1.4 | 6.32 |
| 1.76 | 6.61 | 1.74 | 6.36 | 1.55 | 7.48 |
| | | | | 1.64 | 8.79 |

| TEST 5(f) 8-in.-Deep Bed Stainless-Steel RMI 10 g CalSil (70°F) | | TEST 5(g) 8-in.-Deep Bed Stainless-Steel RMI 20 g CalSil (70°F) | |
|---|---|---|---|
| Velocity (ft/s) | Head Loss (ft-$H_2O$) | Velocity (ft/s) | Head Loss (ft-$H_2O$) |
| 0.122 | 0.2 | 0.061 | 0.05 |
| 0.183 | 0.31 | 0.122 | 0.15 |
| 0.305 | 0.71 | 0.183 | 0.3 |
| 0.68 | 5.85 | 0.244 | 0.68 |
| 0.81 | 9.83 | 0.305 | 0.53 |
| 0.86 | 12.57 | 0.7 | 6.74 |
| 1.03 | 15.99 | 0.77 | 11.47 |
| 1.09 | 17.36 | 0.8 | 14.46 |
| 1.11 | 18.38 | 0.98 | 17.13 |
| 1.12 | 18.47 | 0.99 | 19.71 |
| | | 1.01 | 20.07 |

**APPENDIX C: TEST PROCEDURES**

**C.1.    Debris-Accumulation Tests**

The following general procedure was used to perform debris-accumulation experiments in the large flume:

1.  Debris samples to be used for a particular test were prepared in advance according to the same procedures used in tests conducted in earlier experimental programs for the NRC related to debris transport [Rao, 2002]; i.e.,

    a.  Shredded NUKON™ fiber samples were generated by passing moderately sized (4-in. x 4-in. x 1-in. thick) pieces of fiber blanket through a common leaf shredder. Resulting fiber fragments (fines and small fragments) were presoaked in hot water and occasionally stirred for 10 min. A photograph of the 4-in. x 4-in. blocks and the final shredded fragments is shown in Figure C.1.



**Figure C.1. NUKON™ fiber debris samples.**

    b.  CalSil fragments were presoaked in room temperature water and broken into small fragments by hand. A representative sample is shown in Figure C.2.

    c.  RMI debris was generated by hand-cutting 2-in. x 2-in. pieces of foil from large sheets of stainless-steel foil (see Figure C.3). The flat pieces then were crumpled by hand until flat portions of the foil could no longer be folded with bare hands (see Figure C.4). The final result was a loose pile of crumpled foil debris (Figure C.5).

2.  When debris samples were ready, the test section was filled with water to a level of 18 in. using the transfer pump that draws water from the below-grade reservoir in the UNM Hydraulics Laboratory. When the desired level was achieved, the transfer pump was isolated.

3.  The recirculation pump, which draws water directly from piping connected to the exit of the flume, was turned on and allowed to run for 1 to 3 min, allowing air to be flushed out of recirculation loop piping.

**Figure C.2. Hand-crushed CalSil debris.**



**Figure C.3. Cutting RMI foil.**



**Figure C.4. Hand-crumpling foil.**



**Figure C.5. Stainless-steel RMI debris used in experiments.**

4. The butterfly flow control valve downstream of the recirculation pump was set to a precalibrated position to generate an average flow rate in the flume that produces the desired approach velocity at the debris screen.

5. Electronic pressure instruments positioned up- and down-stream of the debris screen were confirmed to be operating.

6. A 10-in.-diameter, 3-ft-long PVC pipe (open at both ends) was lowered (vertically) into the flow stream approximately midway through the converging section of the flume (~4 ft upstream of the screen). Debris samples were poured into the open pipe and allowed to settle to the floor of the flume (typically ~2 min). The standing pipe was then slowly lifted, allowing debris to be carried downstream toward the screen. Debris was added in this manner in a series of three or four steps (depending on the amount being tested) to prevent the debris fragments from being transported as a single, agglomerated mass to the screen.

7. The geometric pattern the debris assumed on the screen was sketched and photographed.

8. Head loss (differential pressure) across the debris bed was recorded from the pressure gauges.

## C.2. Head-Loss Tests in the Closed-Loop Facility

The following general procedure was used to perform head-loss experiments in the closed-loop hydraulic facility:

1. The top flange at the top of the 12-in. vertical test section was removed.

2. A precut circular 1/8-in.-mesh screen matching the inner diameter of the test section was lowered into the vertical test section using a set of four strings tied to the screen's outer radius at 90º intervals. The screen was placed on the supporting rim mounted on the inner wall of the transparent pipe, and the excess length of string was hung over the outer edge of the top flange.

3. A test section was filled with water and air in the recirculation pump, and supporting piping was vented out by opening a stopcock mounted at the top of the pump housing. The specific location at which water was added to the test loop depended on whether the experiment was to be run at room temperature or with heated water. Room temperature water was added through the opening at the top of the vertical test section. Heated water (~125°F) was added through a sealed fill line located near the recirculation pump and connected to a pair of standard domestic hot-water heaters. Water was added until the entire test apparatus was filled flush with the top flange of the vertical test section.

   - Debris samples to be used for a particular test were prepared in advance according to the same procedures used in the debris-accumulation tests (see Section C.1 above.)

4. The top flange was closed and the air gap was filled with additional water. Air was vented out through the vent line in the top flange. (When the vent line ejected water, the fill line was isolated and the vent line closed.)

5. Pressure in the test section was measured at two fixed points above and below the horizontal screen.

6. Before the recirculation pump was started, static head was noted from the difference in pressure readings.

7.  The recirculation pump was started, and the approach velocity in the test section was varied by using the valve.

8.  Pressure gauge readings were noted at different approach velocities.

9.  Head loss across the debris bed is calculated from the difference of pressure gauge readings and static water head values.

10. Flow rate is increased (or decreased after reaching maximum values), and head measurements are noted at the new velocity.

To measure flow velocity at low velocities (<0.3 ft/s), the 2-in. pipe, along with a flow meter, was incorporated into the test setup. At low approach velocity, the 2-in. pipe flow meter was used to read the flow rate Q. When Q exceeded 100 gal./min, flow was switched to the 6-in. pipeline. During the switching from the 2-in. pipeline to the 6-in. pipeline, ~30 s of time is lost. It was noticed that for the same flow, the 6-in. pipe flow meter shows 65 gal./min when the 2-in. pipe flow meter shows 100 gal./min. For each such case, both of the diagrams were shown: one corresponds to the case without correction and the other case corresponds to the corrected Q.

## C.3.    References

Rao, 2002        D. V. Rao et al., "GSI-191: Separate-Effects Characterization of Debris Transport in Water," NUREG/CR-6772, LA-UR-01-6882, Los Alamos National Laboratory, August 2002.

**APPENDIX D: CALIBRATION OF TEST INSTRUMENTATION**

Velocity of water flow through the flume was measured indirectly by measuring the net volumetric flow and dividing it by the flow cross-sectional area. Because the flow velocity is an important experimental parameter, efforts were taken to calibrate the flow meter used to measure the volumetric flow rate.

**D.1.    Calibration of the Hoffer Flow Meter**

The 6-in. recirculation flow line in the large flume is equipped with a Hoffer turbine flow meter and digital readout. A copy of the manufacturer's calibration data sheet is attached to the end of this Appendix. The meter displayed both the instantaneous flow (in gal./min) and cumulative flow (in gallons). Because of fluctuations in the instantaneous flow, it was decided to use cumulative flow readout to average the fluctuations.

Calibration of this flow meter was achieved by measuring the volume pumped into the flume from the underground reservoir over a 2-min time frame with the indicators attached to the pump. The purpose of this experiment was to validate the measurements of the flow meter attached to the variable speed (frequency) centrifugal pump used to fill the large flume. The comparison test checked the accuracy of the indicators by measuring the time taken for the water level to rise 5 in. Test data are provided in Table D.1. The flow meter readings were recorded by noting the difference in the total volume of water (gallons) that flows through the meter over a 2-min interval (measured with a stopwatch). The actual flow was calculated from the test performed by timing the 5-in. rise in the water level. The calibration of the flow meter was achieved using the following procedure.

- A pump frequency was selected and the pump discharge-valve was throttled as needed to set the water flow through the flume. The frequency is listed in Column 2 below.

- The flow meter readout for the cumulative flow through the pump was recorded initially and again after 2 min. The difference was divided by 2 to obtain the flow meter reading in gal./min. These values are listed in Columns 3 through 6 below.

- This value was compared with the "instantaneous" meter readout (which usually fluctuates ±10%).

- The flume discharge valve was closed and the water was allowed to build up in the flume.

- The time taken for the water level to rise 5 in. was measured. This value was used to determine actual gal./min discharged into the flume. These values are listed in Columns 7 and 8.

**Table D.1. Flow Measurements from the Flow Meter vs Volumetric Measurements**

| Test | Pump Freq. (Hz) | Flow Meter Readings | | | | Time for 5 in. (s) | Actual Flow (gal./min) |
|---|---|---|---|---|---|---|---|
| | | Start | Stop | Difference | Flow (gal./min) | | |
| 1 | 33 | N/A | N/A | N/A | 120 | 94.12 | 119 |
| 2 | 36 | 381765 | 382184 | 419 | 210 | 53.94 | 208 |
| 3 | 38 | 383880 | 384505 | 625 | 312 | 34.65 | 324 |
| 4 | 40 | 386398 | 387280 | 882 | 441 | 25.19 | 445 |
| 5 | 42 | 388769 | 389927 | 1158 | 579 | 20.13 | 557 |
| 6 | 46 | 391911 | 393578 | 1667 | 833 | 13.72 | 818 |

Figure D.1 displays the data, along with 5%-error bars. This figure shows that the flow meter performs its intended function adequately.
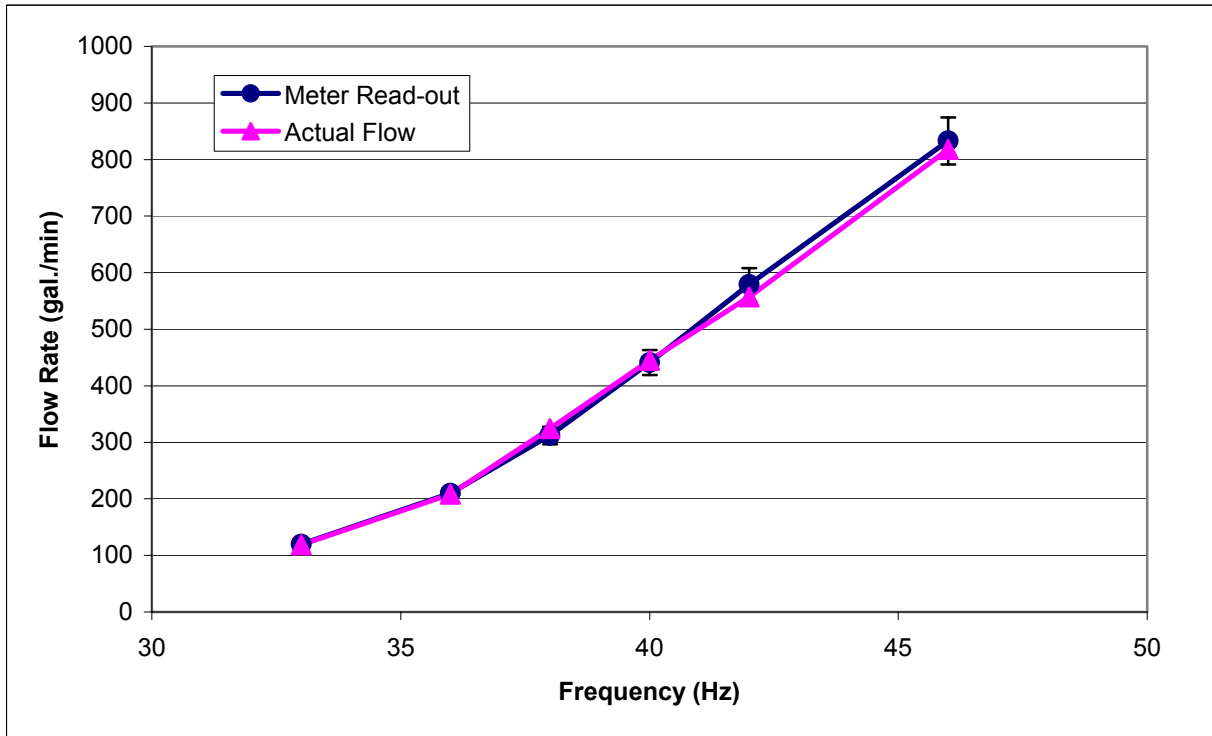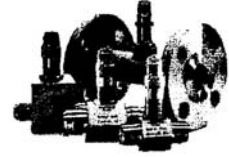


**Figure D.1. Comparison of meter readout with actual flow measurements.**

# **H** HOFFER FLOW CONTROLS, INC.
## The Turbine Flowmeter Company™

107 Kitty Hawk Lane • P.O. Box 2145 • Elizabeth City, North Carolina 27906-2145
1-800-628-4584 • (252) 331-1997 • FAX (252) 331-2886

PAGE    1

CALIBRATION DATA SHEET

MODEL #: HP-B-11/2-1.2-12-2NPT-B-X-13-AL

MEASUREMENT SOLUTIONS
ATTN: ACCOUNTS PAYABLE
1520 WEST PAMPA AVE

MESA, AZ   85202

SERIAL NUMBER: 88512
TEST RANGE: 1.195 to 12.051 FPS
TEST STAND:  1
TEST FLUID: Water at 20C Degrees
COIL TYPE: PC24-45S min  25.00 Mv
DATE:  7/03/00

ACCOUNT NUMBER:   7579
PURCHASE ORDER: R51980
JOB NUMBER:   30760

| # | METER FREQUENCY (HZ) | METER FLOW RATE (FT/SEC) | METER K FACTOR (PLS/FT) | FREQUENCY VISCOSITY (HZ/CTS) |
|---|---|---|---|---|
| 1 | 31.95 | 1.195 | 26.74 | 32.02 |
| 2 | 32.03 | 1.198 | 26.74 | 32.09 |
| 3 | 46.36 | 1.735 | 26.72 | 46.27 |
| 4 | 62.45 | 2.346 | 26.62 | 62.32 |
| 5 | 77.32 | 2.911 | 26.56 | 77.17 |
| 6 | 107.22 | 4.043 | 26.52 | 107.01 |
| 7 | 152.16 | 5.742 | 26.50 | 151.87 |
| 8 | 225.89 | 8.524 | 26.50 | 225.35 |
| 9 | 250.27 | 9.444 | 26.50 | 249.68 |
| 10 | 266.43 | 10.050 | 26.51 | 265.88 |
| 11 | 318.84 | 12.027 | 26.51 | 318.19 |
| 12 | 319.47 | 12.051 | 26.51 | 318.83 |

WE CERTIFY THAT ALL TEST EQUIPMENT USED IN THE PERFORMANCE
OF  THE  CALIBRATIONS  ARE  ACCURATE  AND  TRACEABLE  TO
N.I.S.T.  ALSO,  WE CERTIFY THAT OUR QUALITY ASSURANCE
SYSTEM IS IN COMPLIANCE WITH ISO 9001.

LINEARITY +/- .45    %

'K' AVERAGE   26.5775 PPF

OPERATOR ___KB___

ENGR. APPROVAL ___CH___

**APPENDIX E: INSTRUMENTATION SPECIFICATIONS**

The test instrumentation was upgraded so that time-dependent measurements of the debris-bed head loss, flow rate, and water temperature could be recorded on a computer and saved in spreadsheet format for analysis. The data acquisition system included the Lab View 7.0 data acquisition software to store, process, save, and export the data. Along with the data acquisition software, a differential pressure transmitter, a volumetric turbine flow meter, and a thermocouple were installed to complete the data acquisition system. In addition, water turbidity measurements (a measure of water clarity) were made throughout the testing.

**E.1.    Differential Pressure Transmitter**

The differential pressure transmitter (EW-68071-58) was supplied by Cole Parmer Industries. The sensors within the pressure transmitter allow for wet/wet, wet/dry, or dry/dry connections. The transmitter specifications are listed in Table E.1.1. Figure E.1.1 shows the calibration of the pressure transmitter.

**Table E.1.1. Differential Pressure Transmitter Specification (EW-68071-58)**

| | |
|---|---|
| Range | 0 to 10 psid[a] |
| Accuracy | ±0.25% full scale |
| Output | 4 to 20 mA |
| Temperature range (compensated) | 30 to 150°F (-1 to 65°C) |
| Process connection | 1/4 in. NPT[b] |
| Electrical connections | 1/2-in. internal conduit port |
| Media compatibility | Gases or liquids compatible with 17-4 PH[d] SS[e], silicone and Viton® O-rings. |
| Operating temperature | 0 to 175°F (-17 to 80°C) |
| Dimensions | 3 in. L x 2 1/8 in. W x 3 in. H |
| Power | 11 to 30 VDC[f] (unregulated) |
| Housing | NEMA[g] 6 |

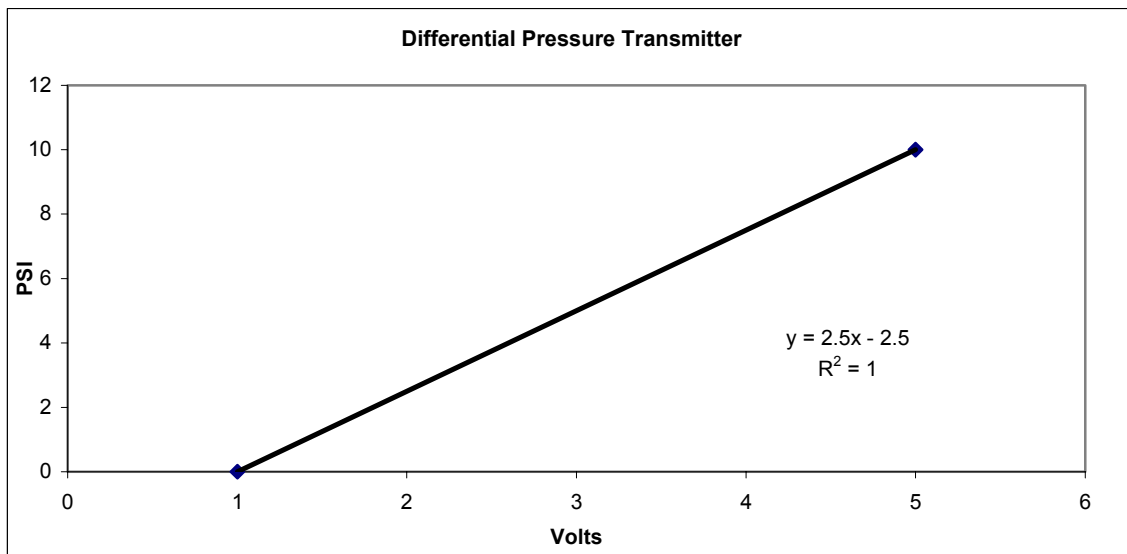[a] psid = pounds per square inch, differential.
[b] NPT =National Pipe Thread..
[d] PH = precipitation hardening.
[e] SS = stainless steel.
[f] VDC = volts direct current.
[g] NEMA = National Electrical Manufacturers Association.



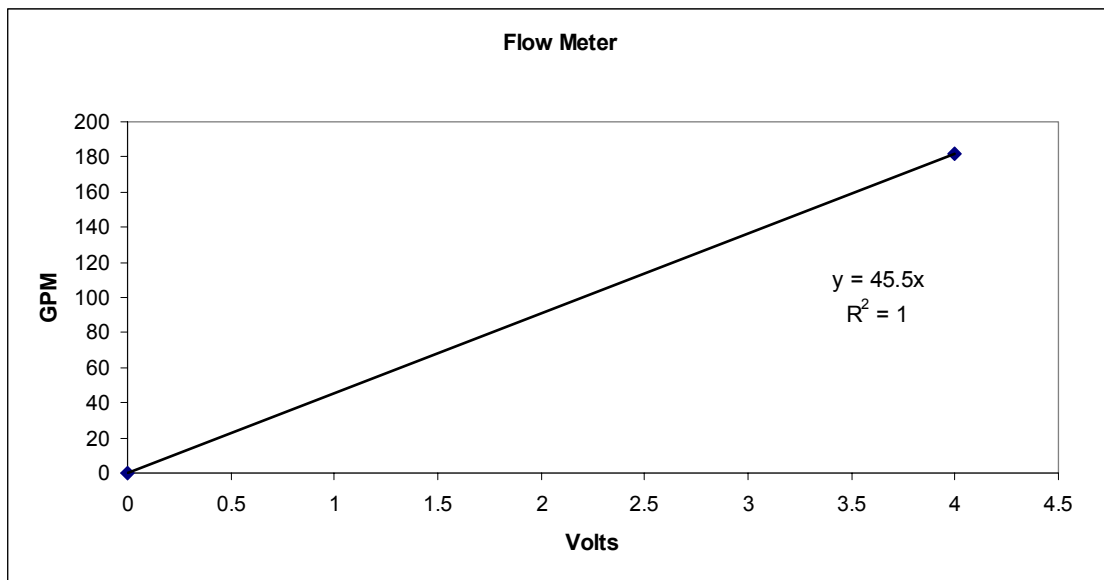**Figure E.1.1. Voltage-transmitter linear range correlation.**

### E.2. Volumetric Flow Meter

The volumetric turbine flow meter (A-05634-72) also was supplied by Cole Parmer Industries. It is a 2-in. turbine aluminum meter rated for 0 to 200 gal./min. Table E.2.1 lists the flow meter specifications. Figure E.2.1 shows the calibration of the flow meter.

**Table E.2.1. Volumetric Flow Meter (A-05634-72)**

| Flow rate | 20 to 200 gal./min |
|---|---|
| Accuracy | ±1% of reading |
| Repeatability | ±0.1% of reading |
| Max pressure | 1500 psi[a] |
| Max particulate size | 500μm |
| Max operating temperature | 140°F (60 °C) |
| Display | Meter-mounted 6-digit LCD[b], 1/2"H (with floating decimal) |
| Housing | Aluminum |
| Connections | 2" NPT(F) |
| Wetted materials | Aluminum, PVDF[c], tungsten carbide, 316 SS, and ceramic |
| Dimensions | 4 1/4 in. W x 4 3/4 in. H x 2 1/2 in. D |

[a] psi = pounds per square inch.
[b] LCD = liquid crystal display.
[c] PVDF = polyvinylidene fluoride.



Figure E.2.1. Voltage-transmitter linear range correlation.

### E.3. Thermocouple

A standard K-type unsheathed thermocouple was used without alterations because of built-in signal conditioning in the equipment. The thermocouple reading was verified with a mercury thermometer.

### E.4.    Water Clarity

Water samples were tested to determine turbidity in Nephelometric turbidity units (NTU), which were calibrated to mass concentration of CalSil particulate. The total water volume of the test loop was measured as ~76.5 gal. The calibration data are shown in Table E.4.1.

**Table E.4.1. Turbidity Calibration**

| Concentration (g/mL) | Turbidity (NTU) |
|---|---|
| 0 | 0 |
| 1E-6 | 1.1 |
| 2E-6 | 2.4 |
| 6E-6 | 4.4 |
| 8E-6 | 5.2 |
| 10E-6 | 6.9 |

**APPENDIX F: RAW TEST DATA FOR THE REFINED HEAD-LOSS TESTS**

Data for the calcium silicate closed-loop head-loss testing were collected both in logbook form and by the data acquisition system. The logbook data included specific information taken for discrete data points when quasi-stable test conditions were established, which included the rate of flow, temperature, debris-bed pressure differential (head loss), debris-bed thickness, water clarity measured in turbidity units, and pertinent observations. The automatic data acquisition system recorded the flow rate, temperature, and head loss, usually at 1-s intervals. The automatically recorded flow rate was available only for Tests 6H and 6I. The logbook data are presented here in tables and the automatically recorded data are shown as time-dependent plots.
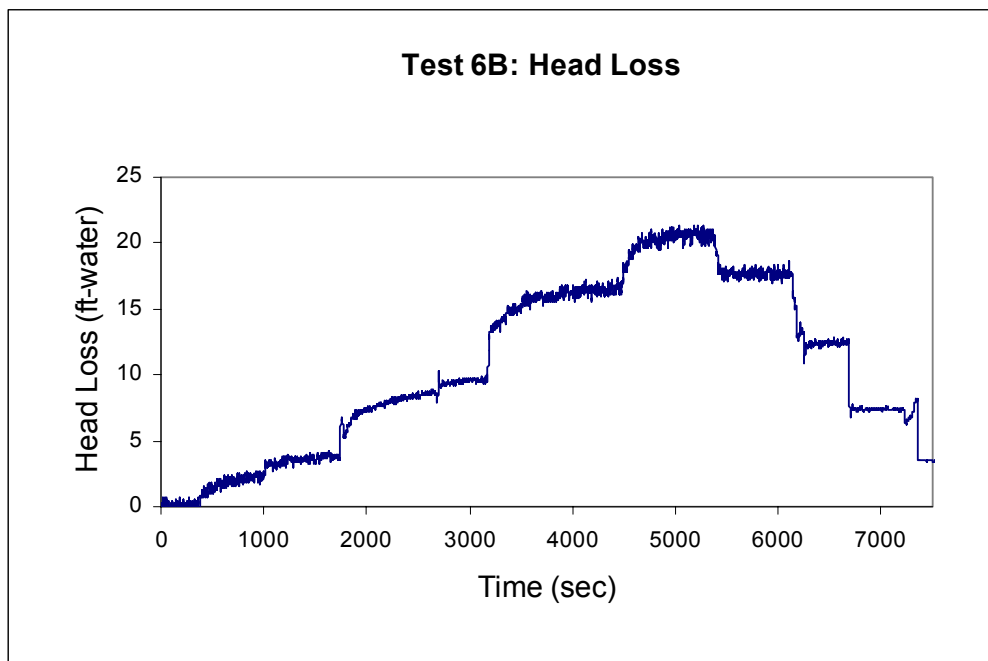
**F.1.     Test 6A: 100 g NUKON™ and 55 g Calcium Silicate**

The data from this test are not useful. This test was used to verify electronics and to test debris preparation.

**F.2.     Test 6B: 100 g NUKON™ and 55 g Calcium Silicate**

**Table F.2.1. Test 6B Logbook Record Test Data**

| Data No. | Flow (gal./min) | Velocity (ft/s) | Head Loss (ft-water) | Temperature (F) | Bed Thickness (in.) | Turbidity (NTU) | Estimated Loop CalSil (g) |
|---|---|---|---|---|---|---|---|
| 1 | 31.7 | 0.100 | 3.63 | 104 | 0.70 | 10.9 | 4.76 |
| 2 | 47.5 | 0.150 | 9.65 | 107 | 0.50 | 1.8 | 0.60 |
| 3 | 63.3 | 0.200 | 16.2 | 109 | 0.44 | 1.8 | 0.60 |
| 4 | 72.7 | 0.229 | 20.5 | 111 | 0.44 | 1.9 | 0.65 |
| 5 | 63.3 | 0.200 | 17.7 | 113 | 0.44 | 2.5 | 0.92 |
| 6 | 47.5 | 0.150 | 12.8 | 114 | 0.46 | 1.8 | 0.60 |
| 7 | 31.7 | 0.100 | 7.41 | 115 | 0.46 | 1.2 | 0.33 |



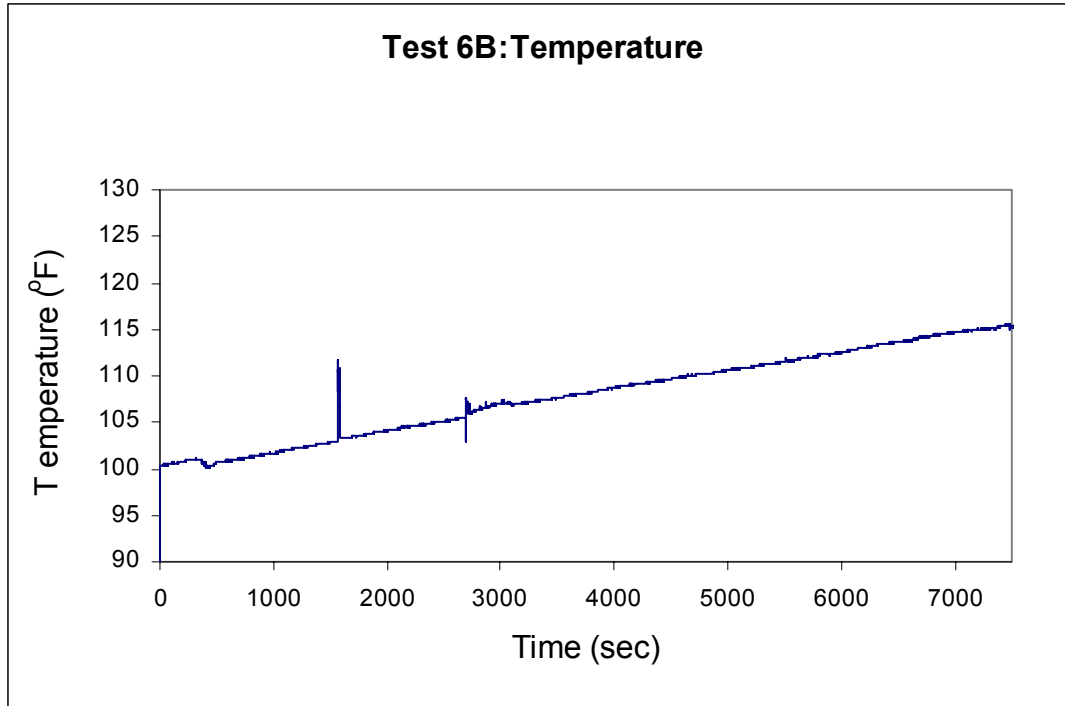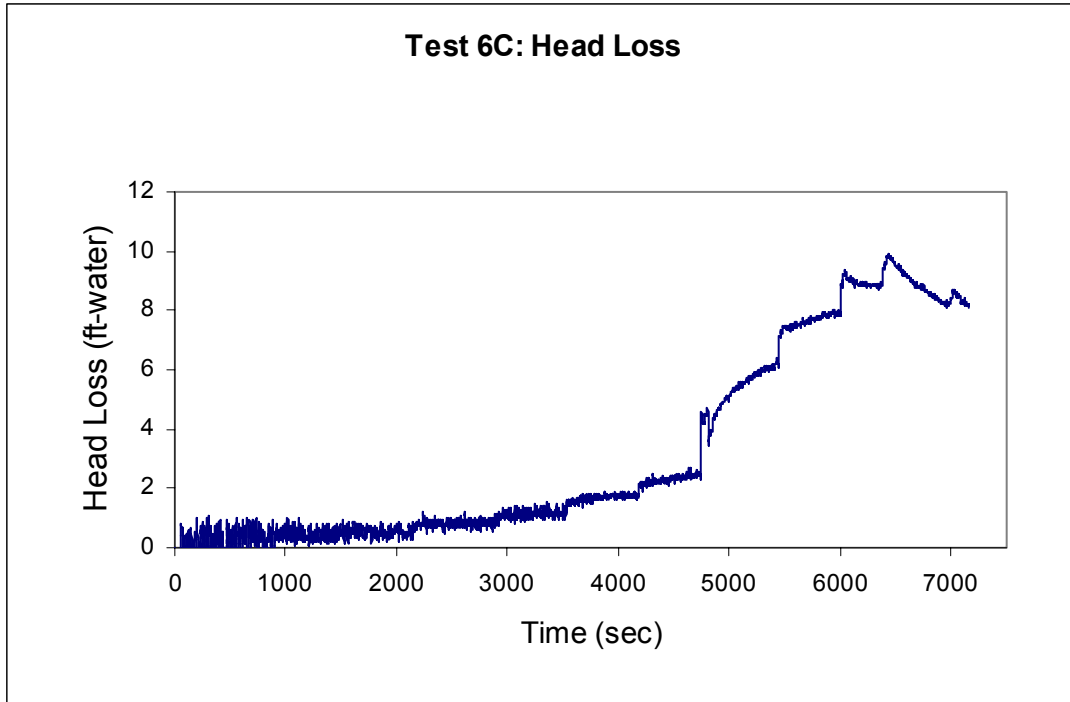**Figure F.2.1. Test 6B head-loss measurements.**

**Figure F.2.2. Test 6B temperature measurements.**

**F.3. Test 6C: 12 g NUKON™ and 6 g Calcium Silicate**

The debris in this test developed holes when the flow was increased beyond 255 gal./min; therefore, all subsequent data were invalid. Also during the test, a transition was made from the two- inch flow meter to the six-inch flow meter, which disturbed the debris bed slightly disturbed during the transition but then the debris resettled into a valid debris bed.

**Table F.3.1. Test 6C Logbook Record Test Data**

| Data No. | Flow (gal./min) | Velocity (ft/s) | Head Loss (ft-water) | Temperature (°F) | Bed Thickness (in.) | Turbidity (NTU) | Estimated Loop CalSil (g) |
|---|---|---|---|---|---|---|---|
| 1 | 32.0 | 0.101 | 0.58 | 120 | 0.38 | 10. | 4.35 |
| 2 | 63.3 | 0.200 | 0.92 | 121 | 0.31 | 4.0 | 1.61 |
| 3 | 94.3 | 0.298 | 1.27 | 122 | 0.31 | 3.5 | 1.38 |
| 4 | 125.4 | 0.396 | 1.73 | 123 | 0.25 | 3.3 | 1.29 |
| 5 | 158.6 | 0.501 | 2.31 | 125 | 0.25 | 3.1 | 1.2 |
| 6 | 183.0 | 0.578 | 6.23 | 126 | 0.19 | 3.0 | 1.15 |
| 7 | 223.0 | 0.704 | 7.97 | 126 | 0.19 | 2.1 | 0.74 |
| 8 | 255.0 | 0.805 | 9.01 | 127 | 0.19 | 2.4 | 0.88 |

**Test 6C: Head Loss**



**Figure F.3.1. Test 6C head-loss measurements.**
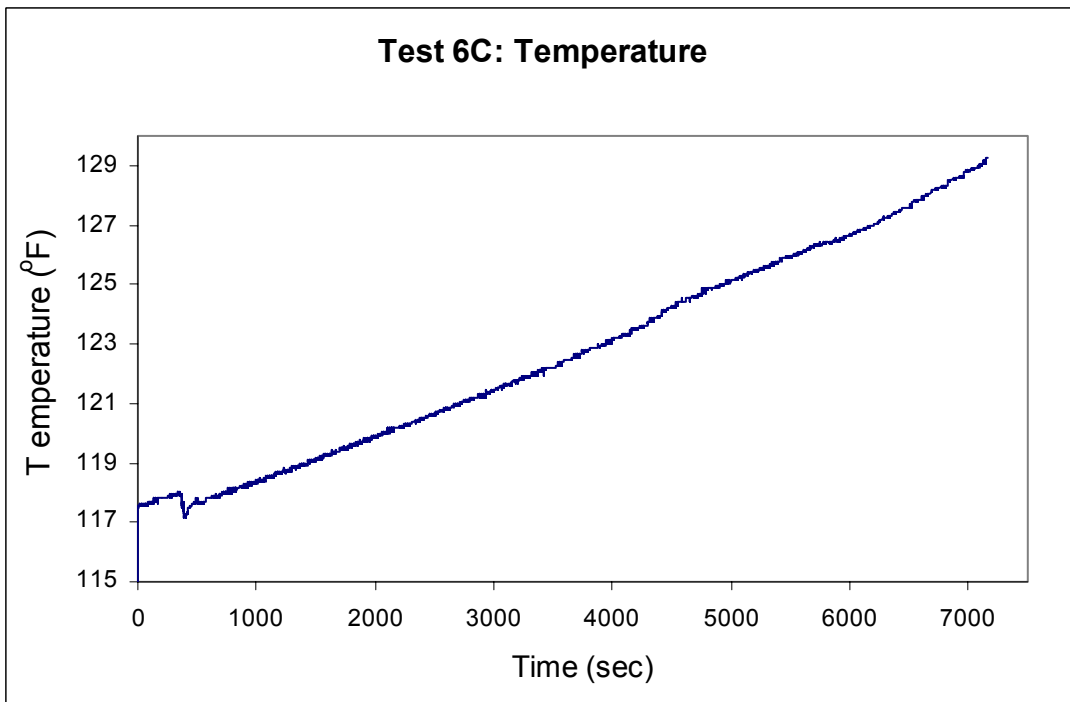
**Test 6C: Temperature**

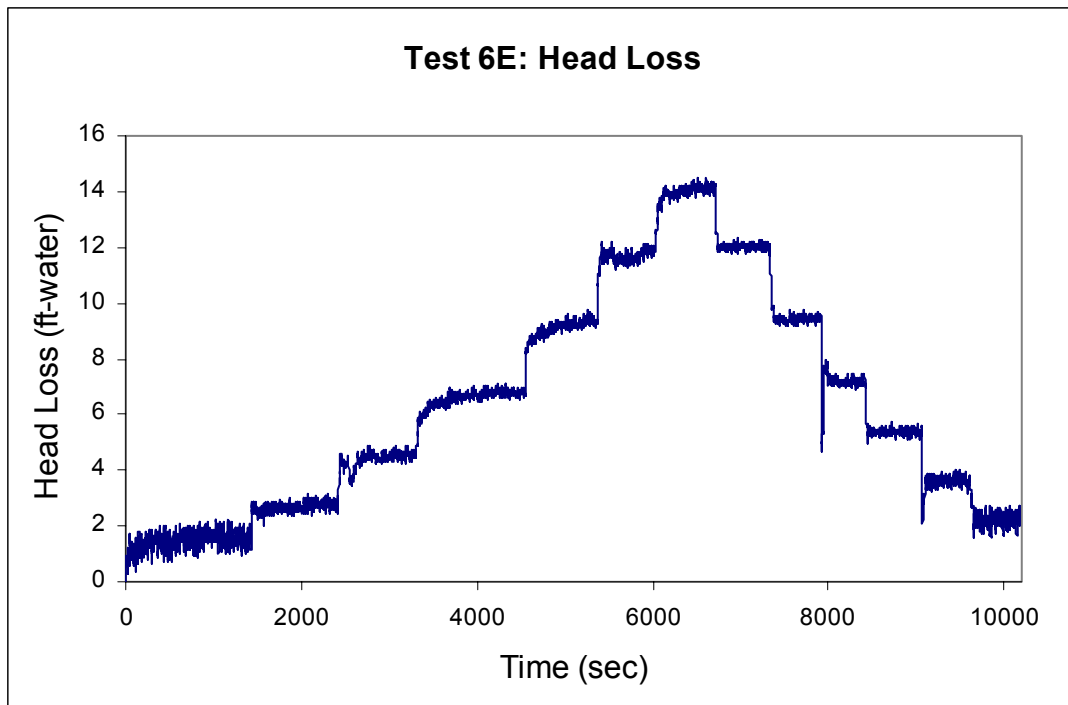

**Figure F.3.2. Test 6C temperature measurements.**

### F.4. Test 6D: 40 g NUKON™ and 20 g Calcium Silicate

The data from this test were not useful due to a data-recording malfunction.

### F.5. Test 6E: 70 g NUKON™ and 35 g Calcium Silicate

**Table F.5.1. Test 6E Logbook Record Test Data**

| Data No. | Flow (gal./min) | Velocity (ft/s) | Head Loss (ft-water) | Temperature (°F) | Bed Thickness (in.) | Turbidity (NTU) | Estimated Loop CalSil (g) |
|---|---|---|---|---|---|---|---|
| 1 | 31.8 | 0.100 | 1.89 | 121 | 0.50 | 6.0 | 2.52 |
| 2 | 46.7 | 0.147 | 2.93 | 123 | 0.50 | 2.5 | 0.92 |
| 3 | 63.4 | 0.200 | 4.66 | 124 | 0.44 | 1.5 | 0.47 |
| 4 | 79.2 | 0.250 | 6.81 | 126 | 0.44 | 0.68 | 0.20 |
| 5 | 94.2 | 0.297 | 9.58 | 127 | 0.38 | 0.47 | 0.14 |
| 6 | 110.5 | 0.349 | 11.9 | 128 | 0.38 | 1.1 | 0.32 |
| 7 | 124.4 | 0.393 | 14.3 | 129 | 0.38 | 0.68 | 0.20 |
| 8 | 110.9 | 0.350 | 12.2 | 130 | 0.38 | 0.52 | 0.15 |
| 9 | 93.6 | 0.295 | 9.77 | 131 | 0.38 | 0.46 | 0.13 |
| 10 | 77.9 | 0.246 | 7.18 | 132 | 0.38 | 0.17 | 0.05 |
| 11 | 63.8 | 0.201 | 5.36 | 132 | 0.38 | 0.22 | 0.06 |
| 12 | 47.4 | 0.150 | 3.79 | 133 | 0.31 | 0.29 | 0.08 |
| 13 | 32.0 | 0.101 | 1.96 | 134 | 0.31 | 0.45 | 0.13 |



**Figure F.5.1. Test 6E head-loss measurements.**
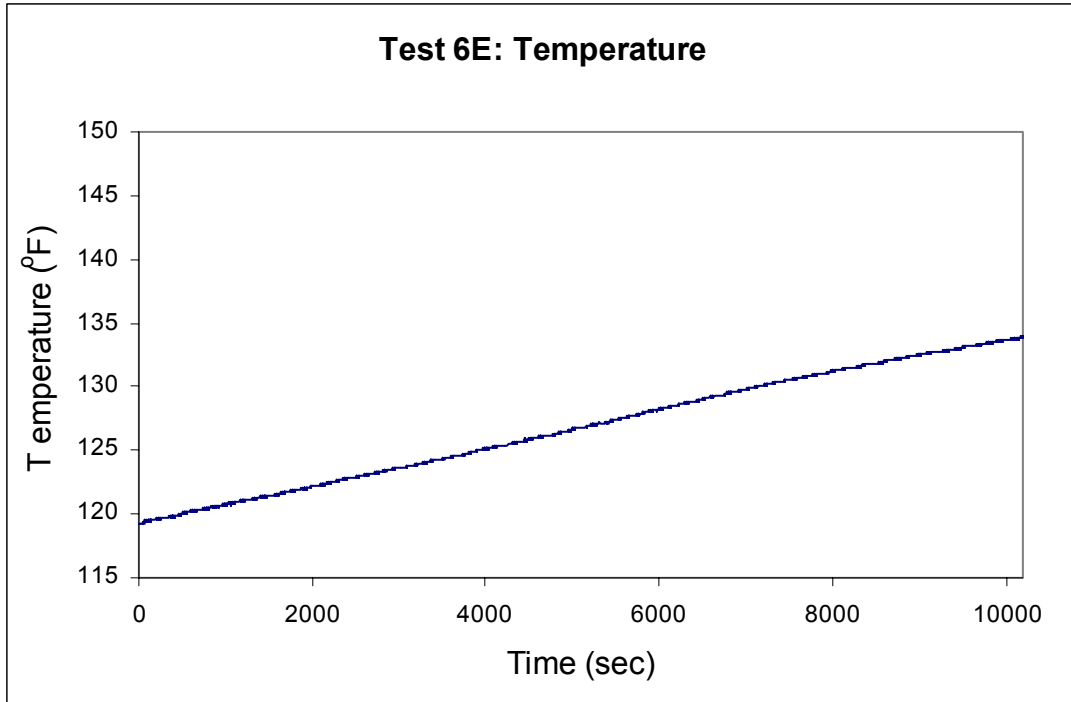
## Test 6E: Temperature



**Figure F.5.2. Test 6E temperature measurements.**

**F.6.    Test 6F: 40 g NUKON™ and 20 g Calcium Silicate**

**Table F.6.1. Test 6F Logbook Record Test Data**

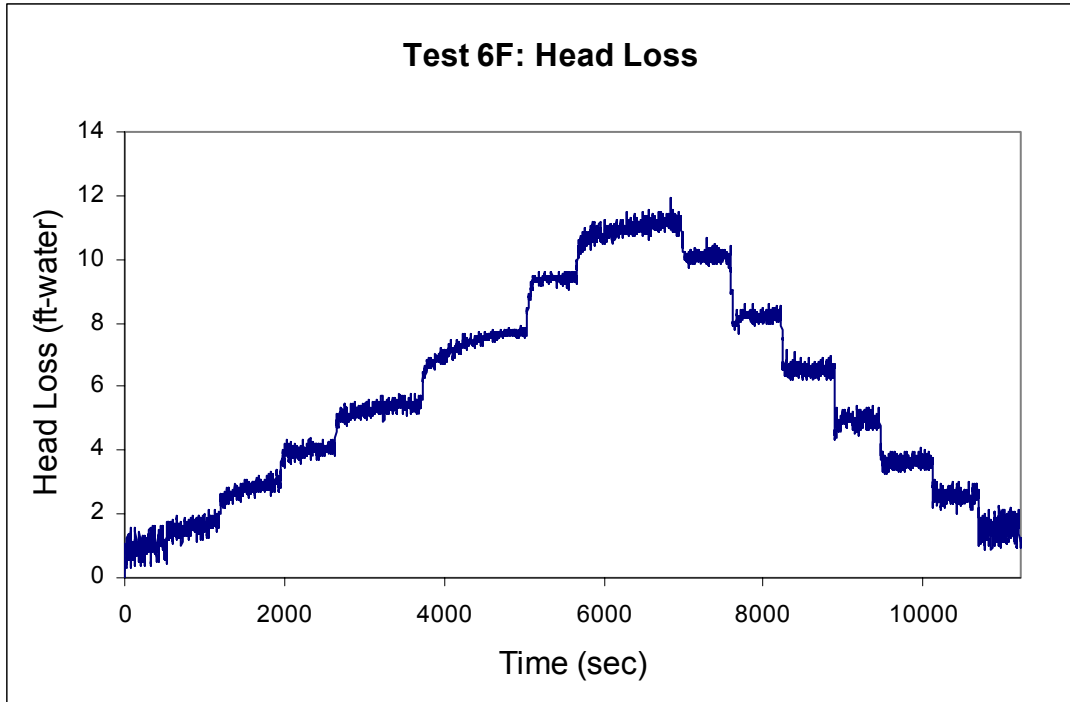| Data No. | Flow (gal./min) | Velocity (ft/s) | Head Loss (ft-water) | Temperature (°F) | Bed Thickness (in.) | Turbidity (NTU) | Estimated Loop CalSil (g) |
|---|---|---|---|---|---|---|---|
| 1 | 33.8 | 0.107 | 0.92 | 134 | 0.38 | 7.7 | 3.30 |
| 2 | 46.4 | 0.147 | 1.73 | 135 | 0.38 | 4.7 | 1.93 |
| 3 | 63.0 | 0.199 | 3.00 | 135 | 0.31 | 2.3 | 0.83 |
| 4 | 77.6 | 0.245 | 4.16 | 136 | 0.31 | 1.2 | 0.33 |
| 5 | 94.5 | 0.298 | 5.77 | 137 | 0.31 | 0.90 | 0.26 |
| 6 | 108.5 | 0.343 | 7.85 | 138 | 0.31 | 0.60 | 0.17 |
| 7 | 127.4 | 0.402 | 9.70 | 139 | 0.25 | 0.75 | 0.22 |
| 8 | 138.1 | 0.436 | 11.4 | 140 | 0.19 | 0.31 | 0.09 |
| 9 | 126.1 | 0.398 | 10.6 | 141 | 0.25 | 0.46 | 0.13 |
| 10 | 110.9 | 0.350 | 8.38 | 142 | 0.25 | 0.08 | 0.02 |
| 11 | 95.5 | 0.301 | 6.70 | 142 | 0.25 | 0.30 | 0.09 |
| 12 | 78.7 | 0.248 | 5.08 | 142 | 0.31 | 0.09 | 0.03 |
| 13 | 62.6 | 0.198 | 3.69 | 143 | 0.31 | 0.13 | 0.04 |
| 14 | 47.2 | 0.149 | 2.56 | 143 | 0.31 | 0.13 | 0.04 |
| 15 | 31.5 | 0.100 | 1.62 | 143 | 0.31 | 0.30 | 0.09 |

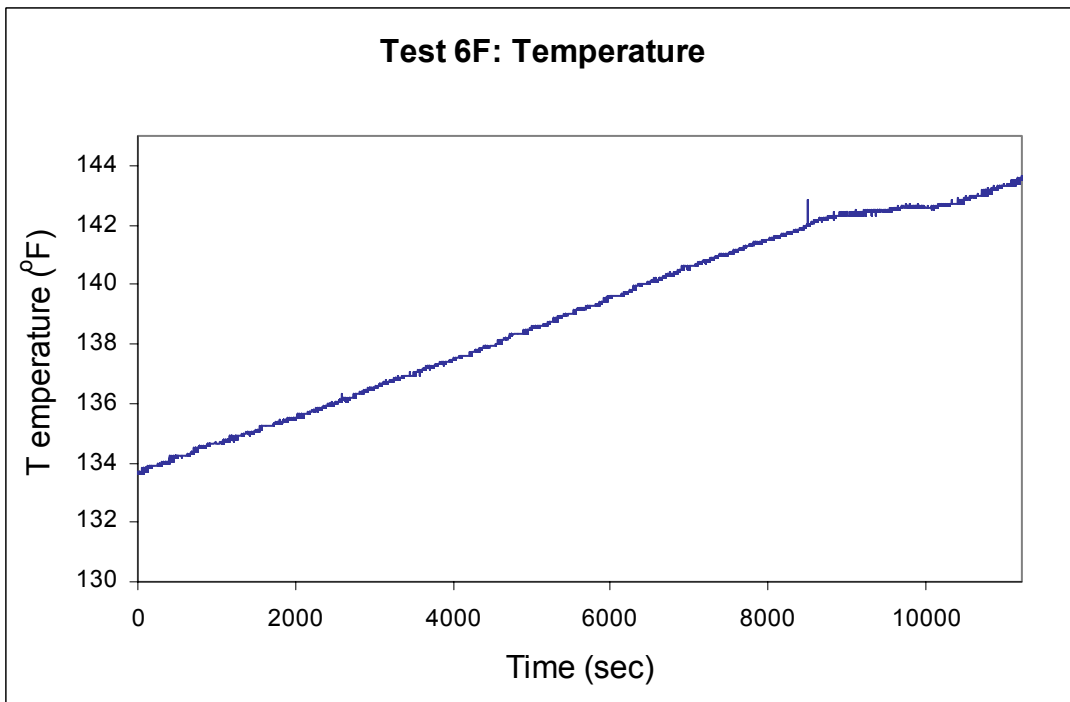**Figure F.6.1. Test 6F head-loss measurements.**



**Figure F.6.2. Test 6F temperature measurements.**

### F.7. Test 6G: 15 g NUKON$^{TM}$ and 7.5 g Calcium Silicate

The test was terminated before planned completion because of a leak that developed in the loop piping. Also, the automatically recorded data were lost because of a software malfunction. During this test, the valve was fully opened at peak velocity.

**Table F.7.1. Test 6G Logbook Record Test Data**

| Data No. | Flow (gal./min) | Velocity (ft/s) | Head Loss (ft-water) | Temperature (°F) | Bed Thickness (in.) | Turbidity (NTU) | Estimated Loop CalSil (g) |
|---|---|---|---|---|---|---|---|
| 1 | 33.3 | 0.105 | 0.58 | 127 | 0.25 | 4.4 | 2.01 |
| 2 | 48.5 | 0.153 | 0.69 | 129 | 0.44 | 2.7 | 1.23 |
| 3 | 64.1 | 0.202 | 0.69 | 129 | 0.38 | 2.8 | 1.28 |
| 4 | 93.5 | 0.295 | 1.04 | 130 | 0.38 | 2.5 | 1.14 |
| 5 | 127.3 | 0.402 | 1.48 | 131 | 0.38 | 2.4 | 1.10 |
| 6 | 158.4 | 0.500 | 13.5 | 134 | 0.38 | - | - |

### F.8. Test 6H: 15 g NUKON$^{TM}$ and 7.5 g Calcium Silicate

**Table F.8.1. Test 6H Logbook Record Test Data**

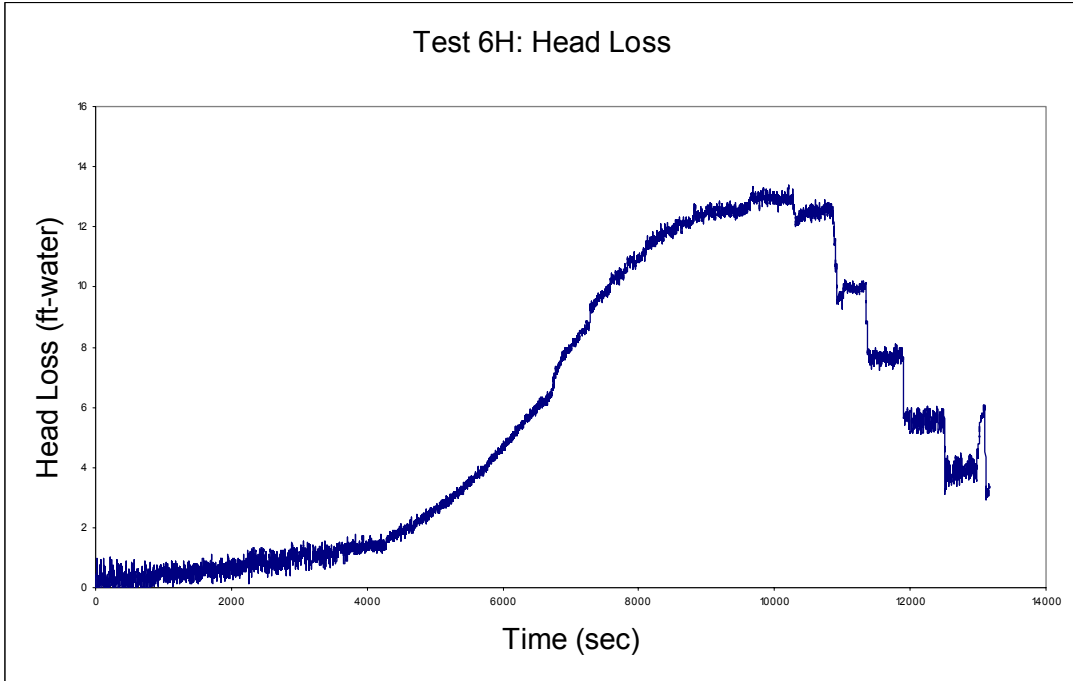| Data No. | Flow (gal./min) | Velocity (ft/s) | Head Loss (ft-water) | Temperature (°F) | Bed Thickness (in.) | Turbidity (NTU) | Estimated Loop CalSil (g) |
|---|---|---|---|---|---|---|---|
| 1 | 33.7 | 0.106 | 0.35 | 89 | 0.19 | 6.20 | 2.61 |
| 2 | 47.3 | 0.149 | 0.46 | 90 | 0.19 | 4.10 | 1.65 |
| 3 | 62.7 | 0.198 | 0.62 | 91 | 0.19 | 4.20 | 1.70 |
| 4 | 78.9 | 0.249 | 0.72 | 93 | 0.19 | 3.40 | 1.33 |
| 5 | 93.4 | 0.295 | 0.95 | 95 | 0.19 | 3.10 | 1.20 |
| 6 | 109.5 | 0.346 | 1.27 | 97 | 0.13 | 2.70 | 1.01 |
| 7 | 126.0 | 0.398 | 12.0 | 107 | 0.13 | 0.95 | 0.28 |
| 8 | 127.7 | 0.403 | 12.7 | 110 | 0.13 | 0.95 | 0.28 |
| 9 | 130.0 | 0.410 | 13.0 | 111 | 0.13 | 0.36 | 0.10 |
| 10 | 126.0 | 0.398 | 12.9 | 113 | 0.13 | 0.45 | 0.13 |
| 11 | 109.8 | 0.347 | 10.3 | 114 | 0.13 | 0.27 | 0.08 |
| 12 | 94.2 | 0.297 | 8.08 | 115 | 0.13 | 0.34 | 0.16 |
| 13 | 78.5 | 0.248 | 5.66 | 116 | 0.13 | 0.42 | 0.12 |
| 14 | 62.8 | 0.198 | 4.11 | 117 | 0.13 | 0.38 | 0.11 |

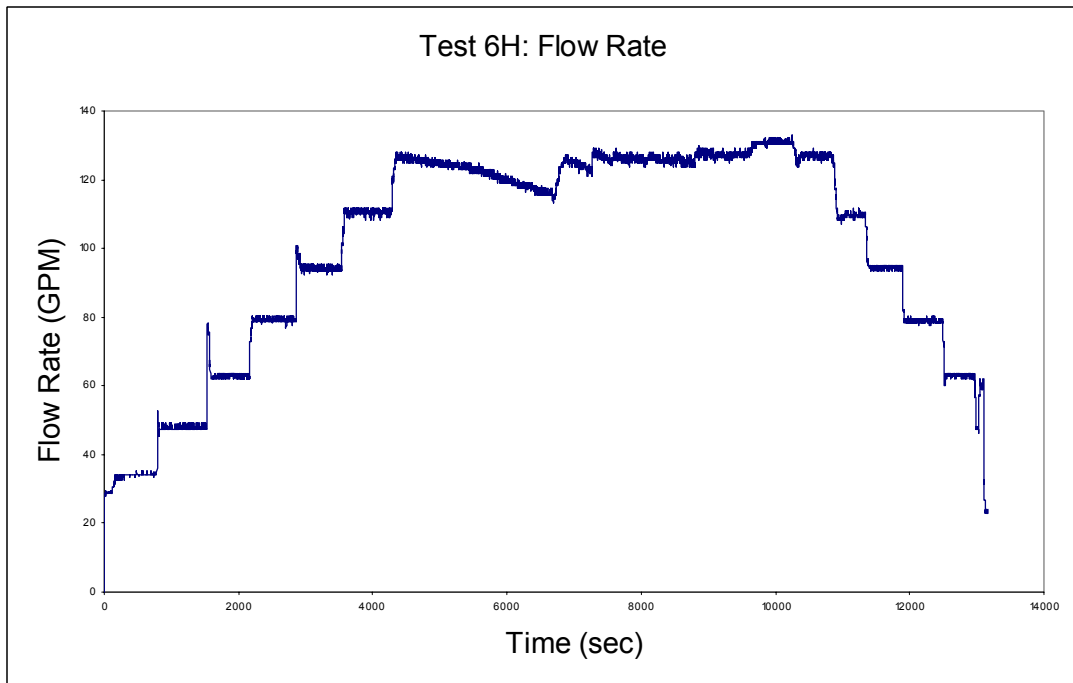**Figure F.8.1. Test 6H Head-loss measurements.**

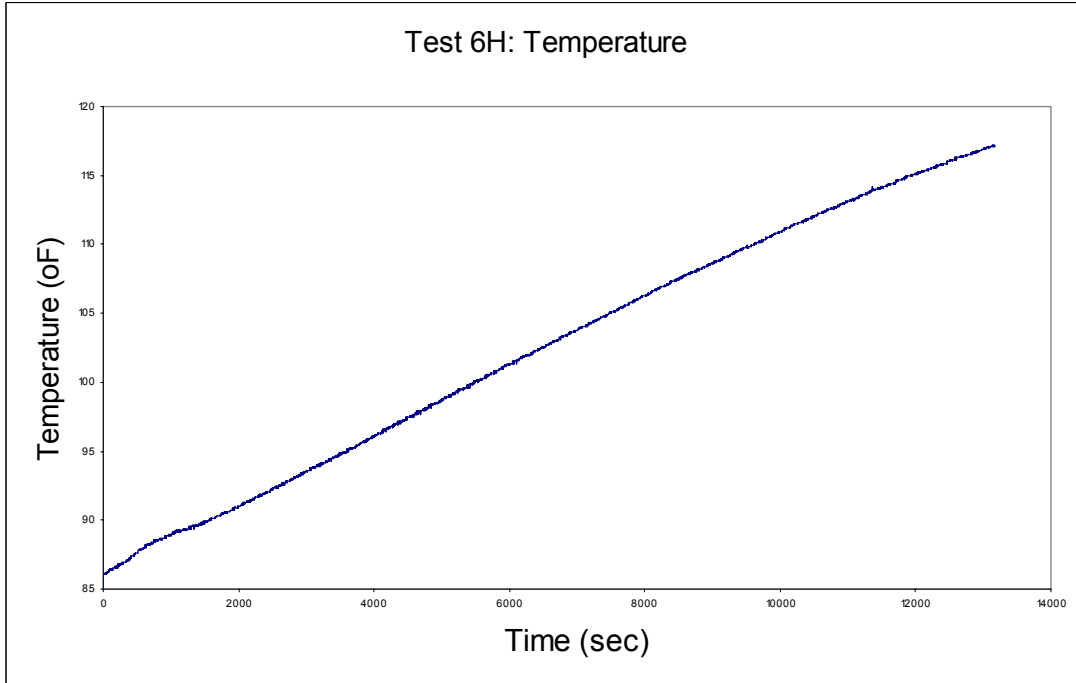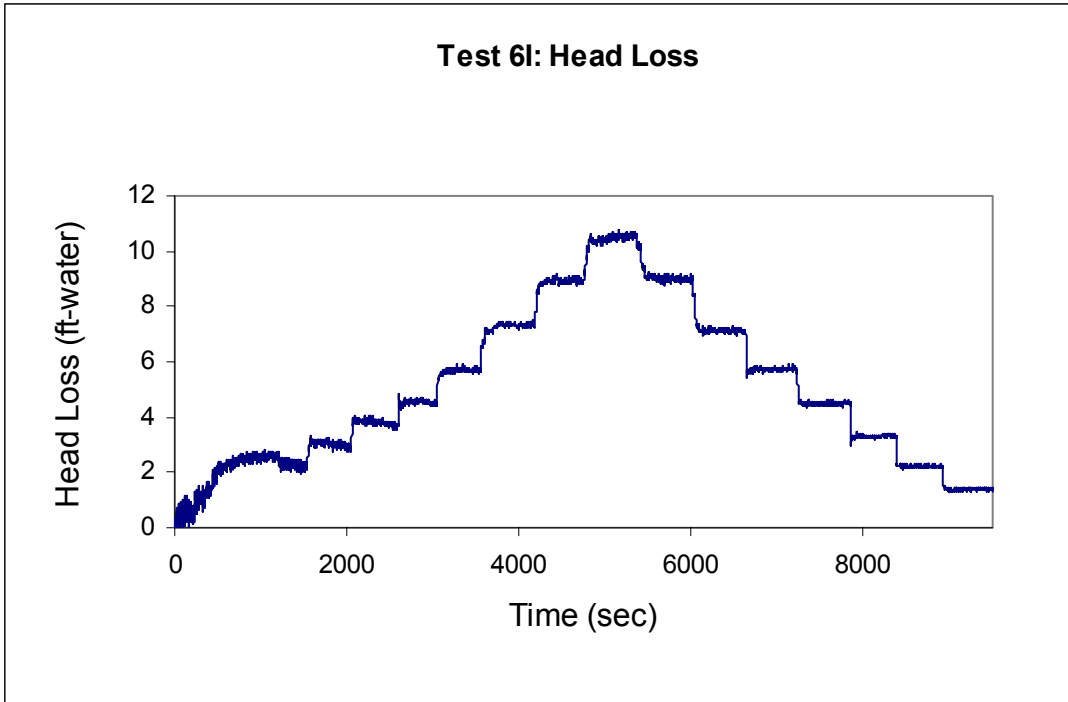

**Figure F.8.2. Test 6H flow measurements.**

**Figure F.8.3. Test 6H temperature measurements.**

## F.9.    Test 6I: 55 g NUKON™ and 27.5 g Calcium Silicate

**Table F.9.1. Test 6I Logbook Record Test Data**

| Data No. | Flow (gal./min) | Velocity (ft/s) | Head Loss (ft-water) | Temperature (°F) | Bed Thickness (in.) | Turbidity (NTU) | Estimated Loop CalSil (g) |
|---|---|---|---|---|---|---|---|
| 1 | 33.1 | 0.105 | 2.31 | 134 | 0.44 | 11.1 | 4.85 |
| 2 | 47.5 | 0.150 | 3.05 | 135 | 0.44 | 3.7 | 1.47 |
| 3 | 65.1 | 0.205 | 3.93 | 135 | 0.44 | 3.5 | 1.38 |
| 4 | 79.5 | 0.251 | 4.62 | 136 | 0.38 | 1.8 | 0.60 |
| 5 | 94.8 | 0.299 | 5.84 | 136 | 0.38 | 1.2 | 0.31 |
| 6 | 110.5 | 0.349 | 7.50 | 137 | 0.31 | 0.83 | 0.24 |
| 7 | 127.6 | 0.403 | 9.14 | 138 | 0.31 | 0.66 | 0.19 |
| 8 | 141.2 | 0.446 | 10.8 | 138 | 0.25 | 0.37 | 0.11 |
| 9 | 126.6 | 0.400 | 9.17 | 139 | 0.31 | 0.32 | 0.09 |
| 10 | 110.4 | 0.349 | 7.37 | 139 | 0.31 | 0.26 | 0.08 |
| 11 | 94.4 | 0.298 | 5.87 | 140 | 0.31 | 0.23 | 0.07 |
| 12 | 79.3 | 0.250 | 4.69 | 141 | 0.31 | 0.26 | 0.08 |
| 13 | 64.0 | 0.202 | 3.37 | 141 | 0.38 | 0.35 | 0.10 |
| 14 | 46.8 | 0.148 | 2.26 | 141 | 0.38 | 0.36 | 0.10 |
| 15 | 31.3 | 0.099 | 1.39 | 142 | 0.38 | 0.35 | 0.10 |

## Test 6I: Head Loss



**Figure F.9.1. Test 6I head-loss measurements.**
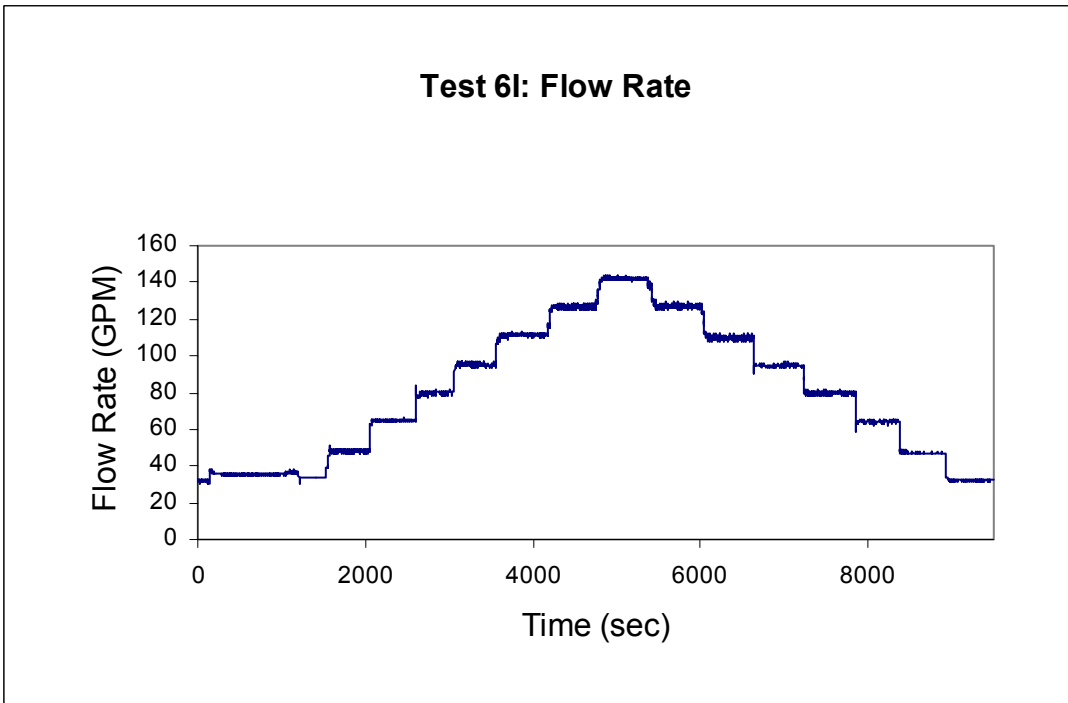
## Test 6I: Flow Rate



**Figure F.9.2. Test 6I flow measurements.**

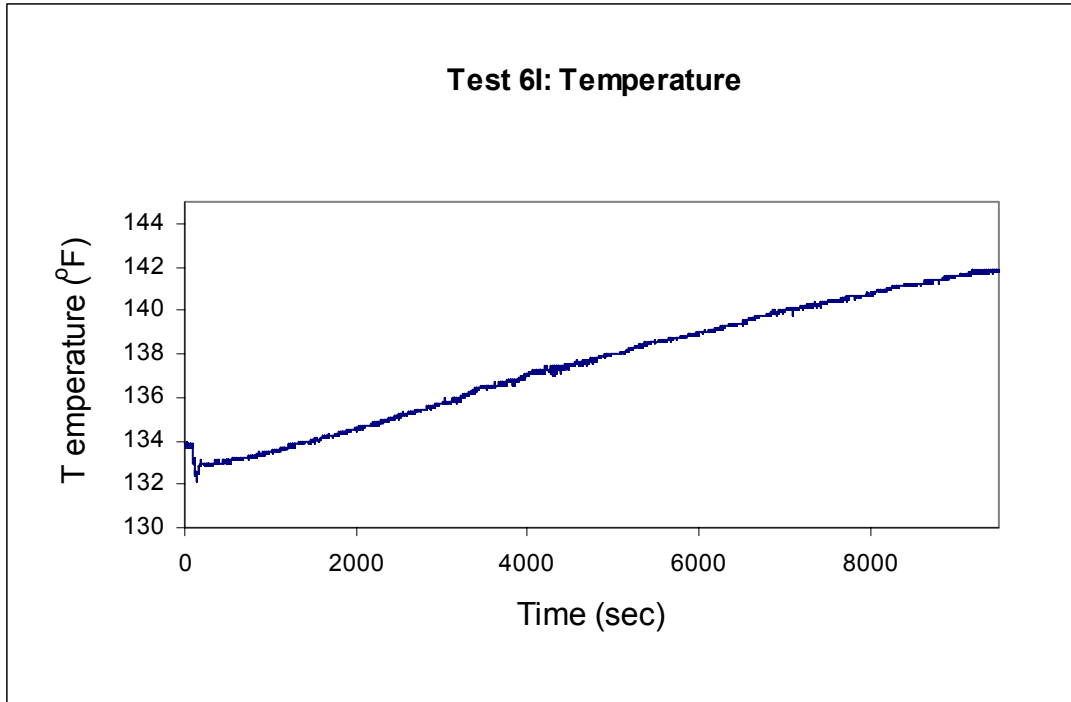## Test 6I: Temperature



**Figure F.9.3. Test 6I temperature measurements.**

## F.10. Test 6J: 18 g NUKON$^{TM}$ and 9 g Calcium Silicate

This test was terminated when the flow regulation valve was fully open and the small flow meter was in operation. The data obtained illustrated relatively low head loss, indicating that the pressure transducer may have malfunctioned. In retrospect, the larger flow meter piping isolation valve should have been opened to increase the flow through the debris bed. Higher flow velocities might have triggered the high thin-bed head losses. The data from this test is questionable; however, it does clearly indicate that the head loss for this test was less severe than that of Test 6H. The test data at the point where the flow regulation valve was fully open are shown in Table F.10.1.

**Table F.10.1. Test 6J Logbook Record Test Data**

| Flow (gal./min) | Velocity (ft/s) | Head Loss (ft-water) | Temperature (°F) | Bed Thickness (in.) | Turbidity (NTU) | Estimated Loop CalSil (g) |
|---|---|---|---|---|---|---|
| 170.2 | 0.537 | 3.35 | 137 | 0.13 | 0.83 | 0.24 |